Lyle, M., Wilson, P.A., Janecek, T.R., et al., 2002
Proceedings of the Ocean Drilling Program, Initial Reports Volume 199

1. Leg 199 Summary[1]

Shipboard Scientific Party[2]

ABSTRACT

Ocean Drilling Program (ODP) Leg 199, "The Paleogene Equatorial Transect" (Sites 1215–1222), was designed to study the evolution of the equatorial Pacific current and wind system as Earth went from maximum Cenozoic warmth to initial Antarctic glaciations. The drilling program was primarily devoted to a transect along the 56- to 57-Ma crust, old enough to capture the Paleocene/Eocene boundary in the basal, more carbonate-rich sediments. The Leg 199 transect extends from a paleolatitude of ~4°N–~4°S to encompass a relatively thick lower Eocene sediment section perhaps 8° north of the paleoequator. One site (1218) was also drilled on ~40-Ma crust to collect a near-equatorial sediment sequence from the middle Eocene to the Oligocene in order to investigate the transition in global climate from the Eocene "greenhouse" to Oligocene "icehouse."

The Pacific plate has drifted northward through Cenozoic time transporting biogenic sediments deposited under the high-productivity equatorial belt into a zone of extremely slow sediment (red clay) accumulation. Thus, the central tropical North Pacific Ocean is an ideal region in which to sample shallowly buried Paleogene sequences of equatorially deposited biogenic sediments. The thin Neogene cover of red clay in the area means that the entire Paleogene sediment section is potentially drillable by ODP advanced piston coring and extended core barrel methods.

[1]Examples of how to reference the whole or part of this volume.
[2]Shipboard Scientific Party addresses.

Ms 199IR-101

BACKGROUND AND OBJECTIVES

Upwelling, Productivity, and Equatorial Sedimentation

The complex system of equatorial currents is one of the most persistent and clear traces of wind-driven circulation in the oceans. The Leg 199 drilling program (Fig. F1; Table T1) was designed to study the evolution of this system in the Pacific Ocean as Earth went from maximum Cenozoic warmth to initial Antarctic glaciations. In the Neogene, the northern position of the Inter-tropical Convergence Zone (ITCZ) relative to the equator has given rise to tradewind-induced divergence at the equator and has caused a narrow band of equatorial upwelling (Fig. F2) as well as an equatorially asymmetric zonal current system. High productivity associated with equatorial upwelling results in a high rain of biogenic debris to the seafloor within 1.5°–2° of the geographic equator, with peak values restricted to an even narrower zone. In the Pacific Ocean, this biogenic rain has built, over Neogene time, a mound of almost pure calcareous and siliceous sediments stretching along the equatorial region and reaching a thickness of >500 m (Fig. F3). The little that we knew about Paleogene sequences in the central tropical Pacific Ocean prior to Leg 199 suggested that pre-Oligocene latitudinal patterns of sedimentation were significantly different than this narrowly focused Neogene arrangement (Moore et al., 2002). Sedimentation rates in the Eocene appear to be significantly slower than Neogene rates, and the distribution of sediments from seismic reflection profiles appears different than a pattern resulting from a narrow, linear, well-focused source of biogenic sediments along the equator. Ocean Drilling Program (ODP) Leg 199 was designed to collect sediments along a latitudinal transect in order to better understand Eocene and Oligocene sedimentation patterns and thereby reconstruct the dynamics of Eocene biogeochemical cycles and paleoceanography.

Pacific Plate Movement and the Cessation of Biogenic Sedimentation

The central equatorial Pacific is unique in the world's oceans because the path of plate motion carries the linear trace of equatorial upwelling and productivity northward with time (van Andel, 1974). There are two clear implications of this northward plate motion: (1) the thickest part of the Neogene equatorial mound of biogenic sediment is displaced several degrees to the north of the equator and (2) sediments deposited a few tens of millions of years ago have moved completely out of the region of high sediment flux. In principle, this set of circumstances presents an excellent opportunity to recover relatively undisturbed sediments through climatologically and paleoceanographically important time intervals that are notorious for extensive chert formation (e.g., the middle Eocene) thus grossly undersampled in the deep oceans.

Despite the high quality of plate tectonic models, the path of movement of the Pacific plate is still not perfectly understood, and it is not yet possible for us to backtrack drill sites to their paleopositions in the early Eocene with confidence. Therefore, paleomagnetic studies aimed at locating our drill sites with respect to the Eocene equator were an important component of the Leg 199 shipboard science. An equally important aim of the shipboard paleomagnetic program was to cross-calibrate geomagnetic reversal stratigraphy with biostratigraphy. In fact,

F1. Leg 199 and DSDP drill sites superimposed on bathymetry and Anomaly C25n, p. 52.

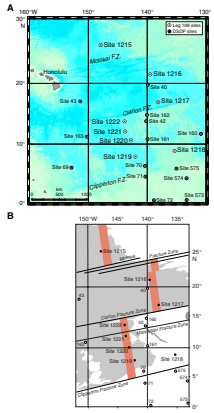

T1. Hole summary, p. 86.

F2. Chlorophyll contents in the Pacific equatorial region, p. 53.

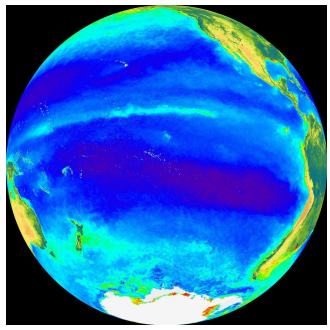

F3. Position, thickness, and mass density of the equatorial sediment bulge in the equatorial Pacific Ocean, p. 54.

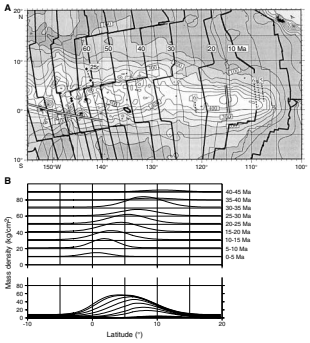

the likelihood of recovering sediments with compositional changes linked to orbitally forced insolation variability made the production of astronomically calibrated timescales an important scientific goal for Leg 199.

Early Paleogene Warm Climates

The early Paleogene, particularly the early Eocene (~55–49 Ma), witnessed the warmest global climates recorded on Earth in the entire Cenozoic, and it has long been appreciated that abyssal ocean-water temperatures were significantly warmer than today (e.g., Shackleton and Kennett, 1975). This observation has led to widespread speculation that these warm temperatures originated through low-latitude water mass formation (e.g., Brass et al., 1982). Yet, this explanation has always posed formidable problems for dynamicists, and recent numerical experiments support the alternative, more conservative, view that the warm, abyssal water masses of the Paleocene and Eocene are more likely linked to deepwater formation in high-latitude regions having warmer sea-surface temperatures than today (Bice and Marotzke, 2001). Support is widespread for the view that surface temperatures were warmer in high-latitude oceans (and the interiors of continents) during the early Paleogene (Zachos et al., 1993). Diverse sets of paleontological, sedimentary, and geochemical proxy records indicate that, at that time, subtropical to temperate fauna and flora extended to subpolar regions of both hemispheres where continental polar ice sheets were conspicuously absent (Shackleton and Kennett, 1975). The surface-temperature regime of the early Paleogene tropics is an ongoing subject of investigation (Bralower et al., 1995; Andreasson and Schmitz, 1998; Pearson et al., 2001), but the very warm temperatures (~12°C) estimated for high latitudes and deep waters mean that there can be little doubt that latitudinal temperature gradients during the early Paleogene were substantially smaller than today (Crowley and Zachos, 2000). This observation raises an intriguing paleoclimate problem because, if warmer high-latitude climates depend on enhanced wind-driven ocean currents or wind-carried heat and moisture to transport heat to the poles, it is difficult to explain how this transport was maintained under the weaker pole-to-equator thermal gradients. Instead, weaker latitudinal temperature gradients should give rise to weaker winds and diminished wind-driven transport. This apparent paradox is a persistent problem in numerical general circulation model reconstructions of warm paleoclimates (Barron and Washington, 1984; Manabe and Bryan, 1985; Sloan and Huber, 2001).

New data from the tropical oceans are necessary to define the climatic and oceanographic processes associated with early Paleogene warmth. Measurement of tropical sea-surface temperature gradients, for example, is an important way to distinguish between greenhouse-induced warming of the poles and warming by either atmospheric or oceanic heat transport (e.g., Crowley, 1991; Bralower et al., 1995; Wilson and Opdyke, 1996; Wilson and Norris, 2001; Pearson et al., 2001). Data on winds and currents are needed to partition heat transport between the atmosphere and oceans. The patterns of tropical wind and ocean circulation are key elements of global circulation, and existing records indicate that these patterns may have been markedly different from today during the early Paleogene (Hovan and Rea, 1992; Janecek and Rea, 1983; Rea et al., 1990).

Leg 199 was designed to drill a lower Paleogene transect across the world's most long-lived wind-driven current structure, which features the confluence of the northern and southern hemispheric winds and has a pattern, strength, and biogenic productivity linked to global climate patterns. The lower Eocene transect was aimed at providing basic records of sediment composition, mass accumulation, plankton communities, sea-surface and abyssal temperatures, and paleoproductivity across the paleoequator. These sorts of data are needed in order to assess the stability of the water column, the magnitude of heat transfer out of the tropics, surface ocean circulation, the location and strength of the trade wind belts, and the location of the ITCZ. The location of the ITCZ and the transition from the trade winds to the westerlies can be determined by the changes in the composition and rates of deposition of wind-blown dust, whereas mass accumulation rates (MARs) of biogenic debris can be used to assess the position and the strength of upwelling zones. Stable carbon isotope data will be used to assess nutrient flows in the water column and to constrain the global carbon cycle.

General Circulation Model Reconstructions

Model reconstructions of the Eocene climate have been hampered by a severe lack of data to constrain marine boundary conditions and, until recently, the need to specify either the atmospheric or oceanic part of the heat transport equation. In addition, lack of adequate control on bathymetry and topography in the Eocene, particularly in ocean gateway regions, severely weakens the capacity to model climate accurately from first principles (Deconto et al., 2000). Finally, computational constraints generally force the number of model years to be short (a few thousand years or less) so long-term transitions cannot be easily modeled. Most paleoclimate modeling is, therefore, performed on time slices for which reasonable initial conditions are established. In order to adequately understand Paleogene ocean dynamics and climate, there must be a strong interaction between paleoceanographers who gather new observations and climate modelers who make use of them to develop more realistic models (Sloan and Huber, 2001; Huber and Sloan, 2000).

One recent development in paleoclimate modeling is the application of coupled, ocean-atmosphere, global circulation models (e.g., **Huber,** this volume, and references therein). These types of models produce physically consistent worlds and can be used to study ocean-atmosphere interactions rather than to specify them. An example of the results of such modeling can be seen in Figure **F4** with the estimated 56-Ma paleopositions of the Leg 199 drill sites superimposed. The figure shows annual upwelling velocity and indicates that the eastern Pacific should have been a relatively productive region, with respect to much of the world ocean, in the early Eocene.

F4. Sites along the 56-Ma Leg 199 transect, superimposed on model estimates of upwelling, p. 55.

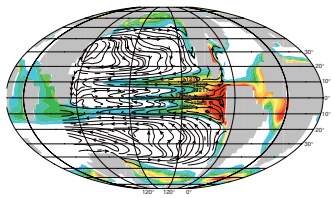

Paleoceanographic Time Slices

We have known for many years that the early Paleogene, particularly the early Eocene (~55–49 Ma), represents the most extreme long-lived interval of global warming witnessed on Earth since the well-documented mid-Cretaceous greenhouse (e.g., Shackleton and Kennett, 1975; Wilson and Norris, 2001). Yet little is known about the number of constituent hyperthermals, the range of temperatures, or their effects on biotic evolution (Thomas and Zachos, 1999). Similarly, although we

know that the Eocene greenhouse period was followed by a long shift toward lower temperatures and ice sheet growth into the late Eocene–Oligocene, the detailed history of these events and consequences for oceanic and atmospheric circulation, carbon cycling, and biotic evolution are only vaguely understood. The late Eocene is also interesting with respect to the response of global climate and biodiversity to the history of large impact extraterrestrial bodies on Earth. Thus, the Paleogene can be thought of as containing numerous critical time slices that provide an excellent opportunity to improve our understanding of important paleoclimatic problems involving the dynamics of greenhouse gas release, warm climate stability, biotic turnover associated with extreme climate transitions, extraterrestrial impacts, and initiation of major continental ice sheets.

Paleocene/Eocene Boundary

It is now well accepted that a substantial (~5°–7°C) warming in the Southern Ocean and subtropics, a 35%–50% extinction of deep-sea benthic foraminifers, and rapid perturbation to the global geochemical carbon cycle took place across the Paleocene/Eocene (P/E) boundary (e.g., Kennett and Stott, 1991; Zachos et al., 1993; Koch et al., 1992). A growing body of evidence attributes these events to the massive release and oxidation of methane from the marine gas hydrate reservoir (e.g., Dickens et al., 1997; Katz et al., 1999). High-resolution stable-isotope records (Bains et al., 1999) and orbitally tuned chronologies from sites in the Atlantic and off Antarctica (Norris and Röhl, 1999) suggest that carbon release occurred extremely rapidly (within one precession cycle). Thus, the P/E boundary event may represent the best example in the geologic record of the response of Earth's ocean-atmosphere climate system to greenhouse warming on a timescale approaching that of the ongoing global anthropogenic experiment. Recently, elevated barium accumulation rates have been reported across the P/E boundary in various deep-sea sites. These data have been interpreted in terms of enhanced deposition of organic matter in deep-sea sediments that may have acted as a negative feedback on atmospheric CO_2 levels and global temperatures to return Earth to average late Paleocene conditions (Bains et al., 2000). Alternatively, this signal may reflect increased ocean barite saturation levels possibly driven by the injection of barium into the global ocean from the marine gas hydrate reservoir (Dickens et al., 2001).

Whereas recently developed data sets lend considerable support to the methane hydrate hypothesis, considerable uncertainty remains about the mechanism and location of carbon release, the response of the calcite compensation depth (CCD), and biotic overturn. Furthermore, the recent discovery of P/E-boundary–like geochemical signals in the Mesozoic (e.g., Opdyke et al., 1999; Hesselbo et al., 2000; Weissert, 2000) raises the distinct possibility that further "hyperthermals" might have existed in Paleogene time (Thomas and Zachos, 1999). Leg 199 presents a major opportunity to help improve our understanding of the climatic chain of events during the Paleogene. Results from the leg should prove particularly useful given the volumetric significance of the Pacific Ocean to geochemical mass-balance simulations (e.g., Dickens et al., 1997) and the current paucity of P/E boundary records from the basin.

Eocene–Oligocene Transition

The Eocene–Oligocene transition represents an important point in the shift from the greenhouse world of the Cretaceous and early Paleogene into the late Paleogene–Neogene icehouse. Attempts to estimate global ice volumes from deep-sea benthic $\delta^{18}O$ records have prompted very different conclusions as to the timing of the onset of the accumulation of continental-scale ice sheets. These range from the Early Cretaceous (Matthews and Poore, 1980) to the middle Miocene (Shackleton and Kennett, 1975). However, recent improvements in the stratigraphic resolution of the $\delta^{18}O$ record have led to suggestions that either the late middle Eocene (~43 Ma) or the earliest Oligocene (~34 Ma) are better estimates of the timing of the initiation of greenhouse to icehouse transition (Shackleton, 1986; Miller et al., 1987, 1991; Zachos et al., 1992). Supporting evidence for this interpretation comes from oceanic records of ice-rafted debris, weathered clay mineral compositions, microfossil assemblages, and sequence stratigraphic analyses (Kennett and Barker, 1990; Browning et al., 1996). Yet, the rarity of complete deep-sea sections across these intervals has limited our understanding of the dynamics of this important step leading to the modern icehouse world.

The Eocene–Oligocene transition is marked by a large rapid increase in the benthic foraminiferal calcite $\delta^{18}O$ record in earliest Oligocene time (Oi-1; Fig. F5). This excursion was first ascribed to a 5°C temperature drop associated with the onset of thermohaline circulation, but more recently Oi-1 has been associated with the onset of continental ice accumulation on Antarctica. Such confusion reflects the long-standing difficulty of separating the effects of temperature and ice on benthic $\delta^{18}O$. Recent application of an independent paleothermometry technique, based on Mg/Ca in benthic foraminifers, shows no significant change corresponding to "Oi-1" (Lear et al., 2000). This result suggests that all of the $\delta^{18}O$ increase associated with Oi-1 can be ascribed to ice growth with no concomitant decrease in polar temperatures. Apparently, according to these data, the trigger for continental glaciation lay in the hydrological cycle rather than the carbon cycle. Specifically, it has been proposed that the opening of the Australian-Antarctic seaway in earliest Oligocene time might have enhanced the supply of moisture as snow to the Antarctica interior (Lear et al., 2000). Support for this suggestion exists from both ocean drilling and numerical modeling experiments (Bartek et al., 1992; Hine et al., 1999). On the other hand, paleoproductivity studies suggest that the near-contemporaneous increase in seawater $\delta^{13}C$ was driven by increased rates of C_{org} burial in marine sediments, and this factor may be implicated in global cooling and ice sheet growth (Diester-Hass and Zahn, 2001). Either way, long-standing global lithologic compilations indicate a pronounced deepening of the CCD associated with the Eocene–Oligocene transition (van Andel et al., 1975) Unfortunately, our most complete records of the Eocene/Oligocene (E/O) boundary come from two midlatitude sites (Deep Sea Drilling Project [DSDP] Site 522 and ODP Site 744). Leg 199 offers an excellent opportunity to generate low-latitude records of the Eocene–Oligocene transition and thereby fully evaluate the competing roles played by global cooling and ice growth in the transition from the Cretaceous greenhouse into the Neogene icehouse.

F5. Compilation of benthic oxygen isotope data for the Cenozoic, p. 56.

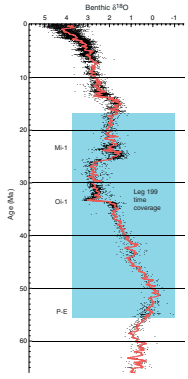

Late Eocene Impact Events

Widespread evidence now exists to support the occurrence of at least two large closely spaced extraterrestrial impact events on Earth during early/late Eocene time. In particular, two large craters (order ~100 km diameter; Chesapeake Bay, North America, and Popigai, northern Siberia) have been proposed to explain impact-ejecta strewn fields that are documented in deep-sea sediments from around the world (e.g., Koeberl et al., 1996; Bottomley et al., 1997). Proxy records for fine-grained extraterrestrial dust (^{3}He measurements) in correlative marine carbonate strata have been interpreted as evidence for a comet shower triggered by an impulsive perturbation of the Oort Cloud (Farley et al., 1998). Intriguingly, unlike the more famous and pronounced precursor extraterrestrial impact event at Cretaceous/Tertiary (K/T) boundary time, biostratigraphic studies indicate that the late Eocene impact horizons do not correspond to major extinctions among marine organisms. Only four or five radiolarian species seem to disappear from the record accompanied by modest compositional changes in planktonic foraminifers and organic walled dinoflagellate cysts (Sanfilippo et al., 1985; Keller, 1986; Brinkhuis and Biffi, 1993). On the other hand, although little evidence exists in the literature for climate change across the K/T boundary, recent work has suggested that the late Eocene impact event was associated with a short-term (~100 k.y.), albeit modest (maximum 2°C), cooling event at high latitude (Vonhof et al., 2000). Leg 199 presents an ideal opportunity to study the climatic and biotic effects of impacts that were too small to precipitate global mass extinctions but were apparently large enough to have engendered regional changes in climate.

Oligocene

In many ways the Oligocene (~33.7–23.8 Ma) represents something of a "neglected middle child" of Cenozoic paleoceanography—caught between the early Paleogene greenhouse and the well-developed Neogene icehouse. This situation is at least partly attributable to the perception that the Oligocene marks a prolonged interval of relative stasis in paleoclimate and biotic turnover reflected in deep-sea micropaleontological communities by conservative body plans, confusing taxonomies, and low biostratigraphic resolution. However, in some respects the Oligocene represents the most interesting piece of the Cenozoic paleoceanographic puzzle because it offers an opportunity to unravel the processes that lie behind the transition from a world free of large-scale continental icecaps and rapid eustatic sea level oscillations to one dominated by these climatic changes. To a large extent, recent progress in our understanding of Oligocene paleoclimates has been driven by seismic stratigraphy and scientific drilling in continental margin sequences (e.g., Browning et al., 1996; Miller et al., 1996; Pekar et al., 2000). In contrast, modern benthic stable-isotope compilations (Fig. **F5**) show that our paleoclimate records for the deep oceans through the Oligocene rely heavily on old DSDP sites largely from the Atlantic Ocean (Miller et al., 1987, 1988, 1990, 1991, 1993). Leg 199 offers an excellent opportunity to generate low-latitude deep-sea records throughout the Oligocene in order to test models developed from continental margin sequences for the pattern and timing of changes in global temperature and continental ice volume.

Previous Drilling

Nearly 30 yr ago, DSDP rotary drilling and coring of the central Pacific equatorial mound of sediments (e.g., DSDP Legs 5, 8, 9, and 16) (Fig. F1) established the general pattern of equatorial sediment accumulation and plate migration through the Neogene and late Paleogene (e.g., van Andel et al., 1975; Berger and Winterer, 1974; Leinen, 1979). However, the rotary coring technology available to these early legs could not provide undisturbed sections or complete recovery and was utterly defeated by middle Eocene chert layers encountered in some of the more deeply buried sections. Since these early efforts, one leg (DSDP Leg 85; Mayer et al., 1985) has revisited the region and obtained hydraulic piston core samples of Neogene sediments. However, the Paleogene sections of the Leg 85 holes were rotary cored because they were deeply buried beneath the Neogene equatorial sediment mound. Much of the Paleogene section was not recovered. For these reasons, even the broad outlines of equatorial sediment accumulation in Paleogene sediments and the link of sedimentation to early Paleogene climate remain poorly defined. The P/E boundary interval in the central tropical Pacific Ocean has not been sampled, primarily because the DSDP sites were mostly placed on crust younger than the boundary. DSDP Site 163 (Fig. F1), on early Campanian-age crust, is the only drill site in the central tropical Pacific that has drilled the interval. Unfortunately, there was poor recovery over the early Eocene caused by closely spaced cherts. The middle Eocene has been sampled at more sites. North of the Clipperton Fracture Zone, where Leg 199 sites are situated, drilling at DSDP Sites 161 and 162 recovered continuous sediment sequences, albeit with core gaps and disturbed by rotary coring, to middle Eocene basalt crust. Sediments from Sites 40 and 41, between the Clarion and Molokai Fracture Zones, were upper to middle Eocene radiolarian oozes beneath a 10-m-thick layer of red clay.

Leg 199 Objectives

Leg 199 drilling was designed to accomplish the following scientific objectives:

1. To define sedimentation, paleoproductivity, circulation, and wind patterns in the Eocene equatorial Pacific;
2. To study the Paleocene–Eocene and Eocene–Oligocene transitions in the equatorial Pacific as well as other boundaries mentioned above; and
3. To obtain complete, continuous Oligocene and lower Miocene paleoceanographic records to study the effects of glaciation in Antarctica upon equatorial Pacific circulation.

In addition, the following important but more general objectives shaped the Leg 199 drilling plan:

1. To collect continuous sequences of Paleogene biogenic sediments, thereby improving Paleogene biostratigraphy, tie this to magnetostratigraphy, and generate high-resolution paleoceanographic records from the Paleogene central tropical Pacific Ocean;

2. To place new constraints on the late Paleocene and early Eocene equatorial position using paleomagnetic and micropaleontologic indicators;
3. To link seismic stratigraphy from the site survey to sediment chronostratigraphy in order to extend the Neogene equatorial Pacific seismic stratigraphy (Mayer et al., 1985, 1986; Bloomer et al., 1995) back in time;
4. To document the transition between American and Asian dust sources in order to understand the primary structure of the Paleogene wind field;
5. To provide new constraints on the early Paleogene mass balance of carbonate and opal (SiO_2) burial and to track the Eocene movement of the CCD in detail;
6. To generate primary geochemical information needed to understand the widespread formation of Eocene cherts; and
7. To collect basal hydrothermal sediment sections for study of hydrothermal activity in the early Paleogene.

RESULTS

Major Lithologies of the Paleogene Equatorial Pacific

The sediments drilled during the Paleogene equatorial transect fall into the following five broad litho-chronostratigraphic units (Fig. F6): (1) a surficial clay unit, sometimes containing a basal radiolarian ooze with a basal age ranging from the middle Miocene in the south of the transect (Site 1218) to the early–middle Eocene in the north (e.g., Sites 1215 and 1216); (2) a nannofossil ooze/chalk unit whose base is at the E/O boundary and whose top is of early Miocene age in the south (Sites 1218 and 1219) and Oligocene age in the central part of the transect (Sites 1217, 1220, 1221, and 1222); Oligocene–Miocene carbonates are nonexistent in the north (Sites 1215 and 1216); (3) a middle–upper Eocene radiolarian ooze and radiolarian clay that is present at all sites except those in the north (Site 1215 and 1216); (4) a lower middle–lower Eocene unit composed of cherts, clays, and radiolarian ooze that is present in varying thicknesses at all Leg 199 sites along the 56-Ma transect except one in the extreme north (Site 1215); and (5) a lower Eocene–upper Paleocene nannofossil ooze or chalk resting upon basalt basement that is recovered at all sites (except Sites 1216 and 1222 where cherts overlie basement and the relevant stratigraphic interval was not drilled).

F6. Lithologic summary, p. 57.

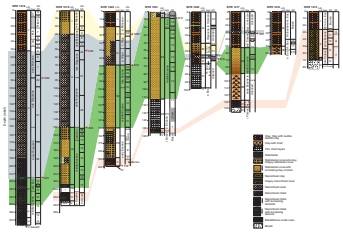

Surficial Clay and Radiolarian Ooze

The upper clay unit is composed of wind-blown dust, clays and radiolarians eroded and reworked from older sediment outcrops, authigenic minerals, and (in sites marginal to the modern equatorial region) freshly deposited radiolarians.

The clay mineral composition of eolian dust transported to Leg 199 sites may provide a way to track the latitudinal position of the ITCZ (Fig. F7). Enhanced precipitation in the ITCZ helps to "wash out" dust particles from the atmosphere, forming an effective barrier to interhemispheric dust transport. In other words, dust generated in the Northern Hemisphere is deposited only in latitudes north of the ITCZ. Today, Asian dust (rich in quartz and illite clays) dominates the compo-

F7. LAS determined concentrations for smectite and illite vs. depth, p. 58.

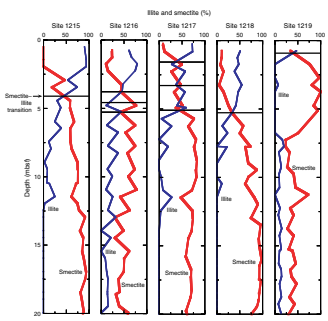

sition of dust deposited in the Pacific north of the ITCZ. In contrast, just south of the ITCZ, a clay mineralogy dominated by smectite is transported via the trade winds from Central and South American source regions. During Leg 199, we used light absorption spectroscopy (LAS) (see **Vanden Berg and Jarrard,** this volume) to produce shipboard estimates of clay mineralogy. In Figure **F7,** plots of LAS-determined mineralogical change downcore are shown vs. depth for Sites 1215–1219. Using paleoposition information, one can then identify the change in ITCZ through time by the change from a smectite-rich to illite-rich clay suite (Fig. **F8**).

Radiolarian ooze or clayey radiolarian ooze are important sediment lithologies in the basal part of the surficial clay unit in Leg 199 sites drilled near the modern equator. These oozes are found at Sites 1219–1221 (Fig. **F6**). In each case, the site occupied an off-equatorial position at the time that the radiolarian ooze was being deposited in the range of 3°–6° north of the paleoequator. Thus, in the Neogene and latest Oligocene, radiolarian ooze is deposited on the fringes of the equatorial upwelling zone. The zone of radiolarian ooze deposition is bound on the south by the appearance of foraminifers and disappears to the north as primary productivity decreases.

F8. Smectite–illite transition plotted as a function of age and latitude, p. 59.

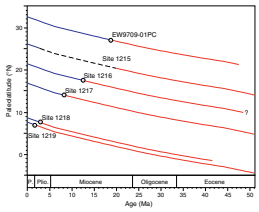

Oligocene–Lower Miocene Nannofossil Ooze/Chalk

The second broad litho-chronostratigraphic unit along the Leg 199 transect is the nannofossil ooze that first appears at the base of the Oligocene. The clay or radiolarian ooze to carbonate transition is an outstanding marker for the E/O boundary because it is very abrupt (see **"Eocene–Oligocene Transition,"** p. 20). The unit has cyclic variations of carbonate content related to orbitally driven changes in insolation. This cyclic variability will allow us to construct an orbitally tuned Oligocene age model of the sediments and to calibrate ages for magnetostratigraphy and biostratigraphy (see **"Stratigraphic Intercalibrations,"** p. 17).

The nannofossil ooze/chalk unit is thickest at sites near the Oligocene equatorial region and thins to the north (Fig. **F6**). Nevertheless, traces of the lower Oligocene carbonate can be found as far north as Site 1217 (16°52′N). At the beginning of the Oligocene, Site 1217 was located ~9° north of the equator at a water depth of 4400 m.

The age of the uppermost nannofossil ooze/chalks depends on the paleoposition and water depth of each drill site. In the south (Sites 1218 and 1219), the uppermost nannofossil ooze unit has an age near the late Miocene. Traversing north, the uppermost nannofossil ooze at Site 1220 (10°11′N) is late Oligocene in age, whereas at Sites 1217 (16°52′N), 1221 (12°02′N), and 1222 (13°49′N), the uppermost nannofossil oozes are early Oligocene in age.

Late–Middle Eocene Radiolarian Ooze

The third broad litho-chronostratigraphic unit along the Leg 199 transect consists of radiolarian ooze, clayey radiolarian ooze, and radiolarian clays (Fig. **F6**). Clay content tends to be higher at the top and bottom of the unit. The radiolarian oozes are characteristic of the Eocene section and are the most enigmatic facies drilled during Leg 199, from a modern perspective, because of the lack of a true modern analog.

In the southern sites of the Leg 199 transect (Site 1219) and in shallower drill sites (Site 1218 and DSDP Site 162), carbonate can be found at low concentrations in the upper Eocene and at higher levels in the middle Eocene, especially in Chron C18 (~39–41 Ma). For the rest of the transect, calcium carbonate ($CaCO_3$) is absent from this unit even in sites located at the contemporaneous paleoequator. The latitudinal width of the late–middle Eocene zone of radiolarian deposition varies through time. The middle Eocene, between ~40 and 45 Ma, represents the greatest latitudinal expansion—radiolarian oozes were found from the equator to a paleolatitude between 10° and 11°N (between DSDP Site 40 and Site 1216). In contrast, radiolarian deposition is confined to within a few degrees of the equator in the uppermost Eocene. Along the 56-Ma transect, radiolarian oozes are deposited only to the south of Site 1221, located at a paleolatitude of ~3°N. The upper Eocene–lower Oligocene sequence is condensed at Site 1221, and Sites 1222 and 162 both have a hiatus just below the Oligocene.

One of the striking features of a unit with such high biogenic silica content is the relative absence of diatoms. Only one major interval in the Eocene radiolarian ooze contains a relatively high diatom content (>10% diatoms in smear slides; Fig. F9). High numbers of diatoms appear in Chron C18 (radiolarian Zone RP15; 39–39.6 Ma) and are associated with the appearance of carbonates in the same sediment interval at Sites 1218 and 1219.

F9. Lithologic columns showing where diatoms are common to abundant, Sites 1218, 1219, 1220 and 1221, p. 60.

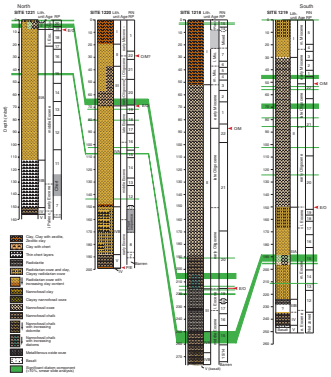

Lower Middle–Lower Eocene Cherts, Clay, and Radiolarian Ooze

The fourth broad litho-chronostratigraphic unit along the Leg 199 transect consists of cherts, clays, and radiolarian oozes (Fig. F6). This unit proved predictably troublesome to recover. Leg 199 drilling results indicate that cherts are present at the boundary between the lower and middle Eocene throughout the transect with the exception of Site 1215 in the extreme north. A younger cherty chalk interval is present at Site 1218 near the middle/upper Eocene boundary, but this interval was continuously cored and recovered with the extended core barrel (XCB) (Fig. F10).

F10. Late Eocene "pentachert" interval, p. 61.

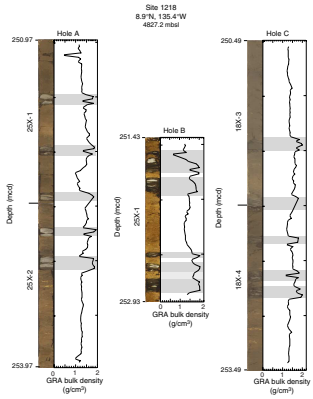

The lower–middle Eocene chert interval is relatively thin at Site 1219 in the south (~8 m thick; 7°48′N) but thickens to the north. At Site 1220 (10°11′N), the unit, including recovered cores of early Eocene radiolarian ooze, spanned 40 m. Poorly recovered cherty intervals span 30–40 m at Sites 1217 (16°52′N), 1221 (12°02′N), and 1222 (13°49′N). The unit is chronologically extensive. It typically first appears in radiolarian Zone RP11–12 (~45–49 Ma) and continues into the lower chalk unit around the top of radiolarian Zone RP7 (~53 Ma). The relationship between these cherts and the lower nannofossil chalk is not yet clear. At Site 1219, a transition from zeolitic clay to nannofossil chalk was recovered, suggesting that the base of the unit may be marked by a gradational transition from clay to $CaCO_3$. However, the chert recovered was associated with most of the basal nannofossil chalk recovered on the leg; this lower unit is not free from chertification.

Lower Eocene–Upper Paleocene Nannofossil Ooze or Chalk

The basal litho-chronostratigraphic unit along the Leg 199 transect consists of nannofossil ooze or chalk of early Eocene–upper Paleocene age overlying basement basalt. Despite high numbers in the rest of the

Eocene, radiolarians are rare to absent in the basal carbonates. This unit is present at all sites except perhaps Sites 1216 (where the relevant stratigraphic interval was not drilled) and 1222, (where only chert was recovered in the one hole drilled to basement). In three of the seven sites targeted to recover the P/E boundary (Sites 1215, 1220, and 1221), this objective was fulfilled (see **"P/E Boundary,"** p. 24). Where present, the basal carbonate unit is most lithified in the south, where overburden is greatest (~250 m burial depth; Sites 1218 and 1219). In contrast, at Site 1215, where the burial depth is significantly shallower (~25 m), we recovered a nannofossil ooze. At three of the sites containing basal chalks (Sites 1217, 1218, and 1220), the sediments are partially to extensively dolomitized. The origin of this dolomite is unclear, but dolomitization appears to be related to proximity to basement rather than location along the latitudinal transect.

Paleogene CCD

One of the most striking features of the Paleogene equatorial Pacific sediments is the rapid appearance and disappearance of $CaCO_3$ through the stratigraphic record. Leg 199 drilling has significantly increased stratigraphic control for many of the Paleogene and early Neogene carbonate–noncarbonate transitions.

Van Andel et al. (1975) compiled DSDP data from all the drill sites in the region and used subsidence curves of ocean crust to develop the Cenozoic history of $CaCO_3$ deposition. This compilation shows that the Eocene was marked by a shallow CCD or level in the water column where the pelagic rain rate of biogenic carbonate is equal to the rate of depth-dependent dissolution. Specifically, the Eocene CCD in the equatorial Pacific is estimated to have been ~3400 m shoaling to ~3200 m beyond 4° from the equator to either the north or south. Furthermore, one of the most prominent changes in the CCD through time captured in this early compilation was a pronounced deepening (by ~1600 m in the equatorial region) associated with the approximate transition from the Eocene to the Oligocene. Shipboard results from Leg 199 support this early interpretation of events. In fact, our shipboard data demonstrate that the correlation between the Eocene–Oligocene transition and the CCD deepening is strikingly precise and consistent across wide tracts of the tropical Pacific. These findings, raise the intriguing possibility that this pronounced deepening of the CCD is in some way related to the first widely accepted sustained glaciation in Antarctica (Oi-1; Fig. **F5**). The nature of the relationship between these two significant paleoceanographic signals will be an important component of shore-based Leg 199 research. In addition, our shipboard data also demonstrate that the transition from silica-rich/carbonate-poor Eocene to silica-poor/carbonate-rich Oligocene deep-sea sediments is remarkably rapid. The transition from carbonate-free to carbonate-bearing sediments is sharp (typically occurring over a 10- to 20-cm interval [Fig. **F11**]), implying that it took only a few tens of thousands of years to introduce the changes in ocean chemistry that depressed the CCD to >1 km below its Eocene depth.

Leg 199 sediments define other major CCD changes in the Eocene that will be better studied after the cruise. The Paleocene–lower Eocene basal chalks define a relatively shallow CCD in the beginning of the interval drilled during Leg 199 (Fig. **F12**). The transition from chalk to clay and radiolarian ooze occurs when near-equatorial sites passed through a water depth of only ~3200–3300 m (Sites 1219–1221),

F11. Cores across the E/O boundary, Site 1218, p. 62.

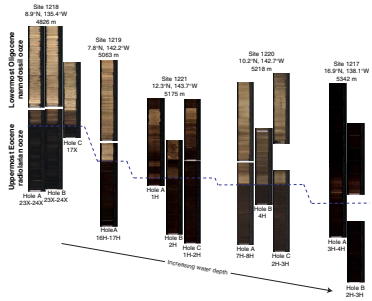

F12. Subsidence history of non-equatorial and equatorial sites, Sites 1215, 1217, and 1221, p. 63.

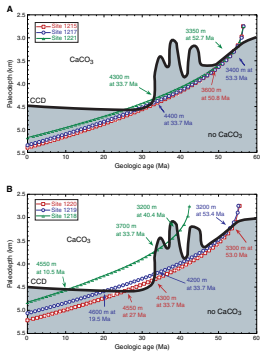

whereas the off-equator sites record a shift from carbonate to clay when they passed below 3400–3600 meters below sea level (mbsl) (Sites 1215 and 1217). In contrast, the Oligocene and Neogene CCD is ~4500–4600 m (Fig. F12). The difference in early Eocene CCD between equatorial and northern sites is greater than the errors associated with the estimation and is the reverse of the Neogene trend. Typically, in the Neogene, the CCD is deeper beneath the equatorial region because of higher carbonate production in the equatorial region relative to periequatorial regions, but this situation seems to have been reversed in the early Eocene.

Although carbonate disappears from the equatorial Pacific in the lower Eocene, $CaCO_3$ is not absent from the Eocene record. A prominent $CaCO_3$ event appears in Chron C18r at ~40–41 Ma (defined by Site 1219 in the south) that can also be found at DSDP Site 162 (van Andel et. al, 1973) (Fig. F12). Smaller carbonate events occur in Chron C20n (~43 Ma) and near the base of C17n (~38 Ma) at Site 1219. The younger event can also be found at Site 1218. In contrast, none of these carbonate events can be found further north, nearer the middle Eocene paleoequator (Site 1220). In fact, there is no $CaCO_3$ in the middle and late Eocene section at Sites 1220, 1221, or 1222.

The transition from chalks to radiolarite at ~40 Ma in Site 1218 appears as abrupt as the transition from radiolarian clay to nannofossil oozes at the E/O boundary. The rapid transitions of sediment type in either direction suggest that there is a strong climate switch at work. Sediments with poor carbonate preservation have also been identified during each of the Oligocene intervals that correlate to warm intervals between the "Oi" glacial advances of Miller et al. (1991). Thus, the Leg 199 shipboard scientists have developed a working hypothesis that carbonate deposition in the tropical Pacific is in some way associated with continental glaciations, whereas tropical Pacific radiolarian oozes are associated with warm global climates. If this hypothesis is substantiated, one implication would be that the transition from cold to warm climates can be as abrupt as the transition from warm to cold climates.

Equatorial Position

Drill sites move with their respective plates and must be backtracked in space as well as depth. Van Andel et al. (1975) recognized the paramount importance of backtracking tropical Pacific drill sites with respect to the motion of the Pacific plate because the equatorial upwelling system leaves a strong imprint on the sediment column when the site passes underneath the equator. This generalization holds for the Oligocene and Neogene. We can recognize the passage of Site 1219 under the equator in the Oligocene by the sedimentary changes, but we find confusing sedimentary signals in the earlier record.

We expected that sedimentation patterns might be different in the Eocene; therefore, we made it a primary leg objective to obtain independent evidence for the position of the paleoequator through the Paleogene. This objective is especially important because the backtrack paths we have used to find paleopositions of Leg 199 sites assume a fixed Hawaiian hotspot, and there is good evidence that the Hawaiian hotspot moved with respect to the Pacific plate prior to 42 Ma (Tarduno, Duncan, Scholl, et al., in press). In addition, small errors in the plate tectonic model, when propogated over long periods of time, may

lead to relatively large errors in a drill site position over long intervals of time.

Shipboard whole-core paleomagnetic analysis has been sufficient to make a preliminary definition of the position of the paleoequator and the change in paleolatitude of Leg 199 drill sites in the Oligocene and in the late middle Miocene (Figs. F13, F14). These data will be refined postcruise with discrete sample analyses. They suggest that the fixed hotspot backtrack of paleopositions is sufficiently accurate to estimate paleopositions back to the middle Eocene. Paleomagnetic analysis of older sediments should yield further evidence for equatorial positions in the early Eocene.

Fluxes and Paleoproductivity

Another primary objective of Leg 199 science is to assess the level of productivity over the Paleogene by using biogenic MARs in concert with other geochemical and micropaleontological data. With this goal in mind we designed a shipboard program to monitor the composition of pore waters in the sediments and measure the bulk chemical composition of recovered sediments.

Organic Carbon Diagenesis and Interstitial Waters

In the context of productivity and biogenic sediment flux considerations, it is notable that none of the Leg 199 sediments contained significant organic carbon (C_{org}). As measured on board the ship, C_{org} levels in Leg 199 sediments were consistently low (~0.1–0.2 wt%), essentially the detection limit for the analysis at sea. Chemical gradients in Leg 199 interstitial waters primarily reflect the relatively limited organic matter diagenesis as well as dissolution of biogenic silica and varying amounts of diffusive influence of reactions in the underlying basalt (Fig. F15). Sulfate concentrations are high (>25 mM) throughout the transect, indicating little oxidation of labile organic matter (Fig. F15). These high sulfate levels mean that barite in the sediments will be well preserved and as a result will potentially be useful for paleoproductivity studies. This is especially important because it appears that any organic matter that may have been delivered to these sites has long since been degraded, if in fact it ever was deposited at all. Ammonium, another by-product of organic matter degradation, is only present in extremely low levels at all sites.

Dissolved silica concentrations generally increase with depth at all sites (Fig. F15). These high interstitial water silica values are consistent with the presence and dissolution of biogenic silica throughout the sediment. Strontium concentrations are generally constant at about seawater value (87 mM) for several of the sites containing little carbonate (Sites 1215–1217, 1220, and 1221), but strontium increases with depth at Sites 1218 and 1219 (Fig. F15) reflecting the presence and dissolution of biogenic carbonate.

Calcium, magnesium, and potassium concentrations at most Leg 199 sites show little evidence for exchange with basalt and subsequent diffusion (Fig. F15). However, the increase in calcium concentration and decrease with depth in magnesium, potassium, and lithium concentrations at Site 1219 are significantly greater than that seen at other Leg 199 sites. These patterns are consistent with alteration of basement rocks and with the recovery of highly altered basalt at Site 1219, unlike the other sites in the Leg 199 transect. The higher levels of lithium at

F13. Relative position of the paleoequator for the middle Eocene and late Oligocene, p. 64.

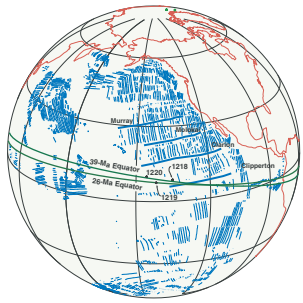

F14. Inferred paleolatitudes, Sites 1218, 1219, and 1220, p. 65.

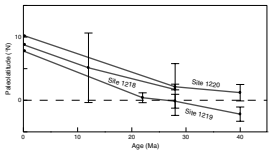

F15. Interstitial water profiles, p. 66.

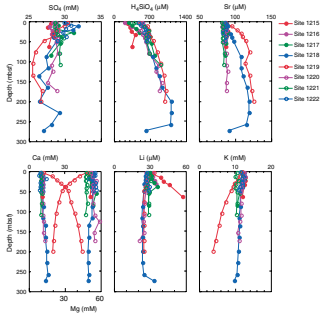

Site 1215 relative to other Leg 199 sites could be linked to the volcanic ash layers recovered at that site.

Bulk-Sediment Analyses

The Leg 199 shipboard geochemical program differed from typical ODP protocol by incorporating relatively detailed downcore profiles of C_{org} composition. The resulting profiles primarily reflect the shifts in lithology between sediments dominated by silica to those dominated by carbonate (Fig. F16). When these data are combined with sedimentation rates (Fig. F17) and bulk density data, it is possible to examine burial fluxes through the Paleogene. MAR calculations are a means to distinguish rates of elemental deposition even under conditions of significant dilution by other sedimentary phases. This is best shown by comparing Si weight percent profiles at Sites 1218 and 1219 to the Si MAR profiles (Fig. F16). Low Si contents between 20 and 30 Ma are primarily caused by dilution of Si by $CaCO_3$. The MAR profile indicates that Si fluxes decreased much less dramatically than percentage data seems to indicate.

Changes in Si MARs should reflect biogenic SiO_2 production because the detrital Si contribution by aluminosilicates is relatively low and constant. Al analyses reflect the detrital aluminosilicate contribution (Fig. F18) and are relatively low with respect to the high Si MAR in the Eocene and Oligocene. A rough indicator of baseline aluminosilicate contribution to Si MARs is given by the Si MAR in the period younger than 15 Ma when clays were the principal sediment accumulating at all Leg 199 drill sites. By comparison to this baseline (15 Ma to present value), it is clear that biogenic Si deposition has decreased since a peak in the middle Eocene between ~38 and 45 Ma.

Virtually all calcium MAR results from the deposition of $CaCO_3$ (Fig. F16). High Ca contents and high Ca MARs occur in the high-$CaCO_3$ intervals of the Oligocene and lower Miocene. Smaller events can be seen in the middle Eocene, particularly ~40 Ma. The lower Eocene Ca MAR is approximately one-half to two-thirds of the high rates of deposition in the Oligocene. Phosphorus burial has a primary source term driven by export productivity (Fig. F18). The phosphorus MAR peaks in the early Oligocene and also in the period ~40–45 Ma in the middle Eocene, which suggests that this part of the middle Eocene had elevated paleoproductivity relative to the late Eocene.

Ratios to an element assumed to be constantly delivered (or nearly so) is another quick way to assess changes in deposition. Figure F19 illustrates this approach by showing ratios of Si, Ba, and Al to Ti. We assume that titanium is bound to aluminosilicates and has relatively constant deposition. The plots of Si/Ti and Ba/Ti suggest that there was relatively high burial of Ba and Si during the Eocene. The relatively constant Al/Ti is an indication that clay minerals are a primary contributor of the Ti flux.

Latitudinal MAR Transects

Observing MARs in time slices along latitudinal transects is another way to assess how sedimentation in the Eocene differs from that in the Oligocene and Neogene. We have chosen three time slices for shipboard comparison: (1) an early Eocene time slice (50–55 Ma), when all parts of the 56-Ma transect were above the CCD; (2) a middle Eocene time slice (38–45 Ma), during the period of highest radiolarian ooze deposition;

F16. Analyses of sedimentary Si and Ca weight percent and MARs, p. 67.

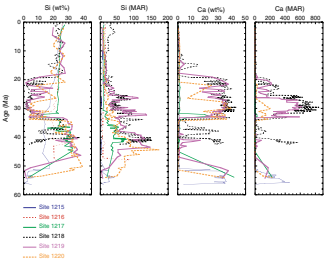

F17. Summary of sedimentation rates derived from age-depth models, p. 68.

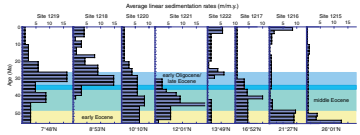

F18. Analyses of sedimentary Al and P weight percent and MARs, p. 69.

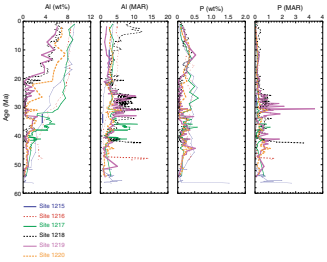

F19. Si/Ti, Ba/Ti, and Al/Ti of Leg 199 sediments, p. 70.

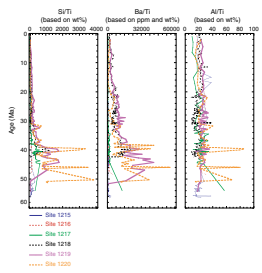

and (3) an Oligocene time slice (25–34 Ma), when high $CaCO_3$ sedimentation had been established.

The Si MAR is highest in the middle Eocene (Fig. **F20**), but the latitudinal gradient of the Si MAR does not peak in the equatorial region as it does in the Neogene. Instead, the Si MAR increases southward. A high Si MAR in the middle Eocene may be due, in part, to the fact that Eocene radiolarians are heavily silicified (Moore, 1969). An individual middle Eocene radiolarian test has an average weight about four or five times that of an average Pleistocene radiolarian test and is much less susceptible to dissolution at the seafloor. The high Si MAR may represent low dissolution prior to burial as well as relatively high Si flux to the sediments.

In the early Eocene, we observe low Si MARs at all latitudes—sufficiently low that a large contribution of Si to sediments must be from clay minerals. Only the Oligocene has a MAR pattern that resembles that of the Neogene with the highest MAR peaking in the equatorial region. The flux of Si at the Oligocene equator is roughly equivalent to the modern MAR at 110°W (Lyle, 1992). Lyle (1992) expressed the modern flux as SiO_2 rather than biogenic Si. The SiO_2 fluxes in the Holocene equatorial region are equivalent, however, to ~50 mg/cm²/k.y. biogenic Si.

Ca MARs in the early Eocene time slice (Fig. **F21**) are actually equivalent to or higher than modern fluxes of Ca from $CaCO_3$ along a 110°W transect, except in the equatorial region (Lyle, 1992). In the early Eocene, however, there is no well-developed equatorial maximum in $CaCO_3$ deposition. In fact, $CaCO_3$ burial in the equatorial region may be only half as much as burial in the subtropical flank of the transect. In the middle Eocene, essentially no $CaCO_3$ is deposited anywhere except the southernmost part of the transect, which reflects the shallow middle Eocene CCD and the lack of $CaCO_3$ deposition in the equatorial region. Only the Oligocene latitudinal transect resembles a Neogene equatorial profile. $CaCO_3$ deposition at the equator is as high as Holocene deposition.

It is clear from our shipboard examination that sedimentation patterns of the Eocene are significantly different from modern equatorial sedimentation. Postcruise analyses utilizing other paleoproductivity indicators will be needed to understand the development of primary and export productivity through the Eocene. Nevertheless, there are few indicators that productivity was high in the Eocene central tropical Pacific Ocean.

One important problem to be approached by postcruise studies is whether C_{org} levels are low in Eocene sediments because of a long period of exposure to oxidants diffusing into the sediment from seawater or whether C_{org} levels were never high in the first place. Shipboard paleomagnetic studies provide circumstantial evidence for the riddle of low C_{org}. Preservation of the paleomagnetic record in sediments strongly depends on diagenesis. For example, Fe^{3+}-Fe^{2+} reduction dissolves magnetite, leading to a decrease of both magnetic susceptibility and magnetic intensity of the sediments. Along the Leg 138 transect, the Neogene equivalent of the Leg 199 transect, sites at the equator or under regions of relatively high C_{org} deposition have magnetostratigraphic records limited to the upper sediments (Mayer, Pisias, Janecek, et al., 1992), whereas sites under regions of low primary productivity have more extended magnetostratigraphic records. The long magnetostratigraphic records obtained on the Leg 199 transect, along with the

F20. Latitudinal transect of Si MARs for the early Oligocene, middle Eocene, and early Eocene, p. 71.

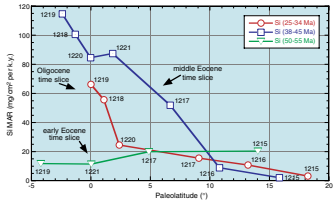

F21. Latitudinal transect of Ca MARs for the early Oligocene, middle Eocene, and early Eocene, p. 72.

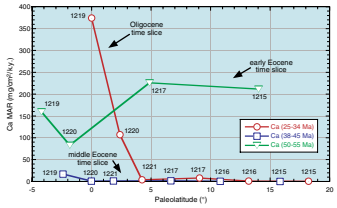

absence of a systematic decrease in magnetic intensity and susceptibility downcore, suggest that there never were high levels of C_{org} deposition in the Eocene.

Stratigraphic Intercalibrations

A major success of Leg 199 is the recovery of continuous sedimentary records with uninterrupted sets of distinct Cenozoic geomagnetic polarity chrons from the paleoequatorial Pacific Ocean (Fig. F22). The sedimentation rates of the recovered and complete composite sections provide acceptable resolution for meaningful magnetobiochronologic calibrations for the early middle Eocene–early Miocene time interval. Biogenic silica is ubiquitously present and will permit, for the first time, the establishment of a precise Cenozoic biochronology of radiolarians, diatoms, and silicoflagellates from a tropical Pacific Ocean setting.

Biogenic carbonate is variably preserved and exhibits moderate to complete dissolution. The upper Paleocene–lower Eocene and Oligocene–lower Miocene intervals have the best preservation, which offers huge potential for establishing a tropical Pacific Ocean biochronology of calcareous nannofossils and planktonic foraminifers tied to magnetostratigraphy. Nannofossils can also be calibrated through much of the Eocene. As most existing age estimates for these groups have been derived from the Atlantic Ocean region, the establishment of an accurate biochronology based on Leg 199 sediments will permit assessments of the degree of interbasin synchrony among the calcareous plankton.

It follows that the sediments recovered during Leg 199 from the paleoequatorial Pacific Ocean will be an exceptionally valuable reference material for years to come for paleoceanography as well as studies of the evolution, biochronology, and intergroup and interbasin correlations among siliceous and calcareous micro- and nannofossils.

One of the enduring legacies of Leg 199 will undoubtedly be the revision of tropical radiolarian biostratigraphy. The opportunity to tie radiolarian biostratigraphic events directly to unambiguous magnetochronology will provide some of the first direct ties between the tropical siliceous microfossil record and the absolute timescale of the Paleogene. Furthermore, the repeated recovery of lower Miocene, Oligocene, and middle and upper Eocene radiolarian-rich sediments at four sites makes it possible to check the reliability of radiolarian events.

Most radiolarian bioevents have been calibrated indirectly to the absolute timescale by correlation to calcareous nannofossil biostratigraphy. During Leg 199, radiolarian bioevents were accompanied by high-resolution magnetostratigraphy, which allows the ages of biozone boundaries to be determined directly from the Cande and Kent (1995), Hilgen (1991a, 1991b), and Shackleton et al. (1995) timescales. Figure F23 shows a comparison between the newly determined zonal boundary ages, calibrated using the reversal stratigraphy from Sites 1218 to 1220, with those estimated by Sanfilippo and Nigrini (1998; SN98). The age estimates of SN98 are based on an unpublished catalog and chart constructed from a reexamination of all Paleogene low- and middle-latitude DSDP/ODP sites from Leg 1 through 135 in which there is a recognizable radiolarian fauna. The published information was reevaluated using current, uniform species concepts and integrated, where possible, with published nannofossil and paleomagnetic data. Sanfilippo and Nigrini (1998) cautioned that their chronology of Paleogene radiolarian zonal boundary events is at best a good approximation.

F22. Synthesis of magnetic stratigraphy, p. 73.

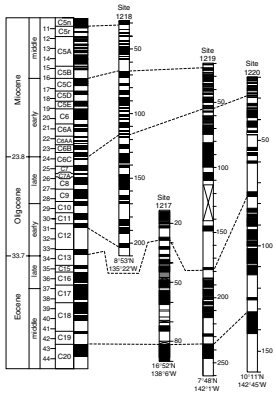

F23. Comparison of estimated ages of radiolarian zones, p. 74.

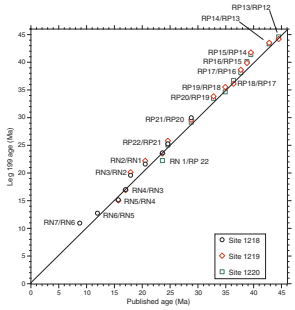

However, it is apparent that most radiolarian events are synchronous (or nearly so) among the Leg 199 sites. The Leg 199 age estimates tend to be older than the published estimates for 11 of 17 events, whereas the others agree to ~100 k.y. or less of previously published ages. Discrepancies in published vs. Leg 199 ages may reflect, for example, uncertainties in the age estimates of SN98 ("at best a good approximation"), paleobiogeographic diachroneity of the events, and difficulties in consistently recognizing evolutionary transitional events. The current radiolarian tropical biostratigraphic zonation includes numerous evolutionary transitions that tend to be subject to interpretation more than distinct first or last occurrence datums.

Postcruise refinements of the biostratigraphy of each site will improve the overall estimate of the ages for both zone marker events and recognition of new bioevents. A cycle stratigraphy based on physical properties measurements in each core will help refine the age estimates of biostratigraphic datums in magnetochrons. The ability to compare the timing of the same events at different Leg 199 sites can identify biostratigraphic datums that may be locally unreliable owing to reworking or latitudinal differences in the timing of evolutionary first or last appearances of species. The abundant, well preserved radiolarian assemblages will permit the recognition of other, easily identified datum levels with a consequent increase in the resolution of siliceous biostratigraphy.

Oligocene–Miocene Boundary Interval

In compilations of benthic foraminifer stable-isotope data, one of the most striking features of the Cenozoic record is also one of the least studied—the late Oligocene (Zachos et al., 2001a, 2001b) (Fig. F5). Much of the Cenozoic record younger than ~51 Ma is characterized by a series of increases in benthic foraminifer $\delta^{18}O$ that record the gradual global refrigeration and polar ice sheet growth that led up to the current icehouse planetary climate. The late Oligocene is a prominent exception to this descent into a glaciated world. Compiled oxygen isotope data from benthic foraminifers display an ~1.5‰ shift to more negative values that results in isotopic ratios in the uppermost Oligocene that are the same as, or even more negative than, the upper Eocene prior to the first large-scale glacial advance on Antarctica (Zachos et al., 2001a). This decrease appears to represent the largest event of its kind in the pre-Pleistocene record of the Cenozoic. At least two competing end-member hypotheses exist to explain this isotope shift: either Antarctica was rapidly deglaciated to a large extent or global deepwater temperatures warmed by 5°–7°C. To date, geochemical data are too sparse for the late Oligocene to either test the deglaciation hypothesis or evaluate the rate and timing of the change in ocean chemistry associated with this climate transition. In fact, because our current records for this time interval are derived from several different sites that lack adequate stratigraphic overlap, even the magnitude and rate of $\delta^{18}O$ decrease across this time interval are poorly constrained.

The late Oligocene deglacial/warm climate state persisted for ~1.5–2 m.y. and was terminated at the Oligocene/Miocene (O/M) boundary by an episode of polar ice buildup and/or global cooling—the Mi-1 event (Fig. F24). An astronomically tuned record in the equatorial Atlantic has been used to suggest that the Mi-1 event represents a glaciation triggered by changes in orbital insolation (e.g., Zachos et al., 2001b). The coincidence of both the $\delta^{18}O$ decrease in the late Oligocene and the Mi-

F24. Digital photograph of the Oligocene–Miocene transition and Mi-1 glacial step, Site 1218, p. 75.

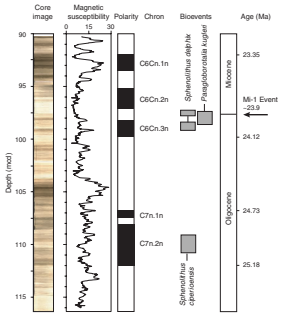

1 event with erosion surfaces and inferred sea level falls provides support for the hypotheses that both involved significant changes in polar ice sheets. However, direct confirmation from coordinated shifts in both benthic and planktonic stable-isotope records or from temperature proxies such as Mg/Ca are mostly lacking.

During Leg 199, we recovered remarkably complete sequences through the upper Oligocene and lower Miocene at Sites 1218 and 1219. These sites display unambiguous magnetostratigraphy, a distinct record of cyclic alternations in sediment physical properties that offers potential for development of an astronomically tuned timescale, and a series of biostratigraphic events in calcareous nannofossils, planktonic foraminifers, and radiolarians that afford direct correlation to previously drilled sites that lack magnetostratigraphy. Sedimentation rates through the late Oligocene and O/M boundary average ~1 cm/k.y. and will permit the development of a standard Pacific reference stable-isotope stratigraphy and Mg/Ca data set that can be correlated at orbital resolution to records throughout the tropical and subtropical oceans. The excellent timescales for Site 1218 and 1219 and potential for further refinements will help to evaluate the rates of change in ice volume and deep-ocean temperatures.

Oligocene

In the context of paleoceanographic research, perhaps the single most important scientific rationale that lies behind scientific ocean drilling is the argument that deep-sea sediments provide the most stratigraphically complete and globally representative proxy records of paleoclimate change. One of the outstanding highlights of Leg 199, in general, is our recovery of stratigraphically complete sequences (the sections drilled are virtually free of hiatuses at the biostratigraphic zone and magnetochron level) representative of substantial tracts of the central tropical Pacific Ocean. Undoubtedly the most elegant demonstration of this important leg highlight is the detailed stratigraphic correlation of Oligocene (including the Eocene–Oligocene and Oligocene–Miocene transitions) sedimentary sequences recovered at Sites 1218 and 1219 as seen in multisensor track (MST) data. These data show consistent cycles between these two sites on a submeter scale, allowing a detailed correlation between the two sites. Consistent cycles persisted over at least 22 m.y., from the early Miocene to the middle Eocene. During coring of Site 1219, it was possible to predict a priori both bio- and magnetostratigraphic datum points from those obtained at Site 1218. This important shipboard finding suggests that it is possible to identify signals that act on a larger scale in the equatorial Pacific, and a close comparison allows the identification and estimation of core gaps and short (subzonal scale) hiatuses.

The quality of the MST data obtained allowed the shipboard construction of not only spliced records from both sites but also an intersite correlation that is supported by available bio- and magnetostratigraphic datum points, which occur at both sites. MST data from Sites 1218 and 1219, illustrated in Figure F25, were adjusted to a common timescale that was obtained mostly from magnetic reversals. The two sites show very similar records down to a small scale for gamma ray attenuation (GRA) bulk density, magnetic susceptibility, and color reflectance data. Yet, the different paleodepths of both sites also lead to differences and offsets (particularly in the Eocene part of the interval) that

F25. MST, paleomagnetic, and biostratigraphic data, Sites 1218 and 1219, p. 76.

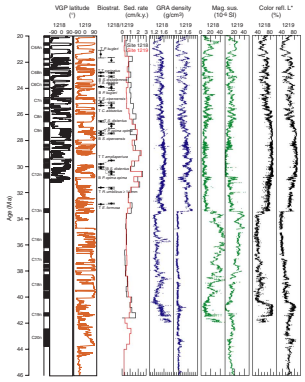

are mostly attributed to different amounts of $CaCO_3$ present in the two sites, probably because of a different paleodepth with respect to the CCD.

The magnetic reversal records from Sites 1218 and 1219 are good and allow the construction of a detailed preliminary timescale. The application of this common timescale to data from both sites allows the calculation of average linear sedimentation rates (LSRs). These are also illustrated in Figure F25, averaged over 400-k.y. segments. Sedimentation rates from both sites track each other well, and Site 1219 shows a consistently slower sedimentation rate throughout the younger two-thirds of the Oligocene. Between ~40 and 42 Ma, an increase in sedimentation rates at both Sites 1218 and 1219 corresponds to the presence of a $CaCO_3$-rich section during a time when the CCD must have fluctuated strongly.

On the shipboard timescale, the MST data show quasi-cyclic patterns where the dominant frequency appears to change throughout time partly as a function of lithology. These cycles are consistent with an orbital forcing that has been observed in the Miocene, Oligocene, and Eocene (Shackleton et al., 1999; Shackleton et al., 2000; Pälike et al., 2001). The lithologic cycles observed will allow the postcruise generation of a detailed astronomical age calibration of bio- and magnetostratigraphic datums throughout the Oligocene and early Miocene. In detail, the shipboard data already allow us to evaluate the quality of previous age calibrations of datum events. For example, the last occurrence of the calcareous nannofossil *Reticulofenestra umbilicus* (≥14 µm) (close to 32 Ma) leads to an exaggerated jump in sedimentation rates at both sites (Fig. F25). Interpolated between the base of Chron C12n and the top of Chron C13n, the stratigraphic position of this biostratigraphic datum suggests an older age that would be compatible with that given by Shackleton et al. (1999). This is just one example of how further postcruise studies will allow the refinement of many datum events throughout the early Cenozoic.

The remarkable fidelity of the correlation between these two sites, separated by >1° latitude and 7° longitude (~800 km), suggests that drilling results from these two sites are representative of large-scale paleoceanographic forcing functions in the late Paleogene eastern equatorial Pacific Ocean. We anticipate that the continuously cored sediments from Site 1218 with supplementary control from correlative sediments in Site 1219 will provide a paleoceanographic reference section for the late Paleogene tropical Pacific Ocean. In particular, these two sites offer an excellent opportunity to generate high-resolution geochemical records in deep-sea foraminiferal calcite with excellent age control throughout the entire Oligocene from a single deep Pacific Ocean site and thereby test models for the pattern and timing of changes in global temperature and continental ice volume developed from Atlantic Ocean DSDP sites and recent ODP transects on continental margin sequences (e.g., Miller et al., 1998, 1991, 1987) and Antarctic drilling (e.g., Wilson et al., 1998).

Eocene–Oligocene Transition

A major highlight of Leg 199 is the recovery of multiple E/O boundary sections from the central tropical Pacific Ocean (Fig. F11). Elsewhere, in the deep oceans, this important paleoceanographic boundary is often marked by condensed sequences containing poorly preserved microfossils or a hiatus. For these reasons, reliable geochemical records

across the E/O boundary are rare and limited to mid- to high-latitude sites from the Southern Hemisphere (e.g., Zachos et al., 1996; Diester-Haas and Zahn, 2001; Gersonde, Hedell, Blum, et al., 1999). Leg 199 recovered E/O boundary sections from five Northern Hemisphere sites (1217, 1218, 1219, 1220, and 1221). Taken together, these sites provide a valuable opportunity to study the chain of events across the E/O boundary within the framework of a depth and latitudinal transect (Figs. **F1, F11**). Throughout this transect, the transition from the Eocene to the Oligocene is instantly recognizable by a sharp upsection shift from SiO_2-rich and carbonate-poor to carbonate-rich and SiO_2-poor sediments (Fig. **F11**).

The pronounced lithologic transition associated with the E/O boundary is sharper in all of the Leg 199 sites drilled on older (~56 Ma) ocean crust than the single site (1218) drilled on 42-Ma crust. Furthermore, among the sites situated on 56-Ma crust, the thickness of the carbonate-rich lowermost Oligocene sediments and their carbonate content generally decreases with increases in both latitude and water depth (Fig. **F11**). These observations indicate that the CCD deepened substantially and rapidly during the Eocene–Oligocene transition (see **"Paleogene CCD,"** p. 12).

In detail, the Eocene–Oligocene transition at Site 1218 is marked by a distinct two-step upsection shift from dark radiolarian-rich clay to pale nannofossil chalk (Fig. **F26**). This two-step shift from carbonate-poor to carbonate-rich sediments is also evident as a two-step increase in GRA bulk density and decrease in magnetic susceptibility values in MST data (Fig. **F26**). At the other deeper and/or higher latitude sites, the lithologic and physical properties transition across the E/O boundary is more of a single, sharp step (Fig. **F26**).

One stratigraphic complication that we faced during Leg 199 is that the E/O boundary is formally defined by the extinction of the planktonic foraminifer genus *Hantkenina* (Zone P18/P16 boundary, Premoli-Silva et al., 1988), but planktonic foraminifers are absent in sediments of this age in all sites. The extinction of the planktonic foraminifer genus *Hantkenina* occurs toward the younger end of Chron C13r and in calcareous nannofossil Subzones CP16a and CP16b (NP21). The age of the P18/P16 boundary, thus, the E/O boundary, is presently estimated to 33.70 Ma on the seafloor magnetic anomaly–based timescale (Cande and Kent, 1995). This age estimate for the E/O boundary will likely be further refined as soon as an astronomically tuned timescale becomes confidently established across the Eocene–Oligocene transition interval.

For the above reasons, the exact placement of the E/O boundary at Leg 199 sites will remain unresolved, perhaps until the problem can be addressed through shore-based high-resolution stable-isotope stratigraphy. Nevertheless, the availability of high-quality magnetic reversal stratigraphies for all of the Leg 199 sites drilled on 56-Ma crust (Sites 1217, 1219, 1220, and 1221) combined with high-resolution nannofossil biostratigraphy made it possible to establish good shipboard approximations for the position of the boundary (Fig. **F27**). Specifically, age control across the Eocene–Oligocene transition in Leg 199 sites is provided by magnetostratigraphy at four of the five sites where the E/O boundary interval was recovered by the ODP advanced piston corer (APC) (Sites 1217, 1219, 1220, and 1221). Calcareous nannofossil and radiolarian biostratigraphy provides the age control at Site 1218 and aids the identification of the geomagnetic polarity zones in the four remaining sites. In order to compare the timing of the lithologic change

F26. Composite digital photographs showing the Eocene–Oligocene sequence and composite GRA bulk density, magnetic susceptibility, and color reflectance data, p. 77.

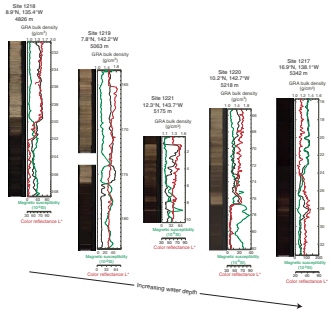

F27. E/O boundary using biostratigraphic and magnetostratigraphic data, p. 78.

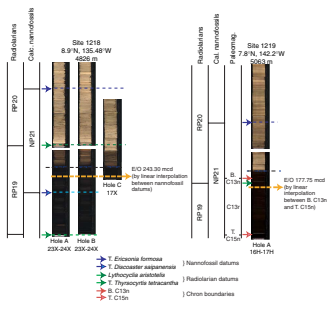

from dark-colored Eocene radiolarite to light-colored Oligocene nannofossil chalk among the five Leg 199 sites with E/O boundary intervals, we have aligned all sites along a 33.7-Ma isochron, calculated through linear interpolation between paleomagnetic and/or biostratigraphic indications (Fig. F28; Table T2).

Discoaster barbadiensis and *Discoaster saipanensis* are constrained to have disappeared over narrow (~20–30 cm) intervals in Site 1218 sediments just below the major change in lithology (Fig. F27). These findings reveal that the entire two-step change in lithology occurred in Zone NP21 (CP16c) above the extinction of the last Eocene discoasters. Based on LSRs, the estimated position of the E/O boundary is at 243.3 meters composite depth (mcd), whereas the midpoint of the initial change in carbonate composition occurs at ~242 mcd (Fig. F27). The midpoint of the second, final step in carbonate composition occurs at ~240 mcd. Thus, our records from Site 1218 imply that the change in CCD occurred in the earliest Oligocene in two steps, as a rapid increase in $CaCO_3$ over 10–20 k.y. followed by a pause of ~100–200 k.y. and then another rapid increase in $CaCO_3$ over 10–20 k.y (see **"Paleogene CCD,"** p. 12). Furthermore, the boundary condition change of the ocean-climate system that caused the first step of this drastic deepening of the CCD and accompanying change in sedimentation in the tropical Pacific Ocean thus occurred near the onset of Oi-1 (33.–33.1 Ma) (Zachos et al., 2001a) (Fig. F5) on the common timescale used (Cande and Kent, 1995).

The above findings raise the intriguing possibility that this pronounced deepening of the CCD associated with the Eocene–Oligocene transition is in some way related to the first widely accepted sustained glaciation in Antarctica (Oi-1; Fig. F5). The nature of the relationship between these two important paleoceanographic signals will be an important component of shore-based Leg 199 research. Calcareous benthic foraminifer assemblages indicate lowermost bathyal and upper abyssal paleodepths at Site 1218. The calculated age-depth curve for Site 1218 indicates a paleodepth of 3700 ± 50 m for sediments of the E/O boundary at this site (Fig. F12). Examination of test walls under transmitted light indicates that benthic foraminifers are well preserved and suitable for benthic foraminifer stable-isotope stratigraphy. Average sedimentation rates in the lower Oligocene are relatively high for a deep-ocean Pacific setting (~1–2 cm/k.y.). Together with the sections from the sites drilled on older (~56 Ma) crust, the section from Site 1218 offers exciting prospects for shore-based investigation of the first Pacific Ocean depth and latitudinal transect across this paleoceanographically important interval. For example, application of combined stable isotope and Mg/Ca records in benthic foraminiferal calcite will allow us to separate the temperature and ice volume components of "Oi-1" (e.g., Lear et al., 2000). This information, together with new constraints on the phase relationships between these signals and the deepening CCD will help to evaluate the role of the hydrological cycle vs. the carbon cycle in triggering the onset of the first persistent large-scale ice sheets during the Cenozoic.

Eocene Radiolarian Ooze

The difference between Eocene equatorial Pacific sediments and those of the Oligocene and Neogene is striking. Everywhere along the Leg 199 transect, upper lower Eocene to uppermost Eocene sediments consist primarily of one microfossil group, the radiolarians, mixed with

F28. Correlation and comparison of the E/O boundary sections, p. 79.

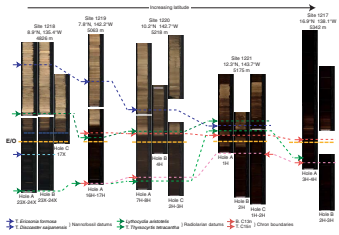

T2. Stratigraphic control around the E/O boundary, p. 87.

varying amounts of clay. In contrast, Oligocene sediments are dominantly nannofossil rich and also contain a diverse mixture of foraminifers, radiolarians, and diatoms. One of the primary postcruise tasks of Leg 199 is to decipher why radiolarian ooze is so common in the Eocene.

The task is made more difficult because analog Neogene and Holocene radiolarian oozes are rare and occupy a specific zone in the equatorial sedimentation regime that is not the same as the equivalent deposit in the Eocene. For example, the "type" Eocene radiolarian ooze (e.g., the middle Eocene ooze of Site 1220 at ~120 meters below seafloor [mbsf]; more specifically, Core 199-1220B-9H; roughly Chron C20n or 43 Ma) consists of 80%–90% radiolarians, <2% diatoms, and 10%–15% clay. The rest of the sediment is made up of opaque minerals. The sedimentation rate for this interval is 8.3 m/m.y. The total thickness of middle–upper Eocene radiolarian ooze at Site 1220 is 80 m, and it was deposited over 13 m.y. During that time, Site 1220 traversed from ~1°S to 1.5°N, based upon a fixed hotspot model, to determine paleopositions. A comparison between these deposits and a good example of a lower Miocene radiolarian ooze cored in the same site shows that the Miocene sediments are also composed dominantly of radiolarians (40%–80%), with traces of diatoms (<2%), and moderate amounts of clay (~20%). However, the remainder of the Miocene sediment is made up of nannofossils. The sedimentation rate is only 2.3 m/m.y., the total thickness of the radiolarian ooze is 18 m, and the sediment was deposited when Site 1220 was between the latitudes of 4° and 6°N. This deposit was formed just beneath the early Miocene CCD but also at the edge of the equatorial productivity zone, which seems typical for modern radiolarian oozes.

Neogene material deposited beneath the equatorial region, even if it was deposited below the CCD, contains large numbers of diatoms and would not be equivalent to the Eocene radiolarian oozes. Site 849 (Leg 138), located at the modern equator, is roughly at the equivalent longitude and latitude as occupied by Site 1220 in the early Eocene. The sediments of Site 849 contain from two to ten times as many diatoms as radiolarians throughout the entire sediment section, based upon smear slides (Mayer, Pisias, Janecek, et al., 1992). In other words, an Eocene radiolarian ooze cannot simply be created by shoaling the CCD in a modern equatorial environment. Diatom production in the Eocene must have been significantly lower than Neogene diatom production. The lack of diatoms is another indication, along with the low levels of C_{org} deposition (see **"Fluxes and Paleoproductivity,"** p. 14) that productivity levels in the Eocene were significantly below Neogene levels.

Diatoms are occasionally found in the Eocene radiolarian oozes in relatively large abundances (Fig. **F29**). We checked whether the presence of diatoms is related to when Leg 199 drill sites crossed the paleoequatorial region. Green arrows on Figure **F29** mark stratigraphic intervals where diatom numbers increase to >5% in smear slide counts. In the Eocene section, they occur primarily around one interval marked by radiolarian Zone RP15 (~39–41.5 Ma based on the preliminary Leg 199 age recalibration) rather than clustering near where we expect equator crossings. The RP15 interval is also the time of maximum radiolarian ooze deposition at Site 1217, then at a paleolatitude of ~8°N. In contrast, maximum sedimentation rates of radiolarian ooze occurred roughly coincident with paleoequator crossings. The presence of diatoms seems to be related to an ecological event that is also associated

F29. Comparison of diatom events to estimated position of equator crossings, p. 80.

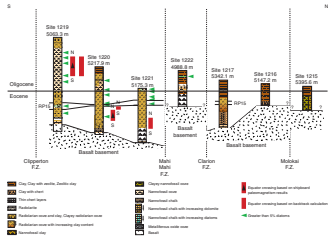

with carbonate deposition at Sites 1218 and 1219, not with passage through the equatorial zone.

One important observation is that the radiolarian deposition zone in the uppermost Eocene is restricted to Sites 1218, 1219, and 1220 in the Leg 199 transect. These sites lie in a paleolatitudinal range from 1° to 2°N. All other sites exhibit a hiatus during this interval or have only clay deposition. The uppermost Eocene is marked by a hiatus of ~2 m.y. at Site 1221 (12°02′N) that expands to 5–6 m.y. at Site 1222 (13°49′N) and at DSDP Site 162 (14°52′N), based upon a recalibration of the DSDP biostratigraphy. Sediments deposited in the late Eocene at Site 1217 (16°52′N) are zeolitic clays. Assuming that radiolarian deposition marks some moderate level of productivity, the latest Eocene was a truly impoverished interval for regions beyond several degrees of latitude from the equator. In contrast, in middle Eocene time, significant radiolarian production occurred over a broad latitudinal range. Siliceous middle Eocene sediments are formed along the entire transect save only for the northernmost sites (1215 and 1216), suggesting the zone of radiolarian production was broader in middle Eocene time (reaching ~10°N latitude) than it was in the late Eocene (when it was only a few degrees wide). Therefore, not only was there a significant change in the type of sediments deposited in the equatorial Pacific during the later Paleogene but also a distinct narrowing of the focus of siliceous sedimentation between the middle Eocene and late Eocene.

P/E Boundary

A principal objective of Leg 199 was to recover shallowly buried sections across the P/E boundary that could be used for paleoclimate and evolutionary studies. It has been known for several years (e.g., Thomas, 1990, 1998; Kaiho et al., 1996; Aubry et al., 1996, 1998; Kelly et al., 1996, 1998; Sanfilippo and Blome, 2001) that the negative carbon isotope anomaly and transient global warming associated with the P/E boundary are accompanied by carbonate-poor sediments overlying more calcareous sediments. A mass extinction of benthic foraminifers occurs at the same time as the carbon-isotope anomaly, which suggests that the boundary records major changes in deep-ocean chemistry and habitats. Carbonate preservation tends to be poorest at the initiation of the carbon isotope anomaly and then improves over an interval several tens of centimeters to several meters thick that records several hundred thousand years of sedimentation. Two drill sites (690 and 1051) have been reported with an interval of laminated sediment just above the base of the carbon isotope anomaly. Laminations have been interpreted to record low-oxygen environments that prevailed during the initial phases of the P/E boundary and may be partially responsible for the benthic foraminifer extinction (Kaiho et al., 1996; Thomas and Shackleton, 1996). Dickens et al. (1995, 2001) have suggested that outgassing of submarine gas hydrate deposits could produce both low-oxygen conditions and carbonate dissolution by oxidation of methane in the water column. However, other than the changes in carbonate content and laminated sediments, most P/E boundary sections display a relatively simple internal stratigraphy.

Leg 199 drilled the first P/E boundary sections (Sites 1215, 1220, and 1221) ever to be sampled in the central tropical Pacific. Furthermore, these sites record a more complex stratigraphy for the P/E boundary than has been recognized previously (Figs. **F30, F31**). Sediments from Sites 1220 and 1221 change from calcareous ooze containing Paleocene

F30. P/E boundary sediments, Sites 1220 and 1221, p. 81.

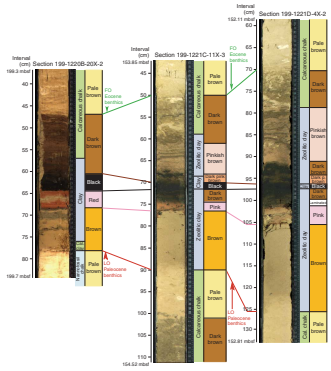

F31. Surface core scrape washed sample from across the P/E boundary, p. 82.

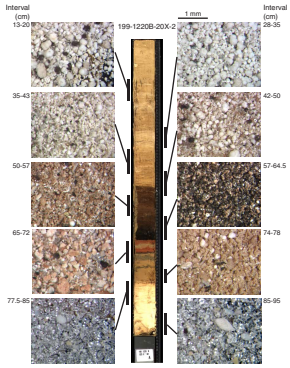

microbiotas to a distinctive layered sedimentary unit in the vicinity of the benthic foraminifer extinction. The first beds at or above the benthic foraminifer extinction horizon consist of brown sediments 8–12 cm thick. The brown bed contains layers of volcanic ash at Site 1220 but is massive at Site 1221. The top of the brown bed is burrowed and overlain by ~2 cm of rose-pink–colored sediment that displays laminations and a few discrete burrows. A layer of black, manganiferous sediments overlies the rose-pink bed and grades upward into brownish, partly laminated and burrowed calcareous clays. The brown, pink, and black beds all have low carbonate contents typical of the core of the P/E boundary at other localities. However, the interbedding of sediments with different color and sedimentary structures has not been observed in P/E boundary sections from elsewhere in the world. The presence of similar sequences of color bands at Sites 1220 and 1221, situated >200 km from one another, suggests that the stratigraphy of these P/E boundaries has at least regional significance and may record changes in deep-ocean chemistry and sedimentation that reflect different phases of the development of the boundary interval on a global scale.

Biostratigraphy of the P/E Boundary Interval

Although the P/E boundary is marked by a major extinction of benthic foraminifers (~53% species extinction), surface-ocean microbiotas display mostly temporary changes in taxonomic diversity. Unfortunately, most P/E boundary sections are highly condensed or have severely dissolved calcareous faunas, so the sequence of biotic events has not been worked out in detail. A few tropical–subtropical sites record the presence of three short-lived species of planktonic foraminifers ("excursion fauna") (Kelly et al., 1998) that are believed to have evolved shortly after the beginning of the global climate change associated with the P/E boundary and then became extinct ~200 k.y. later. Calcareous nannofossils show elevated rates of both extinction and speciation in the ~500 k.y. after the onset of Eocene time, but the sequence of evolutionary turnovers is still much debated.

Results for Leg 199 drill sites suggest that, contrary to previous interpretations, the various biotic events associated with P/E boundary time (e.g., the extinction of the nannofossil species *Fasciculithus tympaniformis* and many benthic foraminifer taxa together with the evolution of the planktonic foraminifer excursion fauna) are not synchronous in the P/E boundary interval. At Sites 1220 and 1221, Paleocene benthic foraminifers become extinct at the start of the deposition of the sequence of multicolored beds (Fig. **F32**). The reduction in carbonate content (from ~80 to ~12 wt%) associated with the benthic extinction and reduced preservation of foraminifers makes it difficult to define the precise level of the extinction. However, a sharp drop in carbonate content is observed at the same level as the carbon isotope excursion in other deep-sea sites. Therefore, it is reasonable to conclude that the base of the multicolored beds at Leg 199 sites will ultimately prove to contain the initiation of the carbon-isotope anomaly. Data from Site 1220 make it quite clear that the excursion fauna (composed of the planktonic foraminifers, *Acarinina africana, Acarinina sibaiyaensis,* and *Morzovella allisonensis*) predates the extinction of Paleocene benthic foraminifers. Hence, Leg 199 results strongly suggest that the excursion fauna evolved before the P/E boundary. These species also range above the top of the multicolored beds and may survive termination of the carbon isotope anomaly. Counts of the abundance of the calcareous nannofos-

F32. Stratigraphic distribution of benthic foraminifers, p. 83.

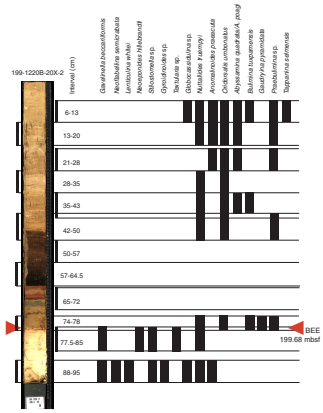

sils at Sites 1220 and 1221 show that *Fasciculithus* is replaced by *Rhomboaster* well above the multicolored beds believed to represent the start of the Paleocene-Eocene thermal maximum. We have also documented the appearance of *Thoracosphaera* cysts in the boundary interval. Thoracosphaerid blooms are frequently associated with sediments immediately above the K/T mass extinction horizon and have been interpreted to represent an opportunistic "disaster" flora (Brinkhuis and Biffi, 1993).

Geochemical Profiles of the P/E Boundary Interval

The shipboard inorganic geochemistry protocol for Leg 199 incorporated a program of bulk-sediment analysis, including a detailed analysis of the P/E boundary interval at Sites 1220 and 1221 (Fig. F33). Results for the two sites are very similar although changes in elemental concentrations are somewhat sharper at Site 1220 than Site 1221. Both sites have a significant enrichment in Mn concentration associated with the black layer, which probably contains Mn oxides. The dark, carbonate-poor portion of the P/E boundary at Sites 1220 and 1221 is associated with high levels of Si, Al, Ti, Fe, and Mg. This is consistent with a higher proportion of silicate minerals such as clays compared to the more carbonate-rich portions of the sediment column and in keeping with the interpretation that the boundary lithology represents an interval of pronounced shoaling of the CCD.

At Sites 1220 and 1221, the P/E boundary is associated with a double peak in levels of Ba and P across the interval of major color change. Superimposed on the center of these broad increases in Ba and P is an interval of very low Ba and P, which corresponds to the black Mn-rich layer and the red layer. Minima in Ba and P also correspond to a minimum in the Sr profile. The Ba and P profiles may be explained in several ways. One possibility is that the double peak seen in the profiles for these elements reflects real changes in the rate of Ba and P delivery to seafloor during P/E boundary time. Alternatively, it is possible that the rates of Ba and P delivery to seafloor were high throughout P/E boundary time, and the double peak is a dilution artifact arising from a shorter interval of rapidly accumulating black and red sediments, possibly as a result of nearby hydrothermal activity. A third possibility is that the double peak in Ba and P arises from diagenetic remobilization of primary Ba and P signals. Regardless, the levels of Ba and P recorded across the P/E boundary at Sites 1220 and 1221 are high in comparison to those measured in other Leg 199 sediments. This observation, together with the congruency of behavior between the two elements, raises the intriguing possibility that the shipboard data record an increase in surface-ocean productivity across this important paleoceanographic interval (Bains et al., 2000) rather than an increase in barite saturation arising from the injection of Ba into the global ocean from the marine gas hydrate reservoir (Dickens et al., 2001).

F33. Analyses of sediment scrapes across the P/E boundary, Sites 1220 and 1221, p. 84.

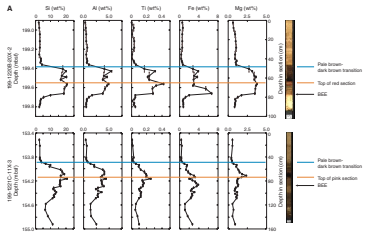

OPERATIONAL AND LOGISTICAL ASPECTS OF THE PALEOGENE TRANSECT

Five logistical issues make the design of the Leg 199 transect (or any other K/T transect) significantly more difficult than the design of a Pleistocene study: (1) the Neogene sediments are overburden, not the target of drilling; (2) because ocean crust is old, the sites are deep; (3) er-

rors in plate tectonic models accumulate, and paleopositions are hard to predict with confidence; (4) the sedimentation regime is more poorly known and the type of sediments that will be encountered can be hard to predict; and (5) cherts commonly occur in the sediments and disrupt recovery, but chert formation is poorly understood and not yet predictable.

The burial (nonburial) history of a Paleogene section by Neogene sediments has an important impact on diagenesis and on the time needed to recover the interval of interest (e.g., Rudnicki et al., 2001). Even modest diagenetic alteration of sediments (e.g., carbonate ooze–chalk transition) can affect core recovery, and this, together with the style of diagenesis, influences the type of paleoceanographic studies for which samples are suitable (Wilson et al., 2002). For example, at Site 1218, deeply buried lower Oligocene nannofossil oozes were converted to chalk at ~200 mbsf, which necessitated a switch from APC to XCB drilling at 189 mbsf. XCB drilling disturbs the sediments more extensively than piston coring and effectively ended our ability to develop a geomagnetic reversal stratigraphy even though a continuous sediment column splice was completed to 263 mbsf. Technologies and strategies are required to maximize APC refusal depths in such cases (e.g., the ability to switch to a 5-m-long APC core barrel). Completing a sediment column splice by multiple offset holes at a drill site is also more of a challenge because significant time can be lost drilling to the target sediments. For example, the presence of the Neogene equatorial sediment bulge immediately to the south of the Clipperton Fracture Zone effectively limited our ability to sample the Eocene from southern tropical paleolatitudes.

Sediments over young ocean crust are relatively shallow and situated under ~3 km of overlying water. Because ocean crust cools and deepens as it ages, a Paleogene transect lies in much deeper water than does a Neogene one. All drill sites along the 56-Ma transect of Leg 199 were deeper than 5 km. Because the water is deeper along an older transect, normal drilling operations such as recovering core take significantly longer than they would along a younger transect. Any failure of equipment leads to a larger time penalty, and standard pipe trips at the beginning and end of a site take significantly more time than in shallow water. Fewer holes can therefore be drilled in the same amount of time for a Paleogene or Cretaceous transect.

Errors in plate-tectonic models are relatively small for the Neogene, but even small errors accumulate with time. The resultant error may amount to several degrees of latitude in the Paleogene Pacific, and the ability to predict paleopositions becomes less reliable. In the case of Leg 199, uncertainties in the motion of the Pacific plate required that we drill a larger latitude span than may have been strictly necessary to study Paleogene equatorial Pacific circulation because prior to drilling we were not certain where the equator crossed our 56-Ma transect in the Eocene and Paleocene.

Even with prior DSDP drilling, it was only possible to predict in a very general way the type of sediments we would find. We were often surprised by the lithologies we drilled, and the scientific party needed to be flexible and ready to revise both the drilling plan and postcruise studies. It is important to have alternate drill sites to choose from after new material is discovered. However, one difficulty that we experienced with the latitudinal-transect approach was that large transit times between sites severely restricted our ability to adopt the flexible approach

that was needed as a result of the significant time penalties that would have been incurred.

The difficulties associated with drilling through cherts are always a consideration when drilling Paleogene and older sediments. Improvements in drilling technology, such as better cutting shoes and active heave compensation, make cherts a less fearsome challenge than early in the DSDP program. Nevertheless, recovery in cherty sediments is still generally poor. In the case of Leg 199, we were able to core a continuous section through cherty chalk at Site 1218 but were generally frustrated in recovering sediments with chert near the early–middle Eocene boundary. We believe that these sediments were still unlithified because we were able to recover radiolarian ooze right up to the upper boundary of chert zones and radiolarian ooze and carbonates below. Understanding where chert zones lie helps to minimize sediment loss, but new drilling technology is still needed.

SITE SUMMARIES

Site 1215

Site 1215 (26°1.77′N, 147°55.99′W) is located north of the Molokai Fracture Zone in 5396-m water depth. It is situated on typical abyssal-hill topography in an area of thin but continuous sediment cover. Based on magnetic lineations, basement age at this site should be in the youngest part of Anomaly An26r, or ~58 Ma. This site was the northernmost of the transect drilled on crust of this age during Leg 199. Double APC/XCB coring at Site 1215 recovered a sedimentary section from red clays at the seafloor to hydrothermal sediments immediately above basalt. The 70-m-thick sediment section consists of pelagic red clay (Unit I; ~0–26 mbsf) overlying 42 m of clayey calcareous ooze with chert (Unit-II; ~26–68 mbsf) and a thin basal unit of hydrothermal sediment (Unit III; ~68–70 mbsf) over basalt. The upper and lower units of the section are unzoned biostratigraphically, but calcareous fauna and flora and magnetostratigraphy indicate that Unit II is complete (to the zone/chron level) from the lower Eocene through upper Paleocene section (NP8 through NP12; C25n–C23n, or ~56.2–52 Ma). Porosity values increase steadily with depth from ~73% near the seafloor to ~91% at the base of the red clay unit (25.8 mbsf) and then decrease steadily to values near 58% at the base of the Unit II carbonates (67.2 mbsf). The one sample analyzed from the lithologic Unit III hydrothermal sediments has a porosity of ~82%. Interstitial pore water profiles from Site 1215 primarily reflect the dissolution of biogenic silica, alteration of underlying basalt, and extremely low levels of labile organic matter available for oxidation.

Highlights

Red Clay Transition

A light to dark color change occurs in the upper portion of lithologic Unit I (red clay) and has been observed in cores of pelagic clay throughout the north central Pacific Ocean. LAS, elemental solid phase chemistry, and both discrete and GRA bulk density data from Site 1215 indicate a downcore transition from illite to smectite between ~5 and 10 mbsf consistent with a change in the source of wind-blown dust from Asia (illite rich) to America (smectite rich) during late Miocene time.

Composite Lower Eocene Section of Clay–Calcareous Ooze Cycles

The interval between ~30 and ~50 mcd at Site 1215 shows a clear succession of cycles in color reflectance and physical properties data on a decimeter scale that appears modulated in amplitude as well as in thickness. This amplitude modulation, when combined with biostratigraphic time control, is consistent with a climatic forcing related to climatic precession (~19,000- to 23,000-yr period). In the $CaCO_3$-bearing sediments, both nannofossil assemblages and planktonic foraminifers are strongly affected by dissolution, but the former provide well-constrained biostratigraphic control. The benthic foraminifers present are characterized by hyaline calcareous tests, are better preserved than the planktonic foraminifers, and are promising for shore-based paleoecological and paleooceanographic studies.

First P/E Boundary Section from the Central Tropical Pacific Ocean

An interval of dark-brown (10YR 2/2) nannofossil clay at ~54.7 mbsf in Hole 1215A (interval 199-1215A-8H-3, 128–148 cm) is interpreted to represent the first P/E boundary section to be recovered from the central tropical Pacific Ocean. Calcareous nannofossil biostratigraphy indicates that the boundary occurs in NP9, and the P/E benthic extinction event is observed between ~54.5 and ~55.5 mbsf.

Site 1216

Site 1216 (21°27.16′N, 139°28.79′W) is located on abyssal hills just south of the Molokai Fracture Zone at a water depth of 5163 m. The crustal age, based on magnetic lineations, is ~57 Ma (magnetic Anomaly An25r). The site was chosen for drilling because it is near the thickest section of lower Eocene sediments along the 56-Ma transect. Based on previous coring and drilling ~1° to the south in latitude, we expected to find a moderately thin red clay section overlying middle Eocene radiolarian oozes and lower Eocene carbonates. Instead, we drilled a 50-m section of red clay overlying thin cherts in sediment and abandoned the site before reaching basement. We recovered only chert in the chert sediment section. Microfossils are absent until ~40 mbsf where small numbers of middle Eocene radiolarians appear. The cherts are early middle Eocene–early Eocene in age. We abandoned the site after drilling to 62 mbsf because of the likelihood of large amounts of chert in the section with little sediment recovery and because we could use the saved time to ensure more complete programs at the remaining sites.

The red clay unit is similar to the red clay section of Site 1215 but expanded (40 m vs. 25 m thick). The upper part of the Site 1216 red clays are illite rich (based upon LAS analyses) grading to smectite rich at the base. The transition begins at ~10 mbsf. Fe-Mn oxyhydroxides are also abundant in the lower part of the red clays, reaching a maximum ~29 mbsf as shown by bulk-sediment analyses and by grain density. A transition from relatively high to low natural gamma ray (NGR) activity occurred at ~25 mbsf. A similar transition in NGR activity was observed at Site 1215.

The sediments at Site 1216 are surprisingly barren of microfossils. Upper middle Eocene radiolarian oozes are absent at the site, and lower middle Eocene radiolarians are not abundant. Calcareous microfossils are absent in the drilled section. Only agglutinated benthic foraminifers were found, but none are age diagnostic. The uppermost radiolarians (from RP13 zone; ~44 Ma) occur at ~40 mbsf. The base of the drilled

section (62.2 mbsf) is in radiolarian Zones RP9 and RP10, which straddle the middle/early Eocene boundary (~49 Ma). The first cherts encountered downhole occurred at ~50 mbsf. These upper cherts, thus, appear in an interval of slow sedimentation rate, at most 4–5 m/m.y., presumably at the top of more rapidly deposited lower Eocene sediments with larger amounts of biogenic components. We estimated from the seismic reflection profile that ~60 m of sediments remained to be drilled in the cherty section until basement was reached.

It was possible to identify magnetic polarity chrons in the red clay section but none in sections with microfossils because of coring disturbance. Based on the microfossil dates, the oldest chron detected is probably C20n. Magnetic intensity of the red clays is strong, and drilling-induced magnetic overprints are mostly removable by standard procedures.

Highlights

Red Clay Section

The red clay section at Site 1216 has several similarities to the red clay section cored at Site 1215, although it is 60% thicker. Both red clay units have a transition from illite to smectite with depth. Both show a significant decrease in NGR activity downcore. The lower parts of each red clay unit are enriched in Fe-Mn oxyhydroxides. When MST records are compared, smaller events appear to correlate between these two sites. Provided that some age control can be developed, it may prove possible to develop a much more detailed red clay stratigraphy for the North Pacific than is now available.

Missing Middle Eocene Radiolarian Oozes

One of the major surprises found from drilling Site 1216 is the remarkable lack of late or middle Eocene radiolarian oozes. These are biogenic sediments that have no modern analog but are prominent sedimentary features from piston cores and drill sites only 1° to the south. DSDP Site 40 recovered 140 m of upper–middle Eocene radiolarian ooze beneath ~10 m of red clay. DSDP Site 41 with a thinner sediment column (34 m of sediment above basalt) contains 16 m of radiolarian ooze below 18 m of red clay. Piston core EW9709-3PC, taken on the site survey for the potential Leg 199 drill site PAT-13 (19°46′N, 138°55′W) also cored 5 m of middle Eocene radiolarian ooze beneath 10 m of red clay. On the basis of this apparent sharp zonation in tropical biotic communities, a major oceanographic boundary must have existed between the paleoposition of Site 1216 and Sites 40 and 41.

Site 1217

Site 1217 (16°52.01′N, 138°06.00′W) is situated ~1° north of the Clarion Fracture Zone on abyssal hill topography at a water depth of 5342 m. The site was chosen for drilling because it is thought to have been located just outside of the equatorial region at 56 Ma (~5°N, 106°W, based upon a fixed hotspot model; Gripp and Gordon, 1990, for the 0- to 5-Ma Pacific hotspot rotation pole; Engebretson et al., 1985, for older poles). At 40 Ma, the site was located at ~8°N, 111°W. Thus, Site 1217 should help define the paleoceanography of the northern tropical Pacific and, in particular, help to locate the ancient North Equatorial Countercurrent (NECC) region. Based on site survey seismic data and piston coring together with results from the nearest drill site (DSDP Site

162, situated on 48-Ma crust ~300 km south and west), we expected the sedimentary sequence at Site 1217 to comprise a relatively thick (25–35 m thick) section of red clays, overlying a radiolarian ooze. We also expected a basal carbonate section with possible chert near basement (estimated total depth of ~125–150 mbsf) deposited when the site was near the ridge crest in the late Paleocene and early Eocene.

The sedimentary section overlying basalt at Site 1217 is ~138 m thick and records a lower Eocene nannofossil chalk overlain by a poorly recovered lower–middle Eocene chert-clay sequence. Middle Eocene–Holocene deposition is represented by radiolarian ooze followed by red clays at the surface. The recovered sediments from all three holes at Site 1217 were affected by coring disturbance, downhole debris, and flow-in associated with chert fragments blocking the core liner. One stratigraphic interval in the APC-cored section was highly disturbed or not recovered in all three holes (~37–49 mbsf), which prevented the recovery of a complete continuous sedimentary section. Nevertheless, it was possible to generate a spliced, but discontinuous, record in the upper 90 m of the section.

The uppermost red clays at Site 1217 (Unit I) are ~39 m thick. The clays show an uphole mineralogical transition from smectite rich to illite rich at~7 mbsf, which indicates a change in wind-blown dust provenance from American to Asian sources associated with the movement northward of the Pacific plate. The red clay unit also contains a thin (~2.5 m thick; ~30 mbsf) subunit of nannofossil ooze interbedded with nannofossil clay. Below the red clays are a radiolarian ooze with clay grading to clayey radiolarian ooze (Unit II; ~39–90 mbsf). The radiolarian ooze is of middle Eocene age (~38–43 Ma) and contains a rich and well-preserved middle Eocene radiolarian fauna. Below 90 mbsf, we encountered a unit of chert and interbedded clay (90–128 mbsf) before recovering a thin, ~1.13-m-thick, section of early Eocene chalk (Unit III; 128–129 mbsf). The chalk is partially to extensively dolomitized (washed core catcher samples yield abundant near-perfectly euhedral rhombs ~100 mm in size) but contains nannofossils and planktonic and benthic foraminifers. Basement basalt was encountered at 138 mbsf.

Wet bulk density values at Site 1217 are high between the seafloor and 22 mbsf (mean values = 1.37 g/cm^3) and decrease sharply to a minimum of 1.18 g/cm^3 at 25.58 mbsf—a value that is very similar to the density of the radiolarian oozes at the site. In contrast, the wet bulk densities of the Oligocene nannofossil ooze subunit and lower Paleocene nannofossil chalk are distinctly higher (~1.28 and 1.79 g/cm^3, respectively).

The magnetic intensity of the sediments is relatively strong, and drilling-induced magnetization was mostly removed with mild alternating-field (AF) demagnetization. Site 1217 sediments provided a good record of geomagnetic reversals that could be interpreted as chrons. Characteristic remanent magnetization (ChRM) inclinations are usually shallow, as expected in these latitudes. A record from Chron C20 to Chron C12 was established from the middle Eocene to the early Oligocene, but the reversal stratigraphy in the upper 15 m (late Oligocene–Holocene) could not be established because of the low sedimentation rate of the upper sediments and the lack of either core orientation or an independent age model.

High levels of sulfate and concomitant low levels of ammonium in interstitial pore waters at Site 1217 indicate a relatively oxic system consistent with very low levels of labile organic matter, the presence of

metalliferous oxides, and the strong and stable magnetic signature in the host sediments. Relatively high pore water silica concentrations are consistent with dissolution of biogenic silica in the sediments. The solid-phase chemical content reflects the microfossil content and the low level of reductive diagenesis. The whole section at Site 1217 shows relatively high levels of Mn and Fe in the solid phase. Within the upper red clays, solid phase Si levels generally increase southward in the Site 1215, 1216, and 1217 transect, presumably indicating higher export of biogenic debris to the ocean floor closer to the paleoequator.

The average LSRs in the red clays (shallower than 23 mbsf) are very low (~0.8 m/m.y.). Sedimentation rates in the underlying fossiliferous and cherty lower sections are substantially higher but are, nevertheless, modest (~5 m/m.y.).

Highlights

Lower Oligocene Nannofossil Ooze

Assuming that a distinct normal polarity chron seen in paleomagnetic data at 23.27 mbsf in Hole 1217A represents Chron C12n, the succeeding downhole normal polarity interval is interpreted to represent Chron C13n, which lies at the base of the Oligocene. This interpretation is consistent with the underlying spacing and length of several normal and reversed intervals and places the thin subunit of nannofossil-rich carbonate ooze (all from nannofossil Zone NP22) in the lowermost Oligocene. This brief interval of carbonate sediment preservation may represent the dramatic deepening of the CCD recorded elsewhere in the deep-sea tropical Pacific Ocean (e.g., DSDP Sites 42, 70, 161, and 162) associated with the Eocene–Oligocene transition, but this possibility can only be validated by shore-based studies.

Middle Eocene Radiolarian Ooze

At Site 1217, we collected the first near-continuously drilled sequence of Eocene radiolarian oozes by deep-sea drilling. In the presence of a well-defined magnetostratigraphy, this section will help to define and calibrate radiolarian stratigraphic zonation. Radiolarian oozes have no modern analog but are prominent sedimentary features of the middle Eocene low-latitude Pacific Ocean, having been recovered from piston cores and drill sites up to 4° to the north (e.g., DSDP Sites 40 and 41) and 10° to the south (e.g., DSDP Sites 70 and 162). In contrast, middle Eocene radiolarian oozes are absent at Site 1216. Thus, Sites 1216 and 1217, along with DSDP Sites 40 and 41, appear to define the northern extent of this type of biogenic sedimentation.

Lower–Middle Eocene Chert and Dolomitized Nannofossil Chalk

By coring to basement at Site 1217, we recovered sediments needed to address a number of Leg 199 objectives, including an improvement in our understanding of the following: (1) the location of the Paleocene/Eocene paleoequator, (2) the biotic composition and rate of accumulation of sediments in the tropical Eocene Pacific Ocean, and (3) the behavior of the silica budget and CCD during the early Eocene. Broadly speaking, the sequence drilled at Site 1217 conforms to the classical sedimentary succession predicted for a deep-sea drill site situated on relatively old oceanic crust in the Central Pacific (red clays overlying siliceous and, in turn, carbonate biogenic sediments). However, the lowermost sediments drilled (lower–middle Eocene chert and chalk) surprised us in two ways. First, these sediments show average LSRs are

relatively slow (<5 m/m.y.), consistent with results from Site 1216. Second, the basal lower Eocene chalks that overlie basement are, like their Site 1215 counterparts, dolomitized—an intriguing discovery given their proximity to what is generally considered to be a kinetically more favorable geochemical sink for Mg (alteration minerals in the upper oceanic crust).

Site 1218

Site 1218 (8°53.38′N, 135°22.00′W) is the only Leg 199 drill site from the 40-Ma transect and is situated at a water depth of 4826 m. It was chosen for drilling in order to investigate paleoceanographic processes in the equatorial Paleogene Pacific Ocean during the inferred transition of Earth's climate from the early Paleogene greenhouse into the late Paleogene icehouse state. Site 1218 is situated on a basement swell ~3°N of the Clipperton Fracture Zone in the central tropical Pacific at a water depth of 4826 m. Pacific plate motion carried Site 1218 across the equator at ~40 Ma based upon a fixed hotspot model (Gripp and Gordon, 1990, for the 0- to 5-Ma Pacific hotspot rotation pole; Engebretson et al., 1985, for older poles). Based upon the same model, the site remained within 2° of the equator from the time crust was formed (42 Ma) until 27 Ma. The sediments recovered from Site 1218 should therefore record near-equatorial oceanographic conditions from the middle Eocene until the early Oligocene. The precise age of basement at the site was poorly constrained prior to Leg 199 because little magnetic anomaly data are available between the Clipperton and Clarion Fracture Zones (Cande et al., 1989).

At Site 1218, we recovered a complete sediment section to within 15 m of basaltic basement. A continuous spliced section (from 0 to 263 mbsf [~41–42 Ma; nannofossil biostratigraphic Subzone CP14a]) was developed using the three drilled holes. The sediments immediately overlying basalt are from near the CP14a/CP13 boundary (42 Ma), which indicates that basement at Site 1218 is slightly older than originally expected. A full suite of downhole logs were obtained to the base of the Hole 1218A, and the data are of excellent quality.

The sediment column at Site 1218 is made up of four sedimentary units. At the top of the sedimentary column is 52 m of yellowish brown radiolarian clay with occasional barren intervals and intervals with nannofossils. The age of this unit is Pleistocene–middle Miocene. Below this unit are nannofossil oozes and chalks of early Miocene–Oligocene age from 52 to 217 mbsf. The basal boundary is abrupt. The upper Eocene and upper middle Eocene sediments (217–250 mbsf) are composed of radiolarites and nannofossil chalk with occasional chert beds. In contrast to other sites, the cherty sections at Site 1218 were completely recovered by XCB coring, undoubtedly because they were interbedded with chalks rather than ooze. The base of the sediment column is middle Eocene chalk (250–274 mbsf). The lower 7 m of the chalk is dolomitized with up to 20% dolomite in the coarse fraction. Basalt was recovered at the base of the drilled section.

Planktonic foraminifers occur sporadically through the lower Miocene, Oligocene, and middle Eocene sediments at Site 1218 with generally less consistent presence than other calcitic groups such as benthic foraminifers and calcareous nannofossils. Most samples show at least some dissolution of planktonic foraminifers with preferential preservation of large, thick-walled specimens in many cases. Middle Oligocene sediments (Zones P21 and P20) were generally the best preserved and

most species-rich sediments for planktonic foraminifers at Site 1218. Benthic foraminifers are present in core catchers throughout the cored interval except in the upper radiolarian clays and the upper Eocene interval. Calcareous nannofossils, in contrast, are present at varying concentrations and states of preservation from uppermost middle Miocene Zone NN8 (37 mbsf) to the base of the sediment section. Radiolarians were found in all recovered cores.

Pore water chemical profiles at Site 1218 are subtle. Sulfate concentrations are near seawater values throughout the section, indicating the lack of significant organic matter diagenesis, whereas trends in Ca and Mg reflect modest basement alteration. Bulk-sediment concentrations (measured every 1.5 m) outline the major lithologic units described above. Only Ca and Sr concentrations are high in the lower Oligocene–Miocene nannofossil oozes, and all other elements tend to be higher in the clays and radiolarite sediments. Biogenic enrichment of Ba can be detected through Ba/Ti ratios (Fig. **F19**). High Mg concentrations can be found in the basal dolomitized chalk.

Natural remanent magnetization (NRM) intensity of the sediments at Site 1218 is relatively strong, and magnetic overprint from drilling can be mostly removed by AF demagnetization. An excellent record of magnetic reversals was made for the entire APC-cored sediment section (0–210 mcd) to Chron C12r of the early Oligocene. In addition, magnetic inclinations were determined on discrete samples after more thorough demagnetization. Middle and early Miocene samples have an average inclination of 5.2° (+2.2°/8.4°), whereas the Oligocene samples have an average inclination of 3.8° (α_{95} = 6.2), which is indistinguishable from the paleoequator.

Highlights

Composite Section

Recovered sediments at Site 1218 have high-amplitude MST data sets, which gave us the ability to direct drilling (in real time) in Holes 1218B and 1218C in order to construct a complete composite sediment section to a depth of ~263 mbsf (~287 mcd). This section will help to define and calibrate Cenozoic biostratigraphic zonation, to develop an astronomically tuned Cenozoic timescale, and to generate high-resolution paleoceanographic and paleoclimatic records of the Paleogene–Neogene transition.

Oligocene–Miocene Transition

The short range of nannofossil species *Sphenolithus delphix* provides a reliable marker close to the O/M boundary between Subchrons C6Cn.3n and C6Cn.2n (Raffi, 1999), and on this basis, the O/M boundary in Site 1218 occurs at ~98 mbsf. The first occurrence of the planktonic foraminifer *Paragloborotalia kugleri* (the marker for the O/M boundary) and first occurrence of the radiolarian *Cyrtocapsella tetrapera* also occur at this depth.

Calcareous benthic foraminifer assemblages indicate lowermost bathyal and upper abyssal paleodepths at Site 1218. Examination of test walls under transmitted light indicates that most of the benthic foraminifers at this site have suffered little or no postburial diagenetic alternation. Average sedimentation rates across the Oligocene–Miocene transition (~1–2 cm/k.y.) are relatively high for a deep-ocean Pacific setting.

Eocene–Oligocene Transition

The E/O boundary at Site 1218 is characterized by a major lithologic change involving a two-step downcore shift from pale nannofossil chalk to dark radiolarite. This transition from carbonate-rich to carbonate-poor sediments is also evident as a two-step decrease in GRA bulk density and an increase in magnetic susceptibility values in MST data. Based upon biostratigraphic information, this transition occurs across or just above the Eocene–Oligocene transition.

The extinction of the calcareous nannofossil *D. saipanensis* is estimated to have occurred ~0.3 m.y prior to the E/O boundary event sensu stricto (extinction of the planktonic foraminifer genus *Hantkenina*), and the last representative of the Paleogene rosette-shaped discoasters, *Discoaster barbadiensis,* disappeared ~0.2 m.y. before *D. saipanensis*. *D. barbadiensis* and *D. saipanensis* are constrained to have disappeared over narrow (~20–30 cm) intervals in Site 1218 sediments shortly below the major change in lithology. These findings reveal that the entire two-step change in lithology occurred in Zone NP21 (CP16c), above the extinction of the last Eocene discoasters. Based on an LSR the estimated position of the E/O boundary is at 243.3 mcd, whereas the midpoint of the initial change in carbonate composition is at 242.0 mcd (Fig. **F27**). The midpoint of the second, final step in carbonate is at 240.0 mcd. The boundary condition change of the ocean-climate system that caused the first step of this drastic deepening of the CCD and accompanying change in sedimentation in the tropical Pacific Ocean occurred near the middle of Oi-1 (33.5–33.1 Ma) (Zachos et al., 2001a) on the common timescale used (Cande and Kent, 1995). The abrupt change in the lithologies across the Eocene–Oligocene transition is a reflection of the rapid deepening of the CCD (van Andel et al., 1975) in the Oligocene. Site 1218 demonstrates that the change in CCD occurred during the earliest Oligocene in two steps, as a rapid increase in $CaCO_3$ over 10–20 k.y. followed by a pause of ~100–200 k.y. and then another rapid increase in $CaCO_3$ over 10–20 k.y. The CCD was shallower than ~3600 mbsl in the latest Eocene radiolarite interval, based on the paleodepth of Site 1218.

Middle and Late Eocene Radiolarites

From Site 1218, it is clear that radiolarian-rich sediments are characteristic of the late and late–middle Eocene Pacific Ocean even near the equator. Nannofossils occasionally are dominant sediment components, showing that the CCD deepened beyond the paleodepth of Site 1218 at times in the late and middle Eocene. The presence of radiolarians and occasional intervals of nannofossils and the relative absence of diatoms (except in specific intervals near the E/O boundary) is more typical of Neogene plankton assemblages found at the fringes of the equatorial high-productivity zone than in the near-equatorial position that Site 1218 probably occupied during the middle and late Eocene.

Middle Eocene Basal Sediments

The basal nannofossil chalks of Site 1218 abruptly become radiolarites upcore at ~40 Ma (base of nannofossil Subzone CP14b; Core 199-1218C-21X). The transition from chalks to radiolarites occurs over only 1.5 m when the site was at a paleodepth of 3000–3100 m. The middle Eocene rise in CCD at 40 Ma is almost as abrupt as the drop in CCD at the E/O boundary.

Finally, the basal 7 m of nannofossil chalk at Site 1218 that overlies basement is, like its Site 1215 and 1217 counterparts, dolomitized—an

intriguing discovery given its proximity to what is generally considered to be a kinetically more favorable geochemical sink for Mg (alteration minerals in the upper oceanic crust).

Site 1219

Site 1219 (7°48.01′N, 142°00.94′W) is the southernmost site drilled during Leg 199. It is situated on the 56-Ma transect ~3° north of the Clipperton Fracture Zone and is located at a water depth of 5063 m on abyssal hill topography. The age of basement at Site 1219 was poorly constrained prior to Leg 199 because little reliable magnetic anomaly data are available between the Clipperton and Clarion Fracture Zones (Cande et al., 1989). At the outset of Leg 199, based on one interpretation of the location of magnetic Anomaly An25r (~57 Ma) (Petronotis et al., 1994), previous drilling, and assumed spreading rates, we estimated the age of basement at Site 1219 to be ~55 Ma. Site 1219 is the only site drilled during Leg 199 that features all of the seismic horizons identified for a Paleogene equatorial seismic stratigraphy (**Lyle et al.,** this volume).

Based upon a fixed hotspot model (Gripp and Gordon, 1990, for the 0- to 5-Ma Pacific hotspot rotation pole; Engebretson et al., 1985, for older poles), Site 1219 should have been within 2° south of the equator between 40 and 21 Ma and should have crossed the equator at 29 Ma. Thus, the sediments should record equatorial conditions from the late middle Eocene through the early Miocene. In addition, Site 1219 should provide an analog for Site 1218, except that it is on older, deeper crust.

Two holes were drilled at Site 1219. Hole 1219A was a remarkable operations success. We advanced to ~225 mbsf using ODP's APC technology and, thereby, achieved one of our high-priority objectives by recovering sediments suitable for whole-core magnetostratigraphy below the lower Oligocene (including the E/O boundary). Basement was reached at ~250 mbsf shortly after switching to XCB coring. A full suite of downhole logs was obtained to the base of Hole 1219A, and the data are of high quality. In addition to these downhole logs, MST data from the latest Eocene to the earliest Miocene interval in this hole bore a striking resemblance to those recovered from Site 1218, and it was possible to correlate between Sites 1218 and 1219 (which are separated by 7° of longitude and 1° latitude, or ~800 km) to a submeter scale.

In contrast to Hole 1219A, Hole 1219B was terminated when an APC core jammed in the bottom-hole assembly (BHA) at the depth of the E/O boundary (~155 mbsf). In light of these difficulties in Hole 1219B and the successes of both Hole 1219A and Site 1218, the shipboard party took a collective decision to abandon Site 1219 earlier than planned in order to target additional and more complete programs at forthcoming sites having early and middle Eocene objectives.

Holes 1219A and 1219B can be spliced to form a continuous section to 130 mcd (~30 Ma) with two apparent gaps at ~90 and ~100 mcd. Excellent correlations between Site 1218 and 1219 allow us to estimate the properties of the unrecovered intervals, whereas correlations between logging data and the cores can be used to estimate the size of core gaps deeper in the sedimentary section. Sedimentation rates over the Oligocene interval were ~16% slower than at Site 1218 based upon the site-to-site correlation.

The sediment column at Site 1219 has a strong resemblance to that of Site 1218. Thirty meters of clay (lithologic Unit I) overlies Oligocene–

lower Miocene nannofossil ooze (Unit II; 30–151 mbsf). Strong cyclic variations in nannofossil content are apparent in both the upper and lower parts of Unit II. An abrupt change in lithology from nannofossil ooze to radiolarian clay and clayey radiolarian ooze occurs at 151 mbsf in the E/O boundary interval. The lithologic change marks the upper boundary of lithologic Unit III, an upper and middle Eocene unit composed of radiolarian ooze and radiolarian clay, which becomes radiolarite, chert, and zeolitic clay at the base. A short section in Unit III in polarity Chron C18r (40.1–41.3 Ma) contains alternating diatom and nannofossil ooze. Below the cherty, clay-rich section at the base of Unit III are the chalks of lithologic Unit IV (234–243 mbsf; ~53–54.8 Ma). The oldest sediments above basalt are slightly younger than the P/E boundary.

NRM intensity of the sediments at Site 1219 is relatively strong, and magnetic overprint from drilling can be mostly removed by AF demagnetization. An excellent record of magnetic reversals was made for the entire APC-cored sediment section (0–223 mbsf), from Pleistocene Chron C1n to early middle Eocene Chron C20r (43.8–46.3 Ma). This remarkably clean magnetic reversal stratigraphy allows us to calibrate biostratigraphic events and to develop detailed sedimentation rate curves downhole through lower middle Eocene sediments. Inclination patterns in discrete samples show that at least the lower part of the sedimentary section was located in the Southern Hemisphere during deposition. The mean inclination depicts a time-averaged paleolatitude of 1.6°S for the site, but this result is preliminary and will require further testing. The paleolatitude inferred from the inclination is consistent with the expected latitudes as calculated from both paleomagnetic pole positions and those based upon a fixed hotspot model.

Nannofossils are present to abundant in the Oligocene–middle Miocene sediments (~151–10 mbsf) but absent from upper Eocene sediments. Nannofossils reappear briefly in polarity Chron C17r (~38.3 Ma) in the middle Eocene, disappear, and then reappear and are present between the middle of polarity Chron C18r to the base of C20n (~40.5–43.8 Ma) and are found in the chalk in the lower Eocene interval. Planktonic foraminifers are present in the lower Miocene to Oligocene sediments and in the lower Eocene chalks. Preservation quality and abundance are highest in the lower Miocene (Zones M4–M2) and the middle part of the Oligocene (Zones P20 and P21). Benthic foraminifers are consistently present and well preserved through the Miocene and Oligocene at Site 1219 but are scarce and very poorly preserved through much of the Eocene sections. Radiolarians were found in all cores except the deepest one (Core 199-1219A-27X), which recovered chalk over basalt basement.

The magnitude of the downhole calcium concentration increase and magnesium and potassium-concentration decrease in pore waters at Site 1219 is the greatest seen at all sites during Leg 199. This pattern is consistent with the extensive alteration (e.g., chlorite formation) of basement rocks observed here. Depth gradients of pore water alkalinity, pH, sulfate, and ammonium reflect the small amount of organic matter degradation occurring in these sediments, whereas the chlorinity profile may reflect the diffusion of the more saline Pacific bottom water of the last glacial maximum into the sediments. Bulk-sediment geochemical analyses from Site 1219 reflect the shifts in lithology back and forth between sediments dominated by silica and carbonate. Clay-rich units are high in Ti and Al, but they are also high in Fe and Mn, presumably reflecting the deposition of authigenic ferromanganese oxyhydroxides.

Physical properties of the sediments also primarily reflect lithology. The carbonate sediments are higher in density, lower in porosity, and lower in magnetic susceptibility than the clay or radiolarian ooze lithologies. This is true even on a fine scale (see Fig. **F29,** p. 73, and **"Physical Properties,"** p. 28, both in the "Site 1219" chapter. The radiolarian ooze has higher compressional wave velocity than the carbonates despite having higher average porosity.

Highlights

Magnetic Reversal Stratigraphy

The clean record of magnetic reversal history from Site 1219 (for the entire APC-cored sediment section; 0-223 mbsf), from the Pleistocene down to Chron C20r (43.8–46.3 Ma), is remarkable for a tropical site and, together with the superb cyclostratigraphic correlations to Site 1218 (see following paragraph) will provide invaluable time control for shore-based high-resolution paleoceanographic studies.

MST Correlation to Site 1218

The MST data from Site 1219 bear a striking resemblance to those recovered from Site 1218 from the middle Eocene to the lowermost Miocene interval. The excellent match in these data sets between the two sites made it possible to align both records on a common (Site 1218 mcd) depth scale. The two records show such high quality correlation (down to the submeter scale) that successful a priori prediction of biostratigraphic zones and magnetic reversals was possible at Site 1219. The mapping from Site 1219 mcd to Site 1218 mcd results in relative sedimentation rates at Site 1218 that are ~16% higher than at Site 1219 over the Oligocene interval. The remarkable fidelity of the correlation between these two sites, separated by >1° of latitude and 7° of longitude (~800 km), suggests that drilling results from these two sites are representative of large-scale paleoceanographic forcing functions in the late Paleogene eastern equatorial Pacific Ocean. We anticipate that the continuously cored sediments from Site 1218 with supplementary control from correlative sediments in Site 1219 will provide a paleoceanographic reference section for the late Paleogene tropical Pacific Ocean.

Oligocene–Miocene Transition

Calcareous nannofossils suggest a placement of the O/M boundary ~55 mcd in polarity Subchron C6Cn.2r at Site 1219, where the range of *Sphenolithus delphix* was observed. On the Cande and Kent (1995) timescale, an age estimate of 24.28 ± 0.05 Ma is obtained for the base of *S. delphix* at Site 1219. With conversion to the orbitally tuned timescale of Shackleton et al. (2000) by subtracting 0.9 m.y. from the Cande and Kent (1995) timescale estimate, an age of 23.38 Ma is obtained for the base of *S. delphix*. This value is 0.14 m.y. older than the orbitally tuned estimate for this datum derived from the eastern South Atlantic (DSDP Site 522) and the western equatorial Atlantic (Sites 926, 928, and 929) (Shackleton et al., 2000). Yet, the calibration of the *S. delphix* event to the geomagnetic polarity record is remarkably consistent in Chron C6Cn.2, from the South Atlantic Ocean to the Mediterranean region (Raffi, 1999) and to the tropical Pacific Ocean (Site 1219).

Eocene–Oligocene Transition

The Eocene–Oligocene transition at Site 1219 is associated with an abrupt lithologic change from radiolarian clays below to nannofossil

ooze above. This transition is similar to but sharper than that observed at Site 1218, presumably reflecting higher rates of carbonate dissolution at Site 1219 (the contemporaneous paleowater depth is ~400 m deeper at Site 1219 than Site 1218). Together with drilling results from Site 1217, this finding offers exciting prospects for shore-based investigation of the first Pacific Ocean depth and latitudinal transect across this important paleoceanographic boundary.

Eocene Sediments

The Eocene sediments at Site 1219 are dominated by radiolarian oozes from the period between ~45 Ma through the E/O boundary. Nevertheless, there are intervals of carbonate in the section, most notably at ~40.5 Ma but also at ~38.3 and ~43.5 Ma. These carbonate units can be detected by density, reflectivity, velocity, and LAS mineralogy as well as by chemical analyses and microscopic examination of the sediments. The 40.5-Ma event and 38-Ma event are also found at Site 1218, but the oldest of these events is older than the base of the sediment column at Site 1218.

The lower middle Eocene interval is represented by cherty sediments that were not recovered by drilling. This is one of five sites on the 56-Ma transect in which we encountered cherts in roughly the same interval. Immediately below the cherts at Site 1219 are zeolitic clays barren of microfossils, suggesting that the chertified interval was deposited slowly. The uppermost lower Eocene chalk in contact with the zeolitic clay has an age of ~53 Ma (nannofossil Subzone CP9b), whereas the lowermost radiolarian ooze above the cherty interval is dated as ~46 Ma. Thus, the average sedimentation rate over the 10-m-thick cherty interval could be as low as 1.4 m/m.y. The interval has been condensed by diagenesis, but an estimate of the bulk MAR using sediment density measured by downhole logging (~2 g/cm^3) is about half that of the sediments immediately above it.

The lower Eocene chalks were poorly recovered but appear to be typical basal carbonate-rich sediments. There is little evidence of hydrothermal sediments in the chalks.

Site 1220

Site 1220 (10°10.601′N, 142°45.491′W) forms a southerly component of the 56-Ma transect to be drilled during Leg 199. It is situated halfway between the Clipperton and Clarion Fracture Zones at a water depth of 5218 m in typical abyssal hill topography. On the basis of regional magnetic anomalies, we anticipated basement age at Site 1220 to be equivalent to Anomaly An25n (~56 Ma; Cande et al., 1989), slightly older than at Site 1219.

Based upon a fixed hotspot model (Gripp and Gordon, 1990, for the 0- to 5-Ma Pacific hotspot rotation pole; Engebretson et al., 1985, for older poles) Site 1220 should have been located ~3°S of the equator at 56 Ma and in an equatorial position at 40 Ma. Thus, Site 1220 should have been situated beneath the South Equatorial Current in the early Eocene. Site 1220 will act as a deeper analog to Site 1218. Both sites are thought to have been located in an equatorial position at ~40 Ma, but Site 1220 was ~400 m deeper at this time.

Three holes were drilled at Site 1220. Hole 1220A was terminated when an APC core jammed in the BHA at ~100 mbsf, but basement was reached in Holes 1220B and 1220C at ~200 mbsf. Cores from Site 1220 overlap and form a continuous sedimentary sequence down to ~144

mcd (base of Core 199-1220B-10H; Figs. F11, p. 32, and F12, p. 33, in the "Site 1215" chapter). The sedimentary sequence recovered at the site is divided into five major sedimentary units. The uppermost unit (~0–19 mbsf) consists of very dark grayish brown clay with zeolites and is underlain by a lower Miocene–Oligocene Unit II (~19–40 mbsf) of radiolarian and nannofossil oozes with varying clay content. The underlying Oligocene radiolarian and nannofossil oozes of Unit III (~40–70 mbsf) are notable by the presence of a significant (~15%–45%) diatom component toward the base. Unit IV (~70–185 mbsf) consists of upper Eocene radiolarian oozes with clay and middle–lower Eocene chert with clayey radiolarian ooze. These sediments are underlain by a lower Eocene–upper Paleocene unit (~185–200 mbsf) of partially dolomitized nannofossil ooze, radiolarian nannofossil ooze, radiolarian ooze, calcareous chalk, and black clay atop an aphanitic to fine-grained phaneritic basalt.

Paleomagnetic data from Site 1220 gave excellent results and a reliable record of geomagnetic reversals from the early to the middle Eocene to the early Miocene. The composite depth record from Holes 1220A, 1220B, and 1220C shows a remarkable match of the cores between the different holes. In fact, the virtual geomagnetic pole (VGP) latitude changes were used as a basis to help fit the cores to the mcd scale. Correlation of the magnetic stratigraphy at Site 1220 to the geomagnetic polarity timescale (GPTS) shows a record that spans from the top of Chron C21n to Subchron C6An.1n (~20.5–46.3 Ma).

Biostratigraphic results indicate that we recovered a nearly complete sequence of lower Miocene–lower Eocene radiolarian zones at Site 1220, interrupted only by a poorly recovered chert sequence from the uppermost lower Eocene and the lowermost middle Eocene. Calcareous fossils are generally poorly preserved or absent through much of the sequence. Calcareous nannofossils are sufficiently well preserved in the lowermost Miocene and Oligocene to provide a basic zonation. Planktonic foraminifers are almost entirely absent above the lower Eocene, but dissolution-resistant species allow the lower/upper Oligocene boundary to be approximated. Both planktonic foraminifers and calcareous nannofossils provide a detailed zonation of a condensed sequence of lower Eocene nannofossil oozes and chert in the basal 10 m of Site 1220. The extinction of Paleocene benthic foraminifers, the appearance of the nannofossil genus *Rhomboaster,* the extinction of the nannofossil genus *Fasciculithus,* and the presence of excursion fauna of planktonic foraminifers provide a detailed biostratigraphy of the P/E boundary in Unit V. The nannofossil events occur 0.8–1.4 m above the extinction of Paleocene benthic foraminifers. The excursion fauna of planktonic foraminifers is present in sediments below the level of the benthic foraminifer extinction (sediments immediately overlying basalt). Thus, none of these events are precisely synchronous with the benthic foraminifer extinction, the marker we used for the P/E boundary, at this site.

Interstitial pore water profiles from Site 1220 are very similar to the profiles of all other Leg 199 sites (except Site 1219) and primarily reflect minor organic matter degradation, the dissolution of biogenic silica, and minor alteration of underlying basalt. The bulk geochemistry of the sediments from Site 1220 reflect the shifts in lithology between sediments dominated by silica and carbonate.

Physical properties of the sediments also primarily reflect lithology. The carbonate sediments are higher in density, lower in porosity, and lower in magnetic susceptibility than the clay or radiolarian ooze lithologies. The radiolarian-rich sediments of Units II and IV are marked by

high porosities, which average 88% and 85%, respectively. The radiolarian oozes maintain their porosity despite burial. The Eocene radiolarian oozes have the highest *P*-wave velocities of the unconsolidated sediment lithologies.

Highlights

Magnetic Reversal Stratigraphy

The clean record of magnetic reversal history from Site 1220 (for the entire APC-cored sediment section; 0–150 mbsf) spans the lower Miocene to lower–middle Eocene (Subchron C6An.1n to the top of Chron C21; 20.05–46.3 Ma). This record is remarkable for a tropical site and will provide invaluable time control for calibration of radiolarian biostratigraphy. Because there are cyclic variations in radiolarian content of the Site 1220 Eocene section presumably driven by orbital forcing of insolation, this record could be highly important for orbital tuning of the geomagnetic polarity timescale from the middle Eocene to the early Miocene.

E/O Boundary

A combination of magnetostratigraphy and nannofossil biostratigraphy indicates that we recovered a further E/O boundary at Site 1220 (~70 mbsf). Shore-based work on this section, together with those recovered at Sites 1217, 1218, and 1219, will allow us to improve existing constraints on the links between global cooling, Antarctic ice sheet growth, and a deepening CCD across this important paleoceanographic boundary.

P/E Boundary

In Hole 1220B, just above basement basalt, we recovered a lithologically striking interval of calcareous chalk and clay (199–200 mbsf). Based on biostratigraphic data, this sequence represents the P/E boundary. Layers of calcareous chalk and clay display a large range in composition and color downcore. Alternating intervals of white and very pale-brown calcareous chalk occur between 198.9 and 199.4 mbsf and contain a minor amount (5%–10%) of poorly preserved nannofossils. White layers occur between 199.15 and 199.23 mbsf and contain 15%–30% planktonic foraminifers. The sediments below this interval consist of faintly banded, dark yellowish brown calcareous chalk but are barren of microfossils. Dolomite (up to 10%) and clay (10%–35%) also occur in this lithology. Below 199.50 mbsf is a 4-cm-thick layer of very dark-brown (7.5YR 2.5/3) calcareous chalk underlain by a black clay. Major components of both sediments are dolomite, iron manganese oxides, and clay. Volcanic glass occurs as a minor component. Dolomite content decreases over the interval from 199.52 to 199.54 mbsf, and no calcareous or siliceous fossils were observed in corresponding smear slides. Directly beneath the black clay is a 4.5-cm-thick interval of yellowish red calcareous chalk. Within this interval is a 1-cm-thick brownish yellow layer of calcareous chalk. Sediments in the yellowish red layers are weakly laminated and contain clay, dolomite, calcite, and a minor percentage of nannofossils. Iron manganese oxides and opaque minerals are minor components. The brownish yellow chalk layer contains clay, dolomite, iron manganese oxides, volcanic glass, and abundant small mottles. Nannofossils are rare in these layers.

The base of the sedimentary section contains a 9-cm-thick interval of brownish yellow clayey calcareous chalk (199.59–199.68 mbsf) with

thin black laminations. Dolomite comprises up to 10% of these sediments. Zeolites and nannofossils also occur as minor components. Iron manganese oxides are rare. Laminations contain clay, iron manganese oxides, dolomite, zeolites, and small amounts of volcanic ash and are barren of calcareous fossils.

Site 1221

Site 1221 (Fig. F1, p. 25, in the "Site 1221" chapter); 12°01.999′N, 143°41.572′W) forms an equatorial component of the 56-Ma transect drilled during Leg 199. It is situated about three quarters of the way between the Clipperton and Clarion Fracture Zones in typical abyssal hill topography at a water depth of 5175 m. On the basis of regional seafloor magnetic anomalies, we anticipated basement age at Site 1221 to be equivalent to Anomaly An25n (~56 Ma; Cande et al., 1989), about the same age as Site 1220. At the outset of drilling at Site 1221, our estimate for total sediment thickness was ~150 m (Fig. F2, p. 26, in the "Site 1221" chapter).

Based upon a fixed hotspot model (Gripp and Gordon, 1990, for the 0- to 5-Ma Pacific hotspot rotation pole; Engebretson et al., 1985, for older poles) Site 1221 should have been located ~1° south of the equator at 56 Ma, in an equatorial position at ~50 Ma and ~2° north at 40 Ma. Thus, Site 1221 should have been situated underneath the early Eocene equivalent of the South Equatorial Current.

Four holes were drilled at Site 1221. Hole 1221A was abandoned because of a stuck XCB barrel that resulted in a pipe trip to clear the BHA. Hole 1221B recored the Oligocene interval at the top of the sediment column, whereas Hole 1221C was cored to cover the major gaps in the upper sediment column and then cored continuously to basement. Hole 1221D was drilled to obtain a second copy of the lower Eocene and Paleocene sediments.

The heave of the vessel frequently exceeded 5 m while we were drilling at Site 1221. The ship heave compromised the quality and recovery of the core. The uppermost ~20 mbsf encountered severe flow-in problems, whereas in the remaining intervals, the often soupy nature of the sediment (radiolarian ooze) resulted in MST data that were not suitable for correlation purposes, with the exception of the P/E boundary interval. A continuous sediment column could not be correlated below 19.5 mcd.

The sediment column is a variation of lithologies seen at other Leg 199 sites. A very thin clay and radiolarian ooze lithologic unit overlies lower Oligocene nannofossil ooze, terminated by an abrupt transition to clay rapidly grading to radiolarian ooze. The abrupt transition is typical of the E/O boundary. At Site 1221, however, latest Eocene and earliest Oligocene time is represented by a hiatus of ~1 m.y. in extent. The middle and upper Eocene radiolarian ooze section is the thickest of any site of Leg 199. Deposition of the radiolarian ooze was highest in the period between 45 and 43 Ma, when sedimentation rates reached 18 m/m.y.

A chert-rich section covering the time interval from ~48 Ma (radiolarian Zone RP11) to 53.8 Ma (nannofossil Subzone CP9a) lies beneath the radiolarian ooze. Although only chert was recovered, coring times were relatively short, suggesting a significant amount of radiolarian ooze or clay is also present. Hole 1221C drilled somewhat faster than Hole 1221D, indicating some variability in the thickness and areal extent of the chert. In the recovered sediments below the chert unit, clay

layers in Hole 1221C can be correlated to clay layers in Hole 1221D. Beneath the chert-rich interval are nannofossil chalks of early Eocene–Paleocene age that comprise the basal sedimentary unit. Within this basal chalk, we recovered two copies of the P/E boundary interval. The P/E boundary interval is recognizable by a multicolored clay-rich unit remarkably similar in structure to the P/E boundary interval at Site 1220, 206 km to the south. The lowermost chalks above basement were dated at 56.5–57 Ma with foraminifers and nannofossils.

Physical properties of the sediments follow lithology. The densest unit is the lower Eocene chalk (~1.6–1.8 g/cm^3) followed by the upper clays and nannofossil ooze. The radiolarian ooze sediments have the lowest wet bulk densities (~1.14 g/cm^3) and the highest porosities (~84%), as well as the highest velocities of the unconsolidated sediments (1530–1550 m/s).

Biostratigraphic analyses indicate that Site 1221 contains a continuous sequence of radiolarian-bearing sediments from the early Oligocene–early Eocene. The uppermost sequence contains considerable quantities of reworked middle Eocene radiolarians, whereas the interval from ~7 to 111 mbsf is almost exclusively brown radiolarian ooze with a sugary texture. No radiolarians were recovered in the chert-rich interval except in the core catcher of Core 199-1221C-10X at a depth of 141 mbsf. These radiolarians are from the late Paleocene to the early Eocene Zone RP7. No radiolarians are found in the basal chalk.

The sediments of Site 1221 contain calcareous microfossils in only the uppermost and lowermost units. Calcareous microfossils are completely absent in the siliceous sediments between ~7 and ~111 mbsf, and biostratigraphic control through this interval was provided entirely by radiolarians. The carbonate content of sediments increased in the basal reaches of Holes 1221C and 1221D, and nannofossil and planktonic foraminiferal biostratigraphy allow basic zonation of a condensed sequence of lower Eocene nannofossil ooze and chert. Section 199-1221C-11X-3 contains an interval of dramatic and colorful banding, the base of which, as at Site 1220, corresponds to the extinction of Paleocene benthic foraminifers and, therefore, the P/E boundary. Preservation of calcareous microfossils improves below the P/E boundary, and planktonic foraminifers and nannofossils allow a detailed zonation of upper Paleocene nannofossil ooze and clay. Calcareous benthic foraminiferal assemblages occur only in the basal sediments below 140 mbsf. These assemblages are moderately well preserved, but the presence of small calcite microcrystals on the surfaces of the tests indicate some diagenetic alteration.

Interstitial pore water profiles from Site 1220 are very similar to the profiles of all other Leg 199 sites except Site 1219 and primarily reflect minor organic matter degradation, the dissolution of biogenic silica, and minor alteration of underlying basalt. The bulk geochemistry of the sediments from Site 1221 reflect the shifts in lithology between sediments dominated by silica and carbonate.

Highlights

P/E Boundary

The P/E boundary was recovered twice (intervals 199-1221C-11X-3, 50–90 cm, and 199-1221D-4X-2, 70–125 cm). The two intervals are very similar, with the interval in Hole 1221D appearing slightly expanded relative to that in Hole 1221C and exhibiting more disturbance.

The benthic foraminiferal fauna were examined in small surface scrapes prior to more complete shore-based analysis. The first occurrence of Eocene benthic foraminifers is at 50 cm in Section 199-1221C-11X-3, whereas the last occurrence of Paleocene forms is at ~91 cm in the same section.

The Site 1221 P/E boundary interval appears remarkably similar to that recovered at Site 1220. Distinctive brown, pink, black, and dark-brown layering can be correlated between the two sites 206 km apart.

Site 1222

Site 1222 (13°48.98′N, 143°53.35′W) is situated ~2° of south of the Clarion Fracture Zone in typical abyssal hill topography at a water depth of 4989 m. On the basis of regional seafloor magnetic anomalies, we anticipated basement age at Site 1222 to be equivalent to Anomaly An25 (~56–57 Ma; Cande et al., 1989), slightly older than at Site 1219. At the onset of drilling at Site 1222, our estimate for total sediment thickness was ~115 m; based upon a fixed hotspot model (Gripp and Gordon, 1990, for the 0- to 5-Ma Pacific hotspot rotation pole; Engebretson et al., 1985, for older poles) Site 1222 should have been located ~1° north of the equator at 56 Ma and ~4°N at 40 Ma.

Two holes were drilled at Site 1222. Hole 1222A was drilled to basement, which was reached at ~98 mbsf. Hole 1222B recored the APC-suitable portion of the sediment column (to ~60 mbsf). The sediment column at Site 1222 contains a sequence of lithologies significantly different to that found at other Leg 199 sites. Site 1222 recovered a 97.8-m-thick section dominated by clay-rich lithologies and chert. Unit I consists of an ~55-m-thick yellowish brown to dark gray brown clay with zeolites grading to radiolarian clay. A thin interval of diatomaceous clay occurs near 17 mbsf (Sections 199-1222A-3H-2 to 3H-4). Within the diatom clay is an interval with unusual layers of laminated diatom ooze that contain a nearly pure diatom component of Pliocene age. Laminations are mainly white to olive. Diatom frustules in some laminae contain significant pyrite making them appear very dark gray to black. A sharp contact exists at the base of the diatom ooze interval and the underlying clay of Subunit IA. In Hole 1222A, this contact also contains a large (5-cm diameter) botryoidal manganese nodule. Unit II, ~3 m thick, consists of dark-brown to brown nannofossil clay grading downcore to yellowish brown nannofossil ooze. Very pale brown mottles are common. Nannofossil content (estimated from smear slides) gradually increases from 30% in the upper portion to 80% near the base of the unit. Unit III consists of an ~8-m-thick sequence dominated by clay with iron oxides and zeolites. Unit III is underlain by a thick (>30 m) poorly recovered sequence of massive chert that, in turn, overlies basement basalt.

Radiolarians provide the biostratigraphic framework for Site 1222. Planktonic foraminifers are completely dissolved in all samples investigated. Calcareous nannofossils of early Oligocene age occur in Unit II and early Eocene nannofossils were found in chalk attached to a piece of chert occur just above basement. This large chert nodule is rimmed with very pale brown nannofossil chalk that provides datums indicating an early Eocene age (NP10). The biostratigraphic distribution of radiolarians suggests massive reworking and mixed Pliocene assemblages in the uppermost two and a half cores, between ~0 and 21 mbsf. The following two cores, between ~21 mbsf and 40 mbsf, contain upper and lower Miocene radiolarian assemblages. Two cores between ~40 and 60

mbsf hold upper and lower Oligocene radiolarian assemblages. Nannofossils are present between ~55 mbsf and 60 mbsf, supporting the radiolarian biostratigraphy. This upper part of the section at Site 1222 appears to contain several breaks in sedimentation. A major hiatus occurs between the lowermost Oligocene and the middle Eocene, having a duration on the order of ~5–6 m.y.

It was possible to construct a continuous spliced record from Site 1222 down to 34.44 mbsf (37.88 mcd), below which it was possible to align most cores from the two drilled holes to each other, but without continuous overlap. Cores 199-1222A-7H and 199-1222B-7H, however, showed good overlap and allowed the splicing of an additional ~13 m from ~59 to 72 mcd.

The paleomagnetic data from lithologic Subunit IA, down to ~40 mbsf, are not interpretable, except for the very top of the Hole 1222A. A large group of ChRM directions show relatively high magnetic inclinations after demagnetization especially in the most clay-rich lithologic units. The cause of the steep inclinations is unclear and might be indicative of unrecognized deformation and physical grain rotation caused by drilling. A preliminary correlation of the magnetic stratigraphy to the GPTS shows that we were able to identify the bottom of polarity Chron C1n (Brunhes) at the very top of the section. Below 40 mcd, we note magnetic reversals but can only identify Chrons C6Cn to C11n with any confidence.

The pore water profiles from Site 1222 primarily reflect minor organic matter degradation and the dissolution of biogenic silica. Most of the dissolved chemical constituents show a lack of gradient with depth and values similar to or slightly higher than seawater.

REFERENCES

Andreasson, F.P., and Schmitz, B., 1998. Tropical Atlantic seasonal dynamics in the early middle Eocene from stable oxygen and carbon isotope profiles of mollusk shells. *Paleoceangraphy,* 13:183–192.

Aubry, M.-P., Berggren, W.A., Stott, L., and Sinha, A., 1996. The upper Paleocene–lower Eocene stratigraphic record and the Paleocene/Eocene boundary carbon isotope excursion: implications for geochronology. *In* Knox, R.W.O.B., Corfield, R.M., and Dunay, R.E. (Eds.), *Correlation of the Early Paleogene in Northwestern Europe.* Spec. Publ.—Geol. Soc. Am., 101:353–380.

Aubry, M.-P., Berggren, W.A., and Lucas, S.G. (Eds.), 1998. *Late Paleocene–Early Eocene Climatic and Biotic Events in the Marine and Terrestrial Records:* New York (Columbia Univ. Press).

Bains, S., Corfield, R.M., and Norris, R.D., 1999. Mechanisms of climate warming at the end of the Paleocene. *Science,* 285:724–727.

Bains, S., Norris, R.D., Corfield, R.M., and Faul, K.L., 2000. Termination of global warmth at the Palaeocene–Eocene boundary through productivity feedback. *Nature,* 407:171–174.

Barron, E.J., and Washington, W.M., 1984. The role of geographic variables in explaining paleoclimates: results from Cretaceous climate model sensitivity studies. *J. Geophys. Res.,* 89:1267–1279.

Bartek, L.R., Sloan, L.C., Anderson, J.B., and Ross, M.I., 1992. Evidence from the antarctic continental margin of late Paleogene ice sheets: a manifestation of plate reorganization and synchronous changes in atmospheric circulation over the emerging Southern Ocean? *In* Prothero, D.R., and Berggren, W.A. (Eds.), *Eocene–Oligocene Climate and Biotic Evolution:* Princeton (Princeton Univ. Press), 245–271.

Berger, W.H., and Winterer, E.L., 1974. Plate stratigraphy and the fluctuating carbonate line. *In* Hsü, K.J., and Jenkyns, H.C. (Eds.), *Pelagic Sediments on Land and Under the Sea.* Spec. Publ.—Int. Assoc. Sedimentol., 1:11–48.

Bice, K.L., and Marotzke, J., 2001. Numerical evidence against reversed thermohaline circulation in the warm Paleocene/Eocene ocean. *J. Geophys. Res.,* 106:11529–11542.

Bloomer, S.F., Mayer, L.A., and Moore, T.C., 1995. Seismic stratigraphy of the eastern equatorial Pacific Ocean: paleoceanographic implications. *In* Pisias, N.G., Mayer, L.A., Janecek, T.R., Palmer-Julson, A., and van Andel, T.H. (Eds.), *Proc. ODP, Sci. Results,* 138: College Station, TX (Ocean Drilling Program), 537–553.

Bottomley, R., Grieve, R., York, D., and Masaitis, V., 1997. The age of the Popigai impact event and its relation to events at the Eocene/Oligocene boundary. *Nature,* 388:365–368.

Bralower, T.J., Zachos, J.C., Thomas, E., Parrow, M., Paull, C.K., Kelly, D.C., Premoli Silva, I., Sliter, W.V., and Lohmann, K.C., 1995. Late Paleocene to Eocene paleoceanography of the equatorial Pacific Ocean: stable isotopes recorded at Ocean Drilling Program Site 865, Allison Guyot. *Paleoceanography,* 10:841–865.

Brass, G.W., Southam, J.R., and Peterson, W.H., 1982. Warm saline bottom water in the ancient ocean. *Nature,* 296:620–623.

Brinkhuis, H., and Biffi, U., 1993. Dinoflagellate cyst stratigraphy of the Eocene/Oligocene transition in central Italy. *Mar. Micropaleontol.,* 22:131–183.

Browning, J.V., Miller, K.G., and Pak, D.K., 1996. Global implications of lower to middle Eocene sequence boundaries on the New Jersey Coastal Plain—the Icehouse cometh. *Geology,* 24:639–642.

Cande, S.C., and Kent, D.V., 1995. Revised calibration of the geomagnetic polarity timescale for the Late Cretaceous and Cenozoic. *J. Geophys. Res.,* 100:6093–6095.

Cande, S.C., LaBrecque, J.L., Larson, R.L., Pitmann, W.C., III, Golovchenko, X., and Haxby, W.F., 1989. Magnetic lineations of the world's ocean basins. *AAPG,* 13:1.

Crowley, T., 1991. Past CO_2 changes and tropical sea surface temperatures. *Paleoceanography,* 6:387–394.

Crowley, T.J., and Zachos, J.C., 2000. Comparison of zonal temperature profiles for past warm time periods. *In* Huber, B.T., MacLoed, K.G., and Wing, S.L. (Eds.), *Warm Climates in Earth History:* Cambridge (Cambridge Univ. Press), 79–131.

DeConto, R.M., Thompson, S.L., and Pollard, D., 2000. Recent advances in paleoclimate modeling: toward better simulations of warm paleoclimates. *In* Huber, B.T., MacLeod, K.G., and Wing, S.L. (Eds.), *Warm Climates in Earth History:* Cambridge (Cambridge Univ. Press), 21–49.

Diester-Haass, L., and Zahn, R., 2001. Paleoproductivity increase at the Eocene–Oligocene climatic transition: ODP/DSDP Sites 763 and 592. *Palaeogeogr., Palaeoclimatol., Palaeoecol.,* 172:153–170.

Dickens, G.R., 2001. Carbon addition and removal during the Late Palaeocene Thermal Maximum: basic theory with a preliminary treatment of the isotope record at ODP Site 1051, Blake Nose. *In* Kroon, D., Norris, R.D., and Klaus, A. (Eds.), *Western North Atlantic Paleogene and Cretaceous Paleoceanography,* Spec. Publ.—Geol. Soc. London, 183:293–306.

Dickens, G.R., Castillo, M.M., and Walker, J.G.C., 1997. A blast of gas in the latest Paleocene: simulating first-order effects of massive dissociation of oceanic methane hydrate. *Geology,* 25:259–262.

Dickens, G.R., O'Neil, J.R., Rea, D.K., and Owen, R.M., 1995. Dissociation of oceanic methane hydrate as a cause of the carbon isotope excursion at the end of the Paleocene. *Paleoceanography,* 10:965–971.

Engebretson, D.C., Cox, A., and Gordon, R.G., 1985. *Relative Motions Between Oceanic and Continental Plates in the Pacific Basin*. Spec. Pap.—Geol. Soc. Am., 206.

Farley, K.A., Montanari, A., Shoemaker, E.M., and Shoemaker, C.S., 1998. Geochemical evidence for a comet shower in the late Eocene. *Science,* 280:1250–1253.

Gersonde, R., Hodell, D.A., Blum, P., et al., 1999. *Proc. ODP, Init. Repts.,* 177 [CD-ROM]. Available from: Ocean Drilling Program, Texas A&M University, College Station, TX 77845-9547, U.S.A.

Gripp, A.E., and Gordon, R.G., 1990. Current plate velocities relative to the hotspots incorporating the NUVEL-1 global plate motion model. *Geophys. Res. Lett.,* 17:1109–1112.

Hesselbo, S.P., Grocke, D.R., Jenkyns, H.C., Bjerrum, C.J., Farrimond, P., Morgans Bell H.S., and Green, O.R., 2000. Massive dissociation of gas hydrate during a Jurassic oceanic anoxic event. *Nature,* 406:392–395.

Hilgen, F.J., 1991a. Astronomical calibration of Gauss to Matuyama sapropels in the Mediterranean and implication for the geomagnetic polarity time scale. *Earth Planet. Sci. Lett.,* 104:226–244.

————, 1991b. Extension of the astronomically calibrated (polarity) time scale to the Miocene/Pliocene boundary. *Earth Planet. Sci. Lett.,* 107:349–368.

Hine, A.C., Feary, D.A., Malone, M.J., Andres, M., Betzler, C., Brooks, G.R., Brunner, C.A., Fuller, M.D., Holbourn, A.E., Huuse, M., Isern, A.R., James, N.P., Ladner, B.C., Li, Q., Machiyama, H., Mallinson, D.J., Matsuda, H., Mitterer, R.M., Molina, G.R.S., Robin, C., Russell, J.L., Shafik, S., Simo, J.A.T., Smart, P.L., Spence, G.H., Surlyk, F., Swart, P.K., and Wortmann, U.G., 1999. Research in the Great Australian Bight yields exciting early results. *Eos,* 80:521.

Hovan, S.A., and Rea, D.K., 1992. Paleocene/Eocene boundary changes in atmospheric and oceanic circulation: a Southern Hemisphere record. *Geology,* 20:15–18.

Huber, M., and Sloan, L.C., 2000. Climatic response to tropical sea surface temperature changes on a "greenhouse" Earth. *Paleoceanography,* 15:443–450.

Janecek, T.R., and Rea, D.K., 1983. Eolian deposition in the northeast Pacific Ocean: Cenozoic history of atmospheric circulation. *Geol. Soc. Am. Bull.,* 94:730–738.

Kaiho, K., Arinobu, T., Isihwatar, R., Morgans, H.E.G., Okada, H., Takeda, N., Tazaki, K., Zhou, G., Kajiwara, Y., Matsumoto, R., Hirai, A., Niitsuma, N., and Wada, H.,

1996. Latest Paleocene benthic foraminiferal extinction and environmental changes at Tawanui, New Zealand. *Paleoceanography,* 11:447–465.

Katz, M.E., Pak, D.K., Dickens, G.R., and Miller, K.G., 1999. The source and fate of massive carbon input during the Latest Paleocene Thermal Maximum. *Science,* 286:1531–1533.

Keller, G., 1986. Stepwise mass extinctions and impact events: late Eocene to early Oligocene. *Mar. Micropaleontol.,* 10:267–293.

Kelly, D.C., Bralower, T.J., and Zachos, J.C., 1998. Evolutionary consequences of the Latest Paleocene Thermal Maximum for tropical planktonic foraminifera. *Palaeogeogr., Palaeoclimatol., Palaeoecol.,* 141:139–161.

Kelly, D.C., Bralower, T.J., Zachos, J.C., Premoli Silva, I., and Thomas, E., 1996. Rapid diversification of planktonic foraminifera in the tropical Pacific (ODP Site 865) during the last Paleocene Thermal Maximum. *Geology,* 24: 423–426.

Kennett, J.P., and Barker, P.F., 1990. Latest Cretaceous to Cenozoic climate and oceanographic developments in the Weddell Sea, Antarctica: an ocean-drilling perspective. *In* Barker, P.F., Kennett, J.P., et al., *Proc. ODP, Sci. Results,* 113: College Station, TX (Ocean Drilling Program), 937–960.

Kennett, J.P., and Stott, L.D., 1991. Abrupt deep-sea warming, paleoceanographic changes and benthic extinctions at the end of the Paleocene. *Nature,* 353:225–229.

Koch, P.L., Zachos, J.C., and Gingerich, P.D., 1992. Correlation between isotope records in marine and continental carbon reservoirs near the Palaeocene/Eocene boundary. *Nature,* 358:319–322.

Koeberl, C., Poag, C.W., Reimold, W.U., and Brandt, D., 1996. Impact origin of the Chesapeake Bay structure and the source of the North American tectites. *Science,* 271:1263–1266.

Lear, C.H., Elderfield, H., and Wilson, P.A., 2000. Cenozoic deep-sea temperatures and global ice volumes from Mg/Ca in benthic foraminiferal calcite. *Science,* 287:269–272.

Leinen, M., 1979. Biogenic silica accumulation in the central equatorial Pacific and its implications for Cenozoic paleoceanography (Pt. 2). *Geol. Soc. Am. Bull.,* 90:1310–1376.

Lyle, M., 1992. Composition maps of surface sediments of the eastern tropical Pacific Ocean. *In* Mayer, L., Pisias, N., Janecek, T., et al., *Proc. ODP, Init. Repts.,* 138 (Pt. 1): College Station, TX (Ocean Drilling Program), 101–115.

Manabe, S., and Bryan, K., 1985. CO_2-induced change in a coupled ocean-atmosphere model and its paleoclimatic implications. *J. Geophys. Res.,* 90:11689–11708.

Matthews, R.K., and Poore, R.Z., 1980. Tertiary $\delta^{18}O$ record and glacio-eustatic sea-level fluctuations. *Geology,* 8:501–504.

Mayer, L., Pisias, N., Janecek, T., et al., 1992. *Proc. ODP, Init. Repts.,* 138 (Pts. 1 and 2): College Station, TX (Ocean Drilling Program).

Mayer, L.A., Shipley, T.H., Theyer, F., Wilkens, R.H., and Winterer, E.L., 1985. Seismic modeling and paleoceanography at Deep Sea Drilling Project Site 574. *In* Mayer, L., Theyer, F., Thomas, E., et al., *Init. Repts. DSDP,* 85: Washington, (U.S. Govt. Printing Office), 947–970.

Mayer, L.A., Shipley, T.H., and Winterer, E.L., 1986. Equatorial Pacific seismic reflectors as indicators of global oceanographic events. *Science,* 233:761–764.

Miller, K.G., Fairbanks, R.G., and Mountain, G.S., 1987. Tertiary oxygen isotope synthesis, sea-level history, and continental margin erosion. *Paleoceanography,* 2:1–19.

Miller, K.G., Feigenson, M.D., Kent, D.V., and Olsson, R.K., 1988. Upper Eocene to Oligocene isotope ($^{87}Sr/^{86}Sr$, $\delta^{18}O$, $\delta^{13}C$) standard section, Deep Sea Drilling Project Site 522. *Paleoceanography,* 3:223–233.

Miller, K.G., Kent, D.V., Brower, A.N., Bybell, L.M., Feigenson, M.D., Olsson, R.K., and Poore, R.Z., 1990. Eocene–Oligocene sea-level changes on the New Jersey coastal plain linked to the deep-sea record. *Geol. Soc. Am. Bull.,* 102:331–339.

Miller, K.G., Mountain, G.S., Blum, P., Gartner, S., Alm Per, G., Aubry, M.-P., Burckle, L.H., Guerin, G., Katz, M.E., Christensen, B.A., Compton, J., Damuth, J.E., Deconinck, J.F., de Verteuil, L., Fulthorpe, C.S., Hesselbo, S.P., Hoppie, B.W., Kotake, N., Lorenzo, J.M., McCracken, S., McHugh, C.M., Quayle, W.C., Saito, Y., Snyder, S.W., ten Kate, W.G., Urbat, M., Van Fossen, M.C., Vecsei, A., Sugarman, P.J., Mullikin, L., Pekar, S., Browning, J.V., Liu, C., Feigenson, M.D., Goss, M., Gwynn, D., Queen, D.G., Powars, D.S., Heibel, T.D., and Bukry, D., 1996. Drilling and dating New Jersey Oligocene–Miocene sequences: ice volume, global sea level, and Exxon records. *Science,* 271:1092–1095.

Miller, K.G., Mountain, G.S., Browning, J.V., Kominz, M., Sugarman, P.J., Christie-Blick, N., Katz, M.E., and Wright, J.D., 1998. Cenozoic global sea level, sequences, and the New Jersey transect: results from coastal plain and continental slope drilling. *Rev. Geophys.,* 36:569–601.

Miller, K.G., Thompson, P.R., and Kent, D.V., 1993. Integrated late Eocene–Oligocene stratigraphy of the Alabama coastal plain: correlation of hiatuses and stratal surfaces to glacioeustatic lowerings. *Paleoceanography,* 8:313–331.

Miller, K.G., Wright, J.D., and Fairbanks, R.G., 1991. Unlocking the Ice House: Oligocene–Miocene oxygen isotopes, eustasy, and margin erosion. *J. Geophys. Res.,* 96:6829–6848.

Mitchell, N.C., 1998. Modeling Cenozoic sedimentation in the central equatorial Pacific and implications for true polar wander. *J. Geophys. Res.,* 103(B8):17749–17766.

Moore, T.C., Jr., 1969. Radiolaria: change in skeletal weight and resistance to solution. *Geol. Soc. Am. Bull.,* 80:2103–2108.

Moore, T.C., Jr., Rea, D.K., Lyle, M., and Liberty, L.M., 2002. Equatorial Ocean circulation in an extreme warm climate: *Paleoceanography,* 17:5-1–5-6.

Norris, R.D., and Röhl, U., 1999. Carbon cycling and chronology of climate warming during the Palaeocene/Eocene transition. *Nature,* 401:775–778.

Opdyke, B.N., Erba, E., and Larson, R.L., 1999. Hot LIPs and mantle methane. *Eos,* 80:486–487.

Pälike, H., Shackleton, N.J., and Röhl, U., 2001. Astronomical forcing in late Eocene marine sediments. *Earth Planet. Sci. Lett.,* 193:589–602.

Pearson, P.N., Ditchfield, P.W., Singano, J., Harcourt-Brown, K.G., Nicholas, C.J., Olsson, R.K., Shackleton, N.J., and Hall, M.A., 2001. Warm tropical sea surface temperatures in the Late Cretaceous and Eocene epochs. *Nature,* 413:481–487.

Pekar, S.F., Miller, K.G., and Kominz, M.A., 2000. Reconstructing the stratal geometry of latest Eocene to Oligocene sequences in New Jersey: resolving a patchwork distribution into a clear pattern of progradation. *Sediment. Geol.,* 134:93–109.

Petronotis, K.E., Gordon, R.G., and Acton, G.D., 1994. A 57 Ma Pacific plate paleomagnetic pole determined from a skewness analysis of crossings of marine magnetic anomaly 25r, *Geophys. J. Int.,* 118:529-554.

Premoli Silva, I., Coccioni, R., and Montanari, A. (Eds.), 1988. *The Eocene/Oligocene Boundary in the March-Umbria Basin (Italy).* Spec. Publ.—Int. Subcomm. on Paleogene Stratigr., Eocene/Oligocene Boundary Meet., Ancona, 1987.

Raffi, I., 1999. Precision and accuracy of nannofossil biostratigraphic correlation. *Philos. Trans. R. Soc. London A,* 357:1975–1994.

Rea, D.K., Zachos, J.C., Owen, R.M., and Gingerich, P.D., 1990. Global change at the Paleocene–Eocene boundary: climatic and evolutionary consequences of tectonic events. *Palaeogeogr., Palaeoclimatol., Palaeoecol.,* 79:117–128.

Rudnicki, M.D., Wilson, P.A., and Anderson, W.T., 2001. Numerical models of diagenesis, sediment properties and pore fluid chemistry on a paleoceanographic transect: Blake Nose, Ocean Drilling Program Leg 171B. *Paleoceanography,* 16:561–573.

Sanfilippo, A., and Blome, C.D., 2001. Biostratigraphic implications of mid-latitude Palaeocene–Eocene radiolarian faunas from Hole 1051A, ODP Leg 171B, Blake Nose, western North Atlantic. *In* Kroon, D., Norris, R.D., and Klaus, A. (Eds.), *West-*

ern North Atlantic Paleogene and Cretaceous Paleoceanography. Spec. Publ.—Geol. Soc. London, 183:185–224.

Sanfilippo, A., and Nigrini, C., 1998. Code numbers for Cenozoic low latitude radiolarian biostratigraphic zones and GPTS conversion tables. *Mar. Micropaleontol.,* 33:109–156.

Sanfilippo, A., Riedel, W.R., Glass, B.P., and Kyte, F.T., 1985. Late Eocene microtektites and radiolarian extinctions on Barbados. *Nature,* 314:613–615.

Shackleton, N.J., 1986. Palaeogene stable isotope events. *Palaeogeog., Palaeoclimatol., Palaeoecol.,* 57:91–102.

Shackleton, N.J., Crowhurst, S., Hagelberg, T., Pisias, N.G., and Schneider, D.A., 1995. A new late Neogene time scale: application to Leg 138 sites. *In* Pisias, N.G., Mayer, L.A., Janecek, T.R., Palmer-Julson, A., and van Andel, T.H. (Eds.), *Proc. ODP, Sci. Results,* 138: College Station, TX (Ocean Drilling Program), 73–101.

Shackleton, N.J., Hall, M.A., Raffi, I., and Tauxe, L., 2000. Astronomical calibration age of the Miocene–Oligocene boundary, *Geology,* 28:447–450.

Shackleton, N.J., and Kennett, J.P., 1975. Paleotemperature history of the Cenozoic and the initiation of Antarctic glaciation: oxygen and carbon isotope analyses in DSDP Sites 277, 279, and 281. *In* Kennett, J.P., Houtz, R.E., et al., *Init. Repts. DSDP,* 29: Washington (U.S. Govt. Printing Office), 743–755.

Shackleton, N.J., Crowhurst, S.J., Weedon, G.P., and Laskar, J., 1999. Astronomical calibration of Oligocene–Miocene time. *Philos. Trans. R. Soc. London A,* 357:1907–1929.

Sloan, L.C., and Huber, M., 2001. Eocene oceanic responses to orbital forcing on precessional time scales. *Paleoceanography,* 16:101–111.

Tarduno, J.A., Duncan, R.A., Scholl, D.W., et al., 2002. *Proc. ODP, Init. Repts.,* 197 [CD-ROM]. Available from: Ocean Drilling Program, Texas A&M University, College Station TX 77845-9547, USA.

Thomas, E., 1990. Late Cretaceous through Neogene deep-sea benthic foraminifers (Maud Rise, Weddell Sea, Antarctica). *In* Barker, P.F., Kennett, J.P., et al., *Proc. ODP, Sci. Results,* 113: College Station, TX (Ocean Drilling Program), 571–594.

————, 1998. Biogeography of the late Paleocene benthic foraminiferal extinction. *In* Aubry, M.-P., Lucas, S.G., and Berggren, W.A. (Eds.), *Late Paleocene–Early Eocene: Climatic and Biotic Events in the Marine and Terrestrial Records:* New York (Columbia Univ. Press), 214–235.

Thomas, E., and Shackleton, N., 1996. The Palaeocene–Eocene benthic foraminiferal extinction and stable isotope anomalies. *In* Knox, R.W.O'B., Corfield, R.M., and Dunay, R.E. (Eds.), *Correlation of the Early Paleogene in Northwest Europe.* Spec. Publ.—Geol. Soc. London, 101:401–441.

Thomas, E., and Zachos, J.C., 1999. Was the LPTM a unique event? In Schmitz, B., Sundquist, B., and Andreasson, F.P. (Eds.), *Early Paleogene Warm Climates and Biosphere Dynamics,* Geol. Soc. Sweden, 122:169–170.

Torsvik, T.H., and Smethrust, M.A., 1989–1997. GMAP32-Geographic Mapping and Reconstruction System, Geological Survey of Norway.

van Andel, T.H., 1974. Cenozoic migration of the Pacific plate, northward shift of the axis of deposition, and paleobathymetry of the central equatorial Pacific. *Geology,* 2:507–510.

van Andel, T.H., Heath, G.R., et al., 1973. *Init. Repts. DSDP,* 16: Washington (U.S. Govt. Printing Office).

van Andel, T.H., Heath, G.R., and Moore, T.C., Jr., 1975. Cenozoic history and paleoceanography of the central equatorial Pacific Ocean: a regional synthesis of Deep Sea Drilling Project data. *Mem.—Geol. Soc. Am.,* 143.

Vonhof, H.B., Smit, J., Brinkhuis, H., Moutanari, A., and Nederbragt, A.J., 2000. Global cooling accelerated by early–late Eocene impacts? *Geology,* 28:687–690.

Weissert, H., 2000. Global change—deciphering methane's fingerprint. *Nature,* 406:356–357.

Wilson, G.S., Roberts, A.P., Verosub, K.L., Florindo, F., and Sagnotti, L., 1998. Magnetobiostratigraphic chronology of the Eocene–Oligocene transition in the CIROS-1 core, Victoria Land margin, Antarctica: implications for Antarctic glacial history. *Geol. Soc. Am. Bull.,* 110:35–47.

Wilson, P.A., and Norris, R.D., 2001. Warm tropical ocean surface and global anoxia during the mid-Cretaceous period. *Nature,* 412:425–429.

Wilson, P.A., Norris, R.D., and Cooper, M.J., 2002. Testing the Cretaceous greenhouse using glassy foraminfera from the core of the Turonian tropics on Demerara Rise. *Geology,* 30:607–610.

Wilson, P.A., and Opdyke, B.N., 1996. Equatorial sea-surface temperatures for the Maastrichtian revealed through remarkable preservation of metastable carbonate. *Geology,* 24:555–558.

Zachos, J.C., Lohmann, K.C., Walker, J.C.G., and Wise, S.W., Jr., 1993. Abrupt climate changes and transient climates during the Paleogene: a marine perspective. *J. Geol.,* 101:191–213.

Zachos, J.C., Pagani, M., Sloan, L., Thomas, E., and Billups, K., 2001a. Trends, rhythms, and aberrations in global climate 65 Ma to present. *Science,* 292:686–693.

Zachos, J.C., Quinn, R.M., and Salamy, K., 1996. High resolution (104 yr) deep-sea foraminiferal stable isotope records of the Eocene–Oligocene climate transition. *Paleoceanography,* 11:251–266.

Zachos, J.C., Rea, D.K., Seto, K., Niitsuma, N., and Nomura, R., 1992. Paleogene and early Neogene deep water history of the Indian Ocean: inferences from stable isotopic records. In Duncan, R.A., Rea, D.K., Kidd, R.B., von Rad, U., and Weissel, J.K. (Eds.), *Synthesis of Results from Scientific Drilling in the Indian Ocean*. Geophys. Monogr., Am. Geophys. Union, 70:351–386.

Zachos, J.C., Shackleton, N.J., Revenaugh, J.S., Pälike, H., and Flower, B.P., 2001b. Climate response to orbital forcing across the Oligocene–Miocene boundary. *Science,* 292:274–278.

Figure F1. Map of the central tropical Pacific showing (**A**) Leg 199 drill sites and DSDP drill sites in the region superimposed on bathymetry and (**B**) Leg 199 drill sites superimposed on the approximate position of magnetic Anomaly An25n (58.9–56.4 Ma; red), the target crust for the 56-Ma transect. Gray shading = seafloor depths >5000 mbsl.

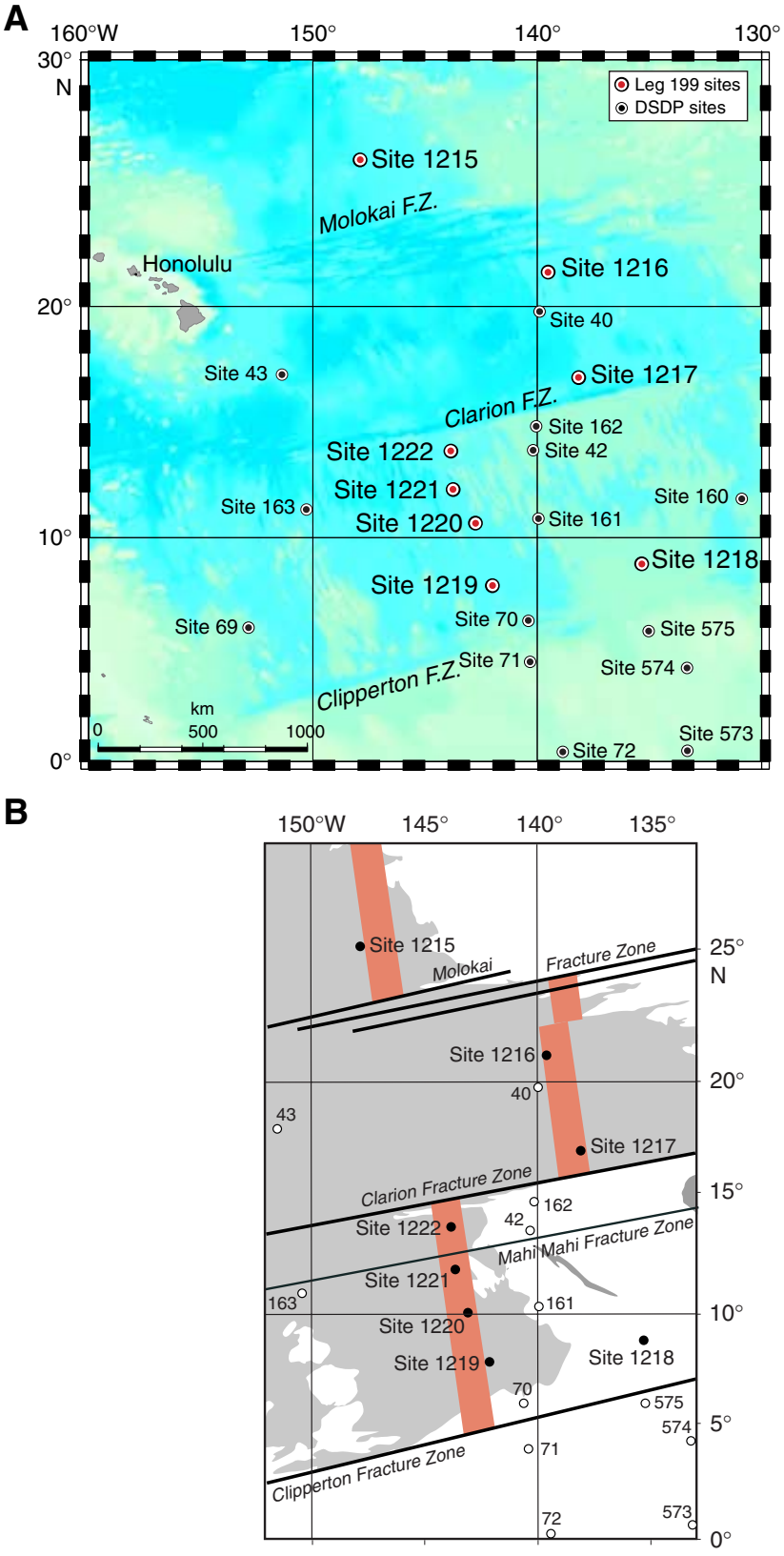

Figure F2. Chlorophyll contents in the Pacific equatorial region, from SeaWIFS satellite, September 1997–July 1998 composite. The high-productivity (light colored) band along the equator is constrained to its position by ocean circulation patterns. Red = highest chlorophyll contents, dark purple = lowest chlorophyll.

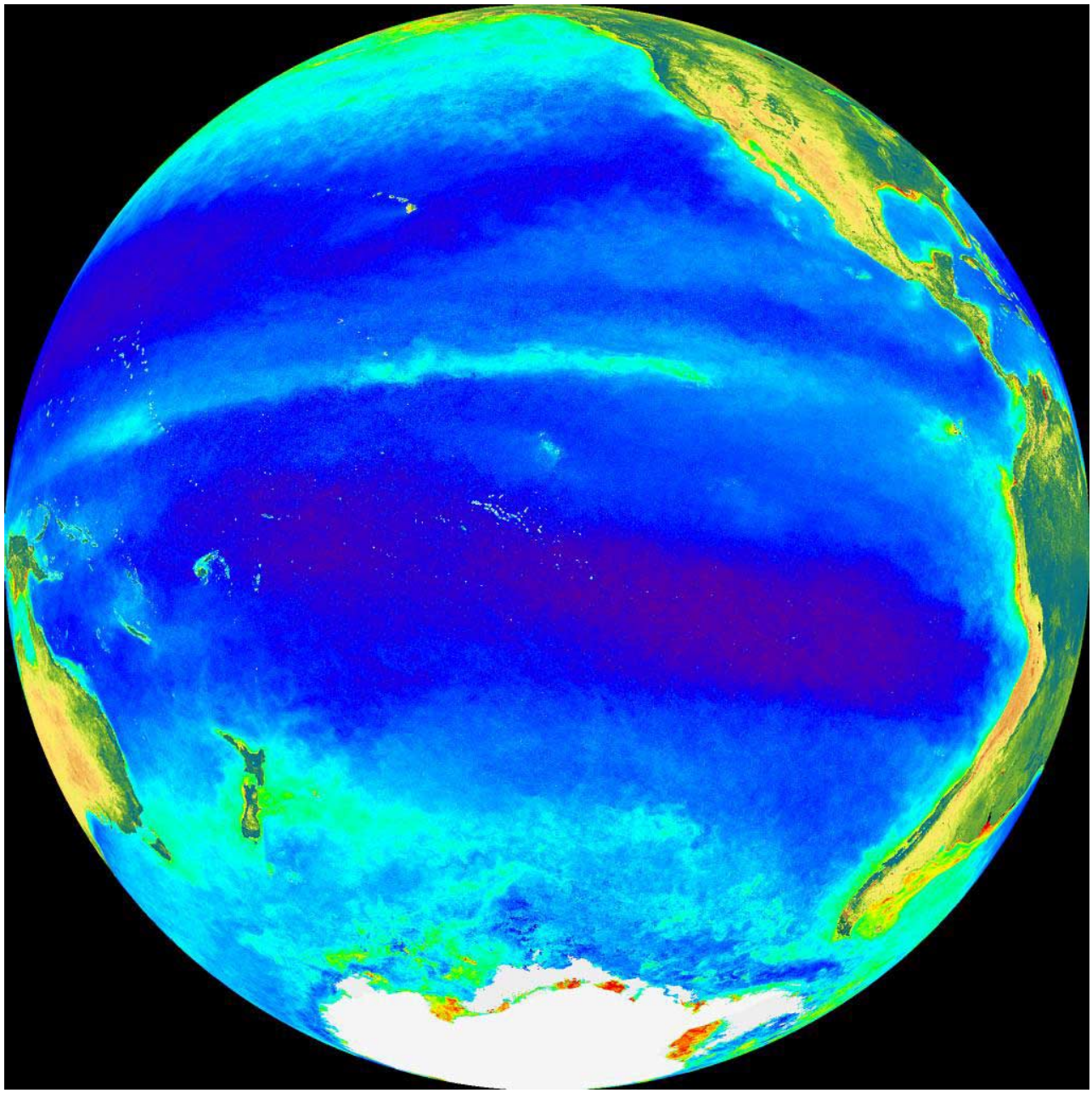

Figure F3. A. Position and thickness in meters of the equatorial sediment bulge in the equatorial Pacific Ocean (after Mitchell, 1998). The thickest pile of sediments is displaced from the equator by the northwestward movement of the Pacific plate. Because of Pacific plate movement, Paleogene equatorial sediments lie beneath a relatively thin Neogene sediment column. **B.** Representative, latitudinal cross-section of sediment mass density in the tropical Pacific Ocean based on previous DSDP results.

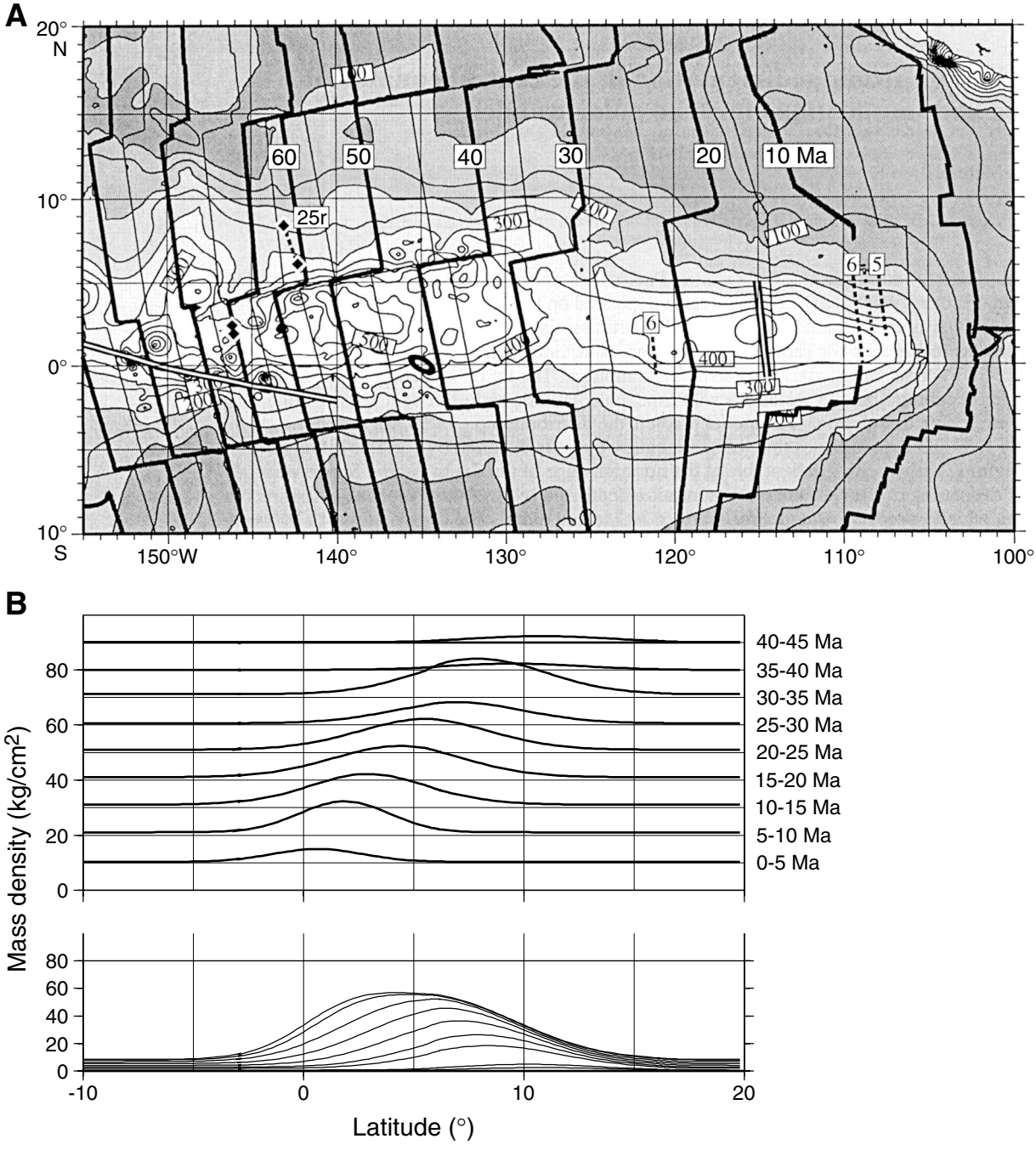

Figure F4. Paleopositions of sites along the 56-Ma Leg 199 transect, superimposed on model estimates of upwelling from a new early Eocene coupled ocean-atmosphere climate model (**Huber,** this volume). Lines with arrows = current streamlines at the approximate depth of the thermocline. Compare the upwelling pattern in this model with the chlorophyll distribution in Figure **F2,** p. 53, an indicator of modern upwelling.

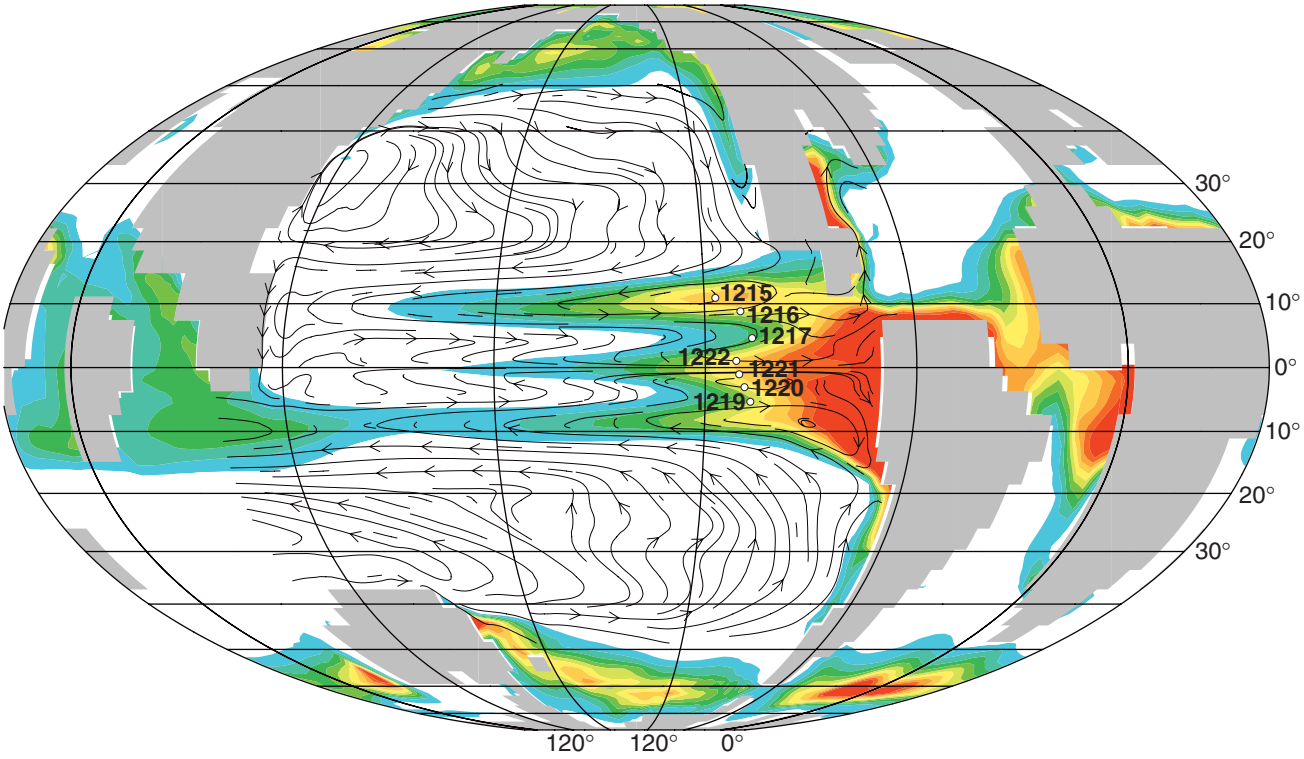

Figure F5. Compilation of benthic oxygen isotope data for the Cenozoic (Zachos et al., 2001a). Also shown is the time window investigated during ODP Leg 199 and the position of three major events targeted by the leg. P/E = Paleocene/Eocene boundary and its associated thermal event. Oi-1 is approximately at the E/O boundary and marks the first major Antarctic glaciation. Mi-1 is near the O/M boundary and marks the beginning of the development of the Neogene cryosphere.

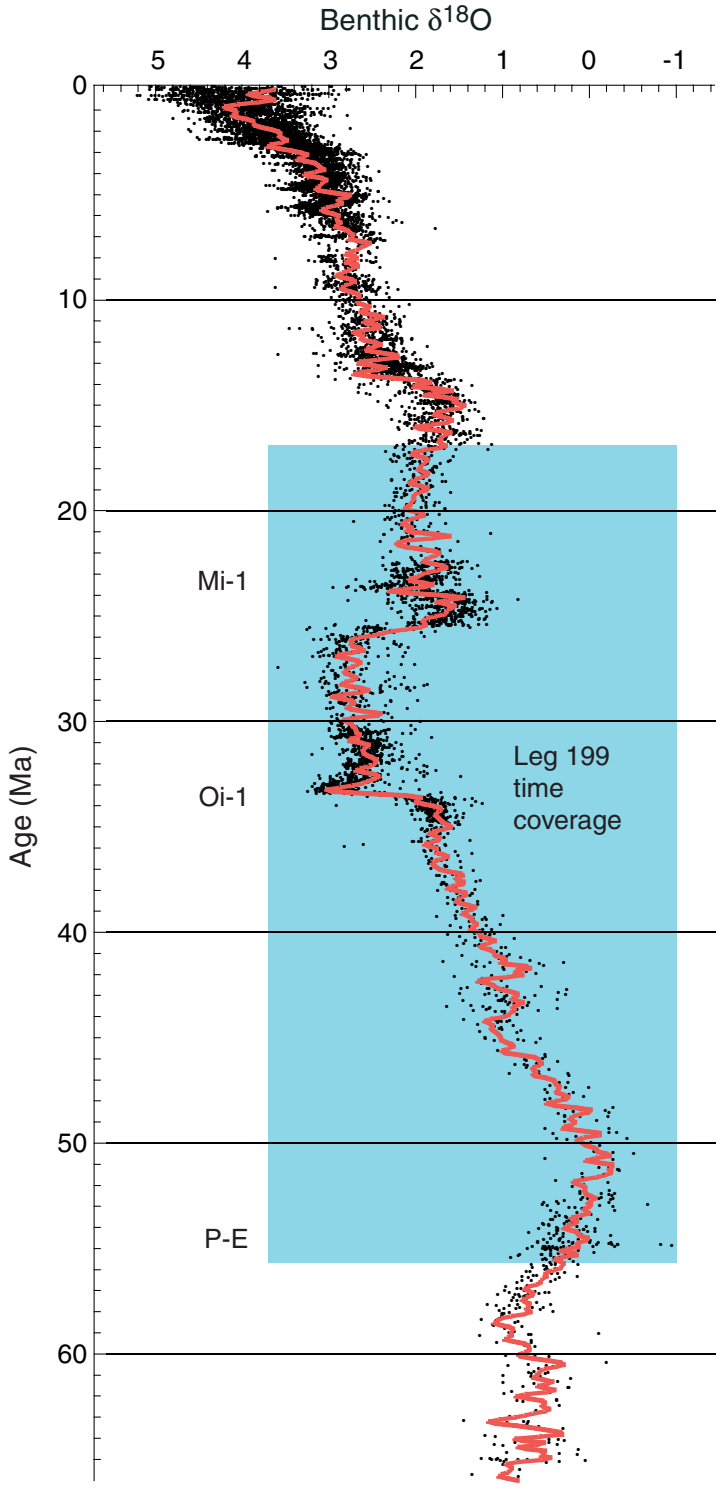

Figure F6. Lithologic summary for Leg 199. Individual units at each site are correlated to each other. The abundance of carbonate ooze in the Oligocene–upper Miocene sequence at Site 1218 suggests this site was above the CCD after the late Eocene. O/M = Oligocene/Miocene boundary, E/O = Eocene/Oligocene boundary, P/E = Paleocene/Eocene boundary. RN = Neogene radiolarians, RP = Paleogene radiolarians, NP = Paleogene nannofossils.

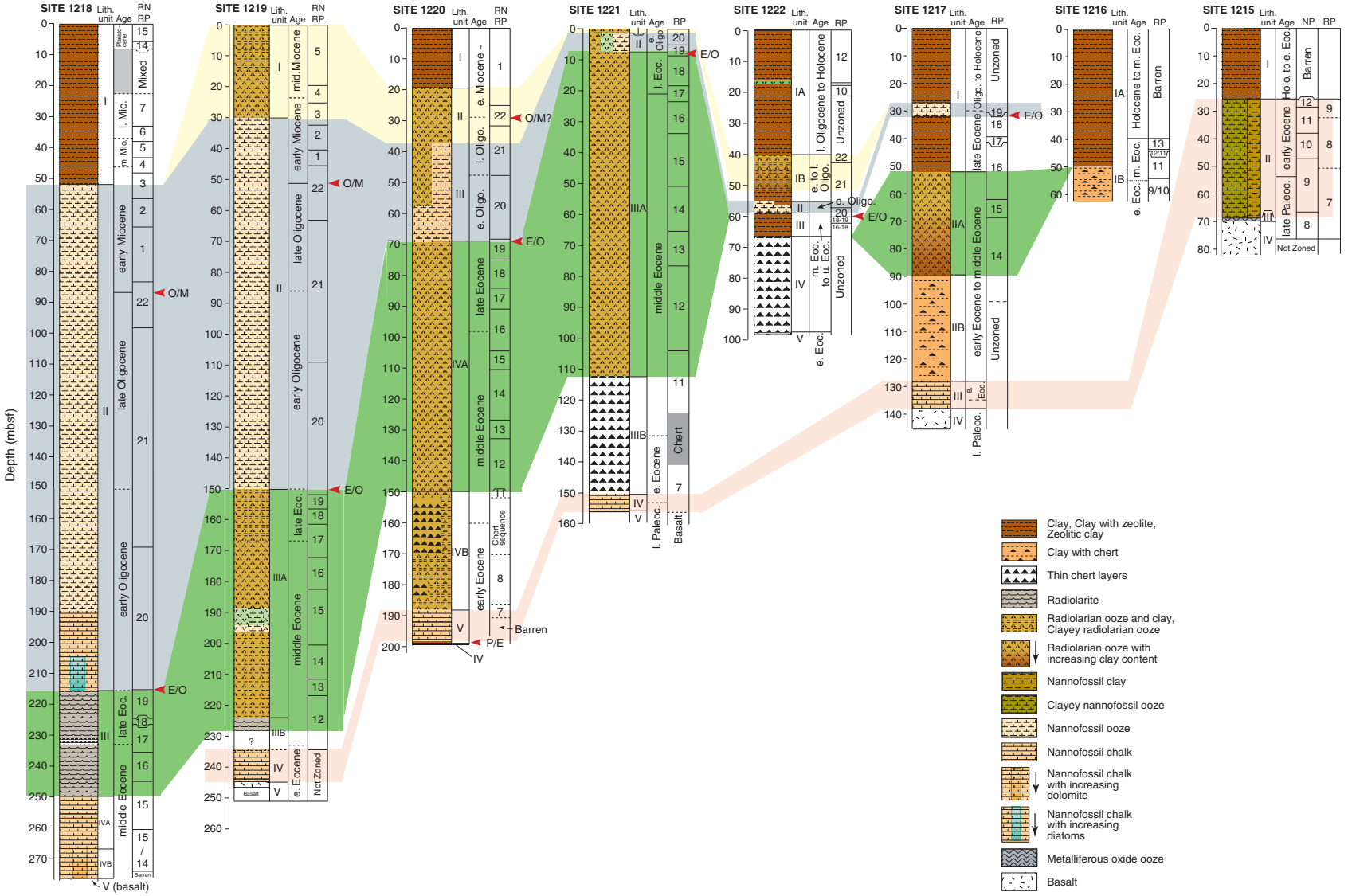

Figure F7. LAS (300–2500 nm) estimated concentrations for smectite and illite vs. depth for sites that contain a smectite (red) to illite (blue) transition.

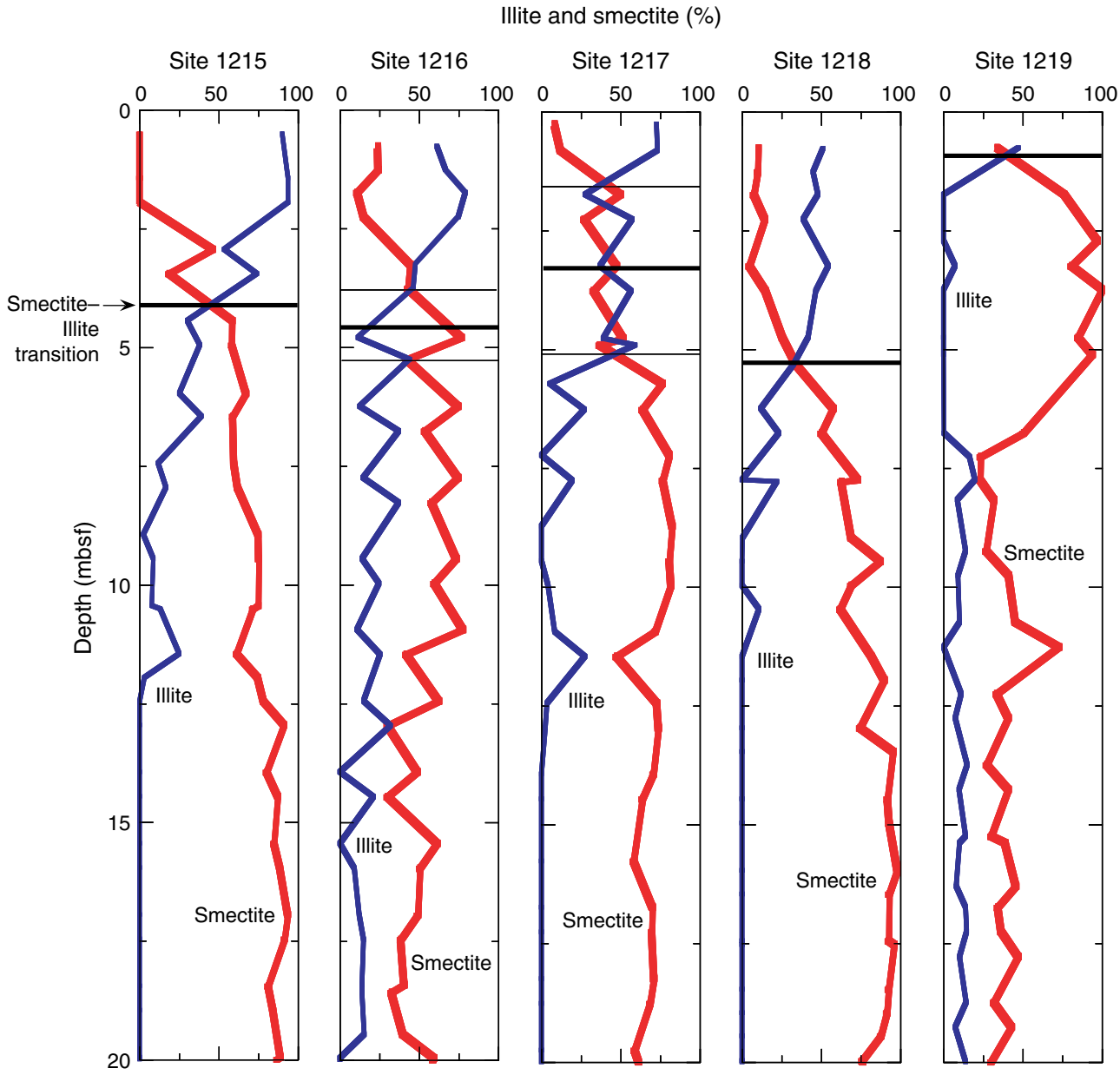

Figure F8. Smectite–illite transition plotted as a function of age and latitude. The transition most likely tracks the paleoposition of the ITCZ because it marks the switch from American dust sources (smectite rich = red) to Asian sources (illite rich = blue). Black dashed line = uncertainty of timing and latitude of transition in Site 1215.

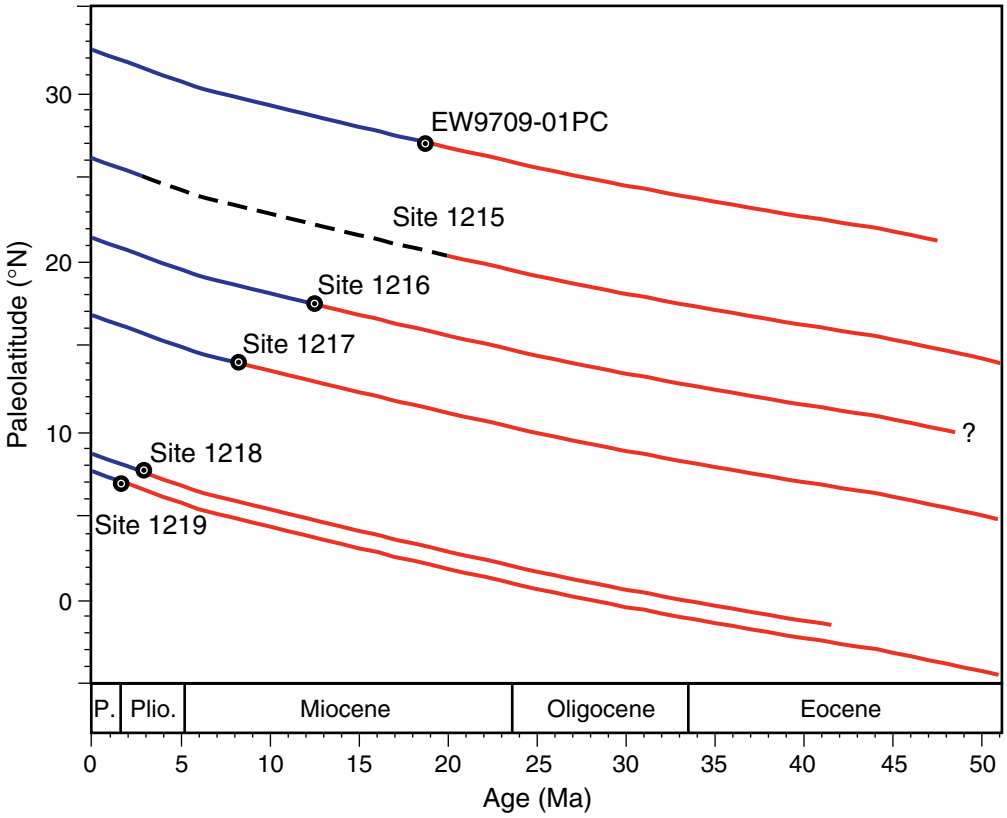

Figure F9. Lithologic columns for Sites 1218, 1219, 1220 and 1221 showing where diatoms are common to abundant (>10% based on smear slide analysis). Diatoms are a significant constituent of sediments from all the southern sites during the RP15 radiolarian zone (upper middle Eocene). Zones RP19 and 20 (basal Oligocene) are diatom rich, with the exception of Site 1219. At Site 1219, a pronounced peak in diatom abundance is found in upper Oligocene sediments. O/M = Oligocene/Miocene boundary, E/O = Eocene/Oligocene boundary, P/E = Paleocene/Eocene boundary. RN = Neogene radiolarians, RP = Paleogene radiolarians.

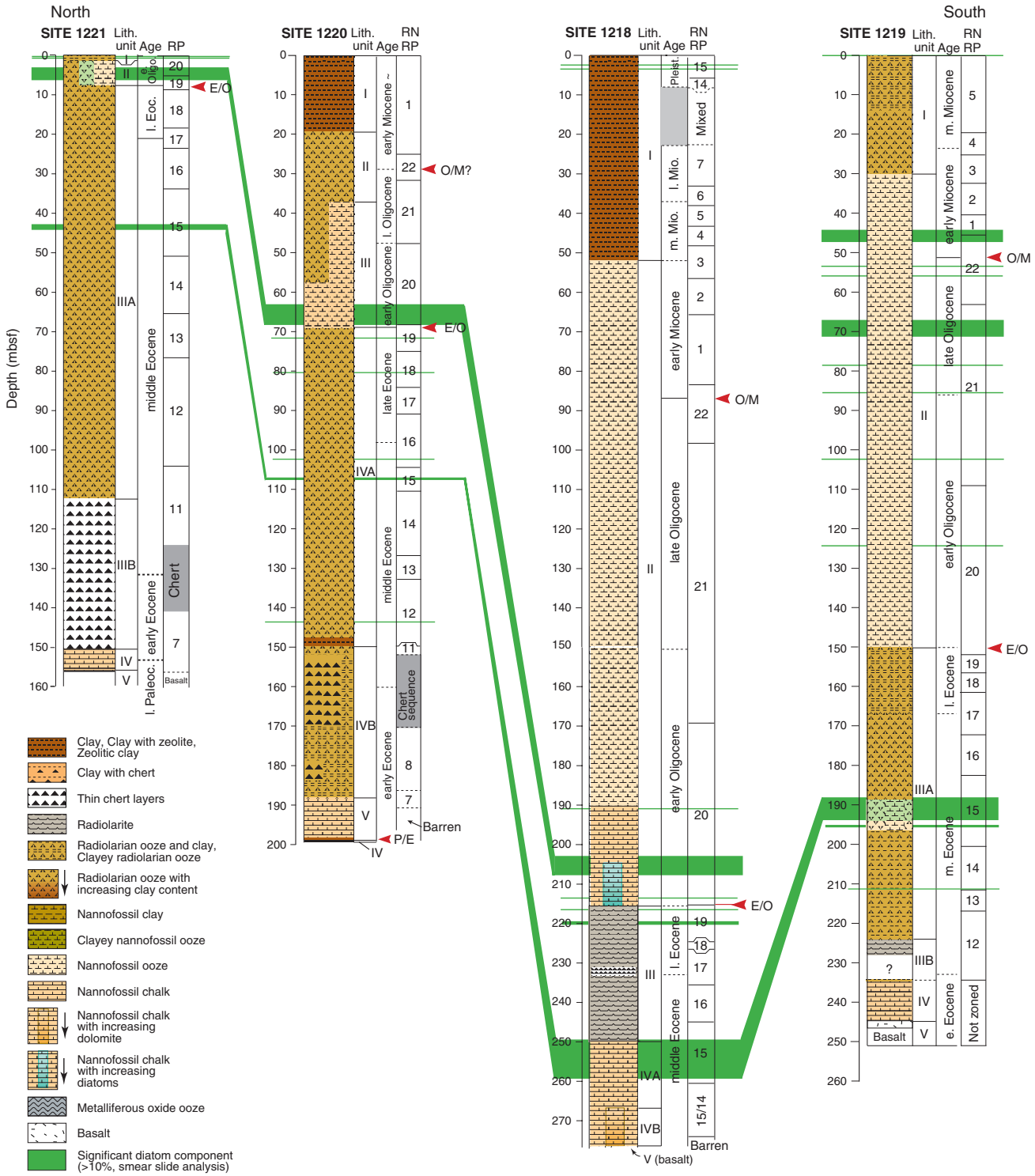

Figure F10. Composite digital photographs of the middle/upper Eocene boundary "pentachert" interval of Site 1218 plotted vs. gamma ray attenuation (GRA) bulk density in Sections 199-1218A-25X-1 and 25X-2, 199-1218B-25X-1, and 199-1218C-18X-3 and 18X-4. Five chert layers in chalks were recovered intact and can be observed through all holes drilled at Site 1218. The contacts of the radiolarite of Unit III and these lithified chert layers are gradational. More of these intact chert layers were observed in Cores 199-1218A-27X and 199-1218C-18X, 19X, and 20X.

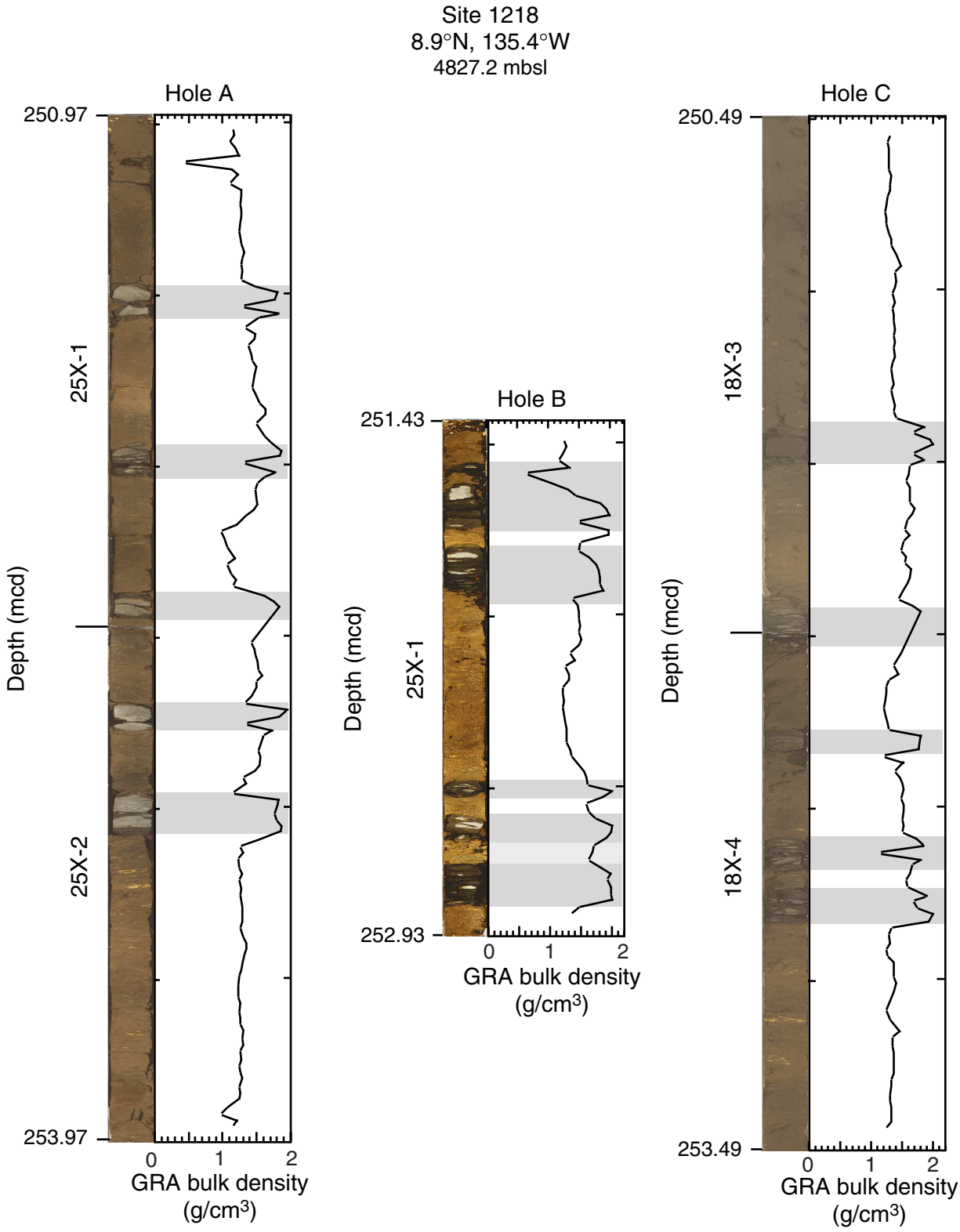

Figure F11. Composite digital images of cores taken across the E/O boundary using the shipboard GEOTEK digital imaging system. At Site 1218 (shallowest crust 42-Ma), it is clear that the Eocene–Oligocene carbonate transition occurs as a two-step shift. At other sites, in deep water, the transition is more abrupt. Dashed line = base of lithologic transition.

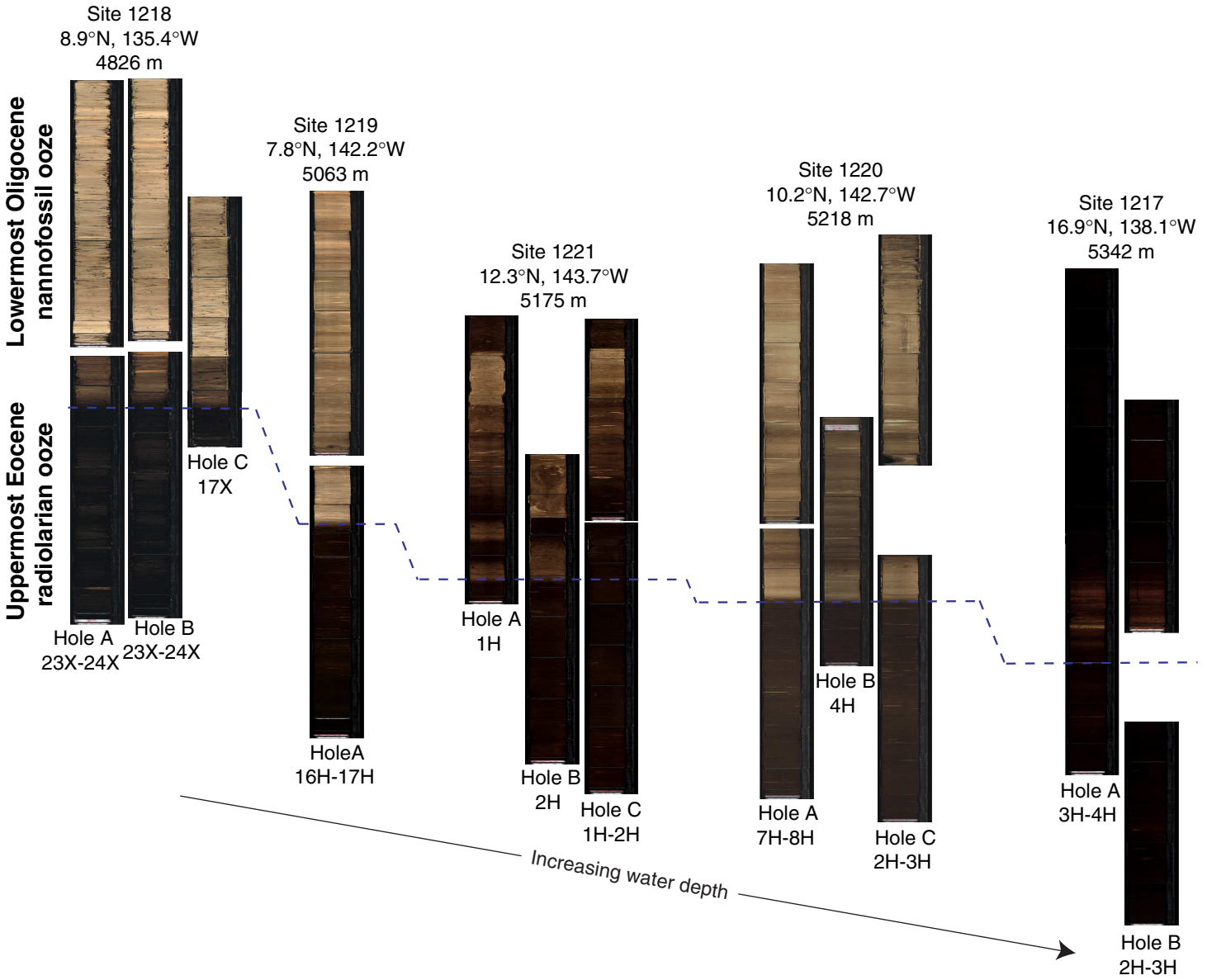

Figure F12. A. Subsidence history of non-paleoequatorial Leg 199 sites (1215, 1217, and 1221). Estimated calcite compensation depth (CCD) based on presence/absence of carbonate is also shown. **B.** Subsidence history of paleoequatorial Leg 199 sites (1218, 1219, and 1220). The estimated CCD (thick line) based on presence/absence of carbonate is also shown.

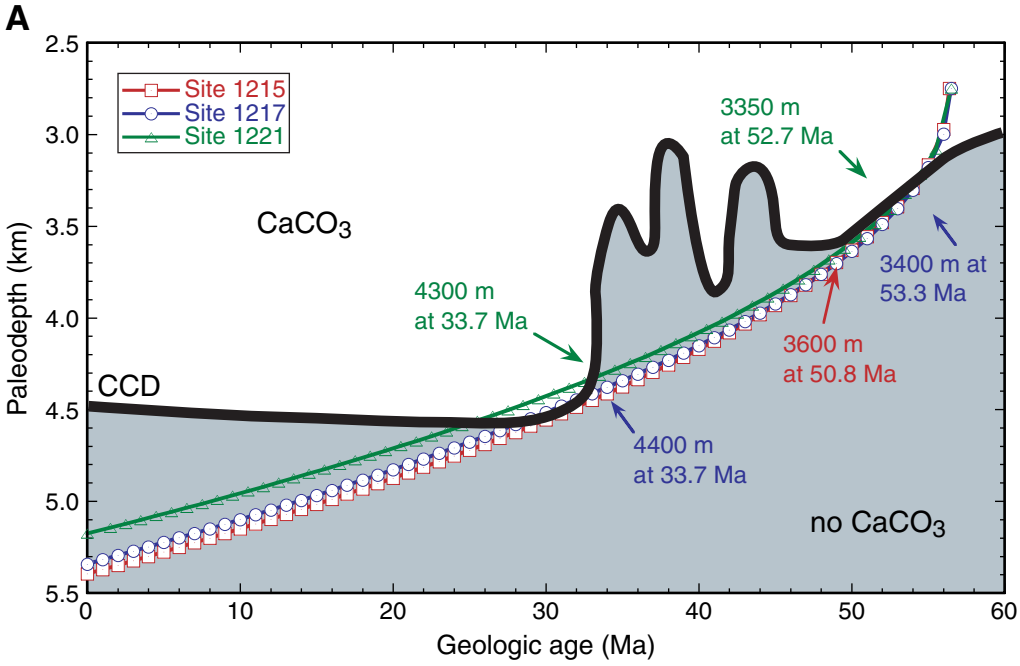

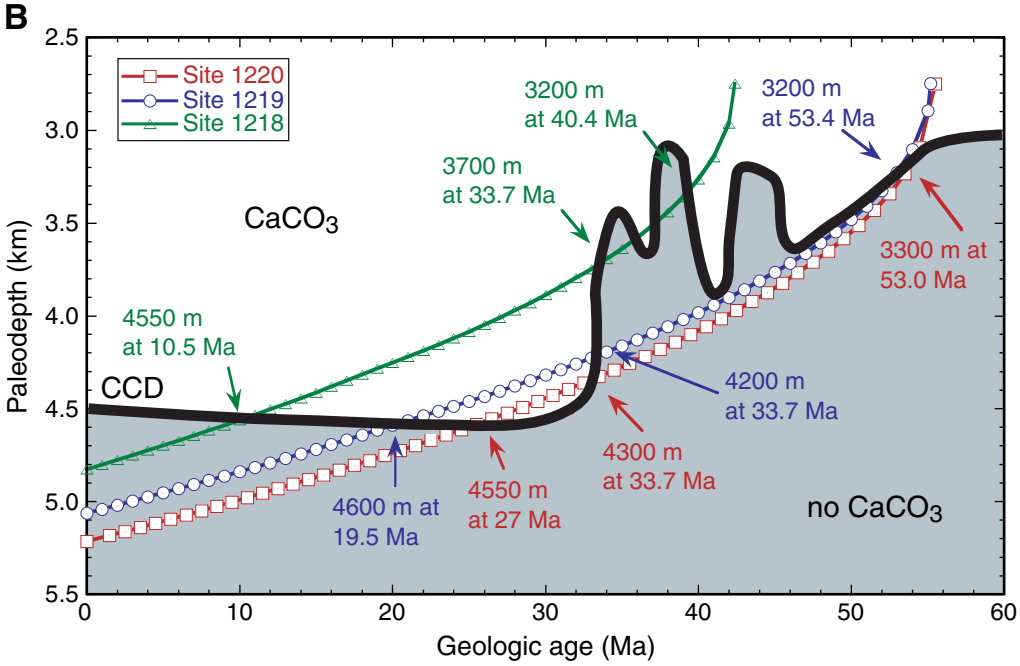

Figure F13. Relative position of the paleoequator for the middle Eocene and late Oligocene based on data from Sites 1218, 1219, and 1220. The main seafloor magnetic anomalies as well as the major fracture zones are shown in blue. For each site, we have computed a mean declination and inclination for two different intervals, 26 and 39 Ma. Mean declinations have then been rotated for the expected paleomagnetic pole for the Pacific plate of the appropriate age. The map was constructed using GMAP32 (Torsvik and Smethrust, 1989–1997).

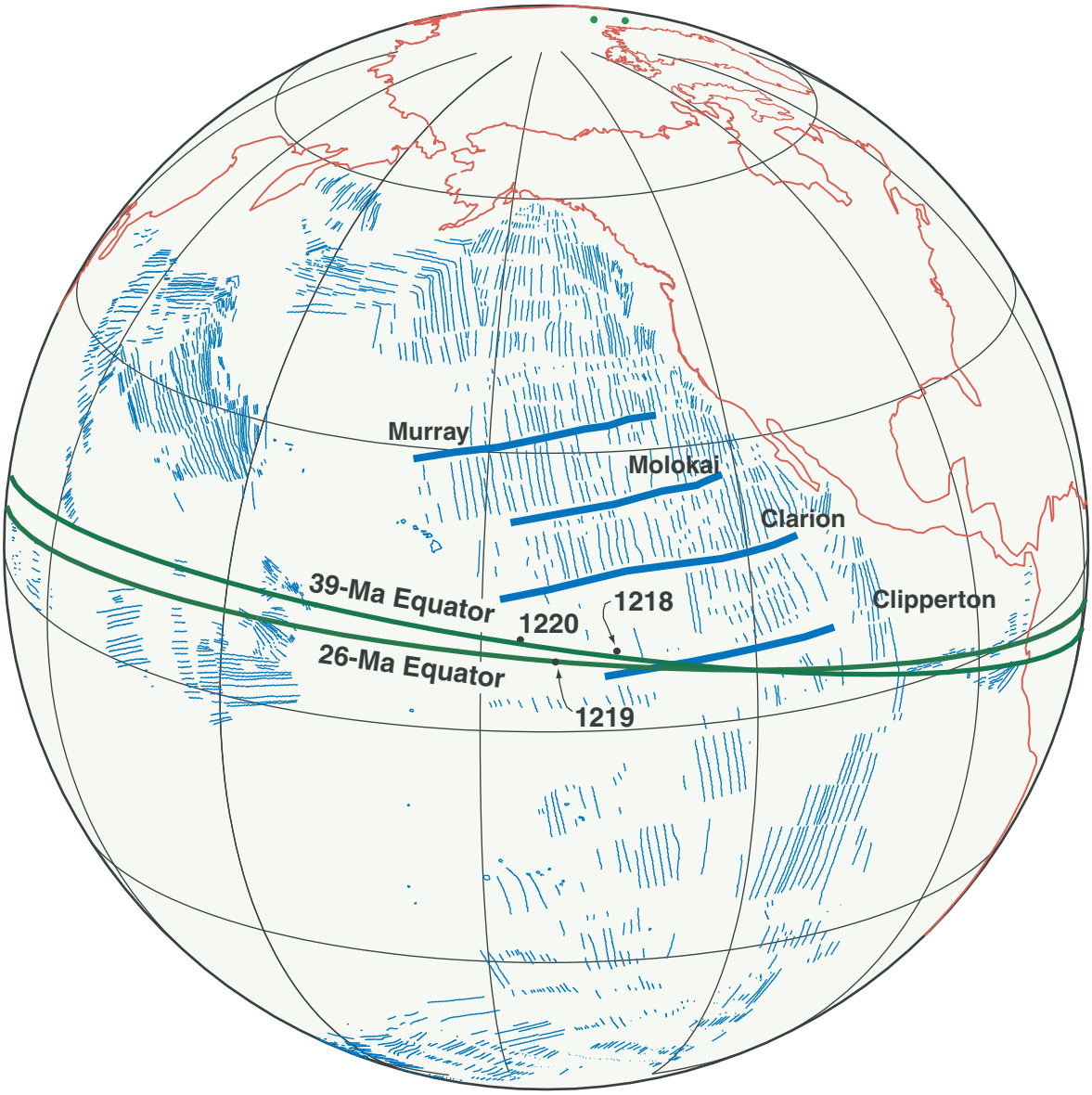

Figure F14. Inferred paleolatitudes for Sites 1218, 1219, and 1220 based on mean paleomagnetic inclinations, using the dipole formula. Error bars represent the maximum difference obtained from different holes around their mean. Site 1218 has not produced data older than the Oligocene. Notice that Site 1219 crosses the equator much later than Site 1220. Data points at 0 Ma are the present-day latitudes of the studied sites.

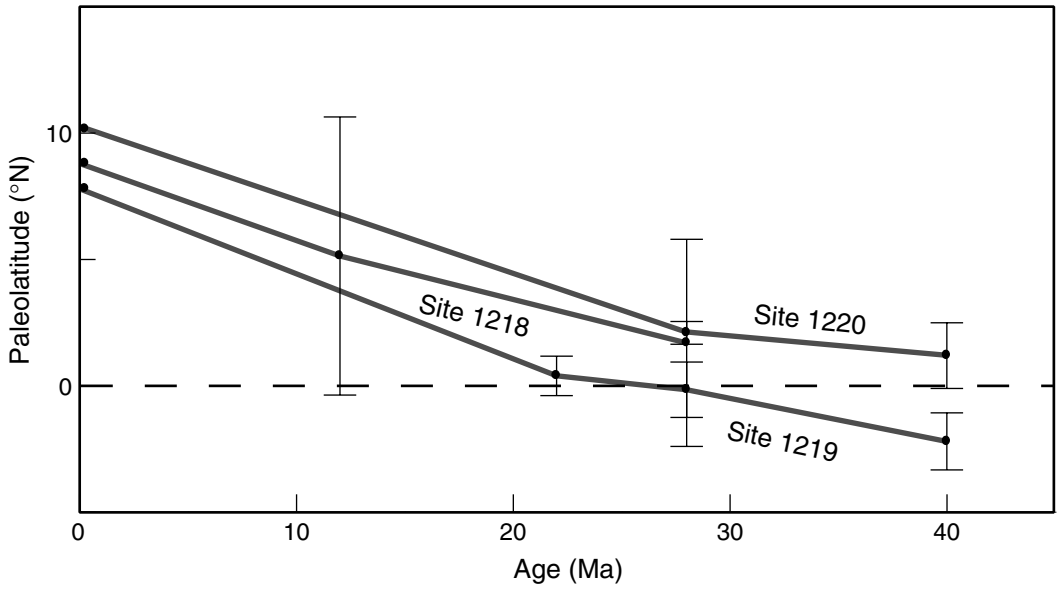

Figure F15. Interstitial water profiles from Leg 199 sites. Profiles reflect the limited organic matter diagenesis and relatively high biogenic silica contents at these sites. Only Site 1219 has the "typical" Ca and Mg profile, indicating an exchange of seawater Mg for basalt Ca during crustal alteration.

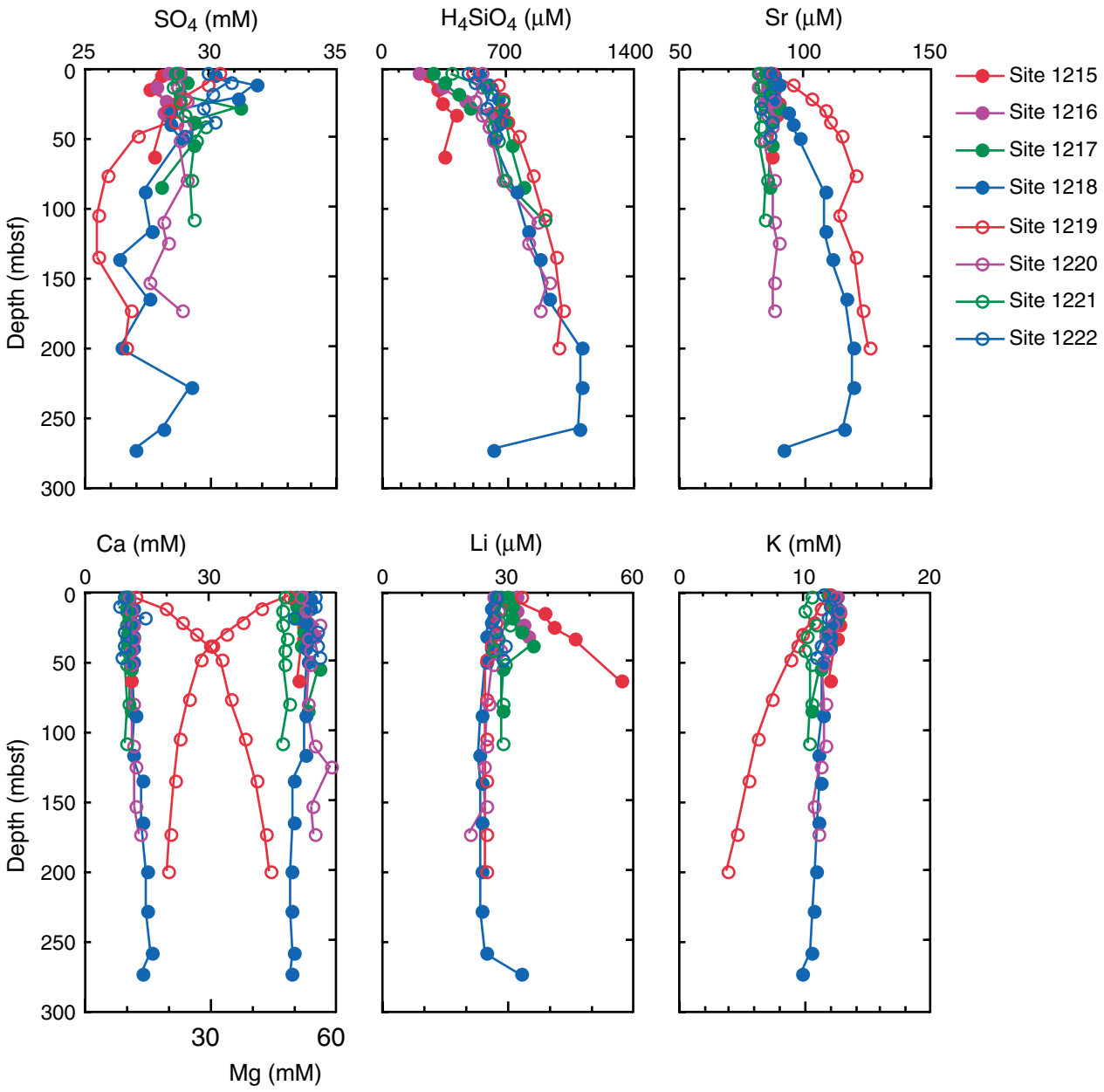

Figure F16. Shipboard ICP-AES analyses of sedimentary Si and Ca weight percent and mass accumulation rates (MARs). MAR is a product of sedimentation rate, elemental weight percent, and dry bulk density. Si largely represents biogenic silica, whereas Ca represents $CaCO_3$.

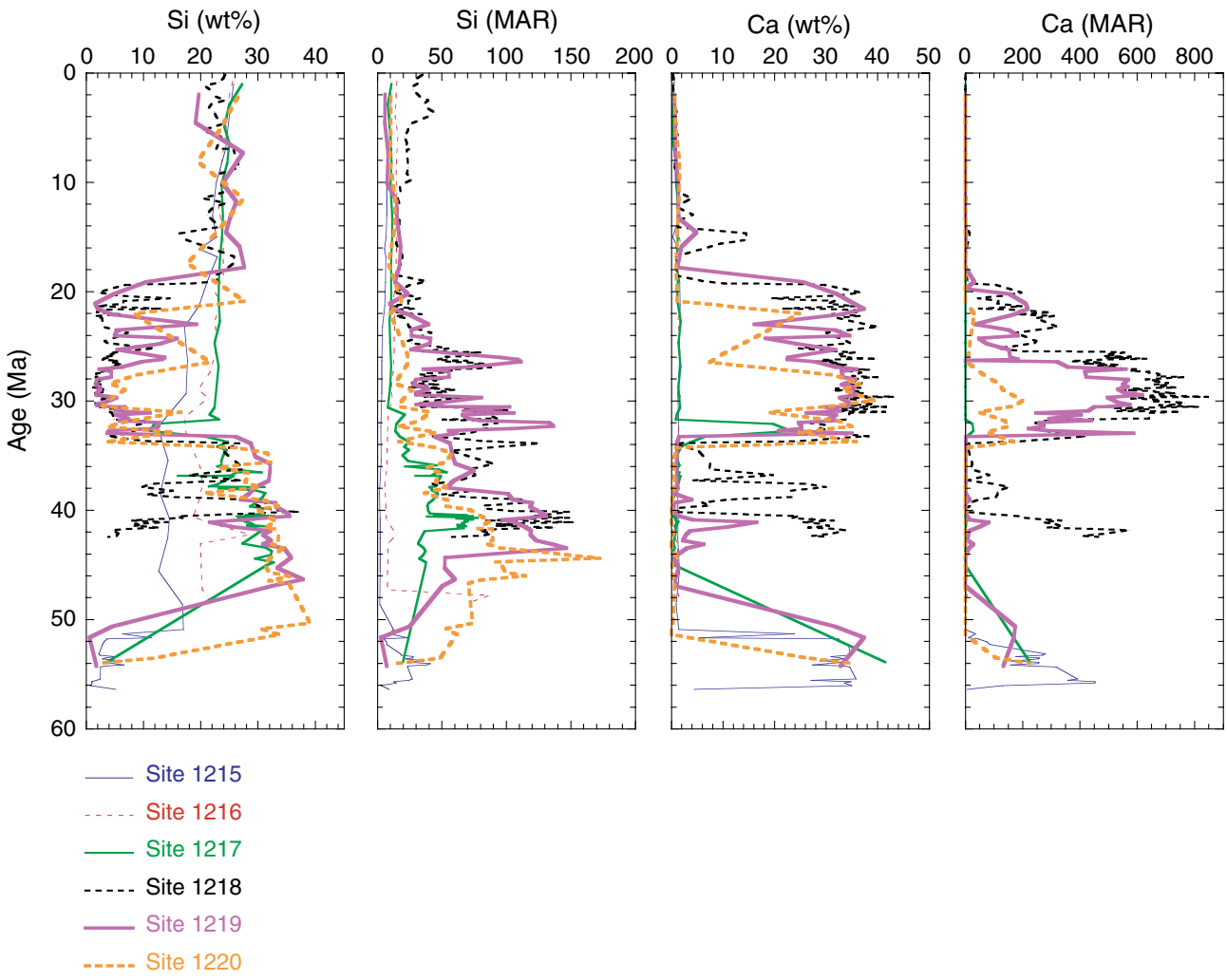

Figure F17. Summary of sedimentation rates derived from age-depth models at each of the Leg 199 sites.

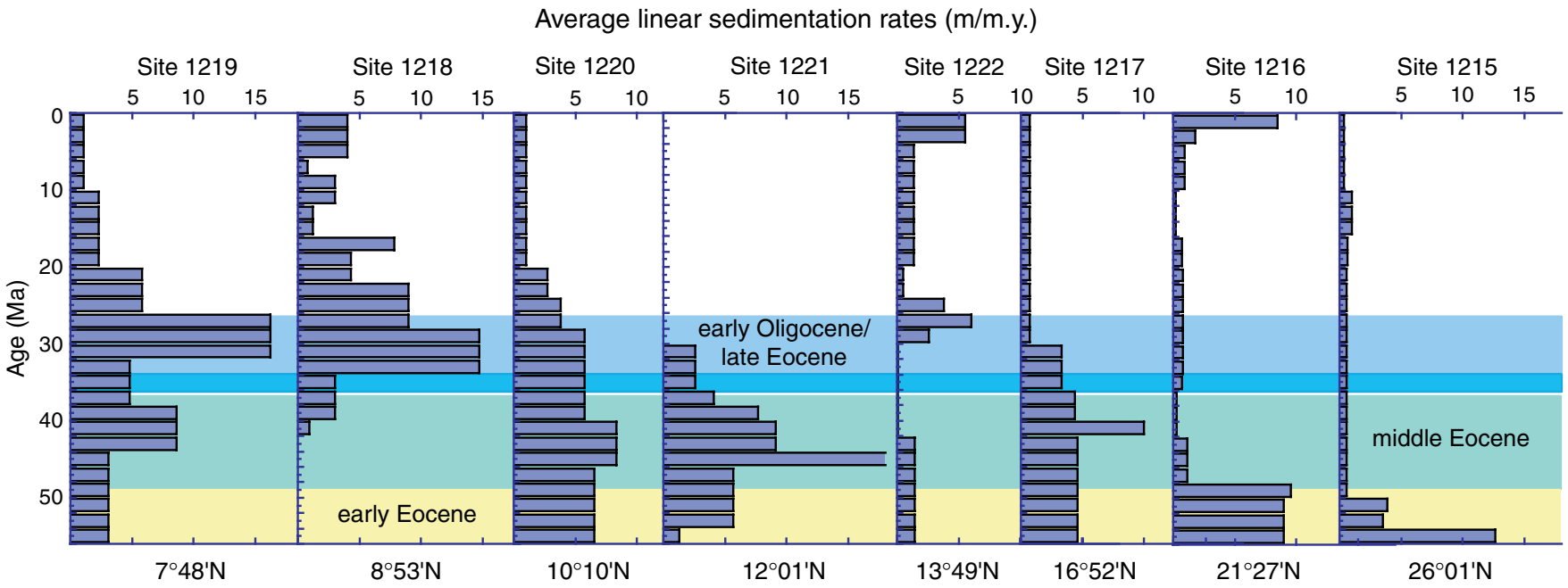

Figure F18. Shipboard ICP-AES analyses of sedimentary Al and P weight percent and mass accumulation rates (MARs). MAR is a product of sedimentation rate, elemental weight percent, and dry bulk density.

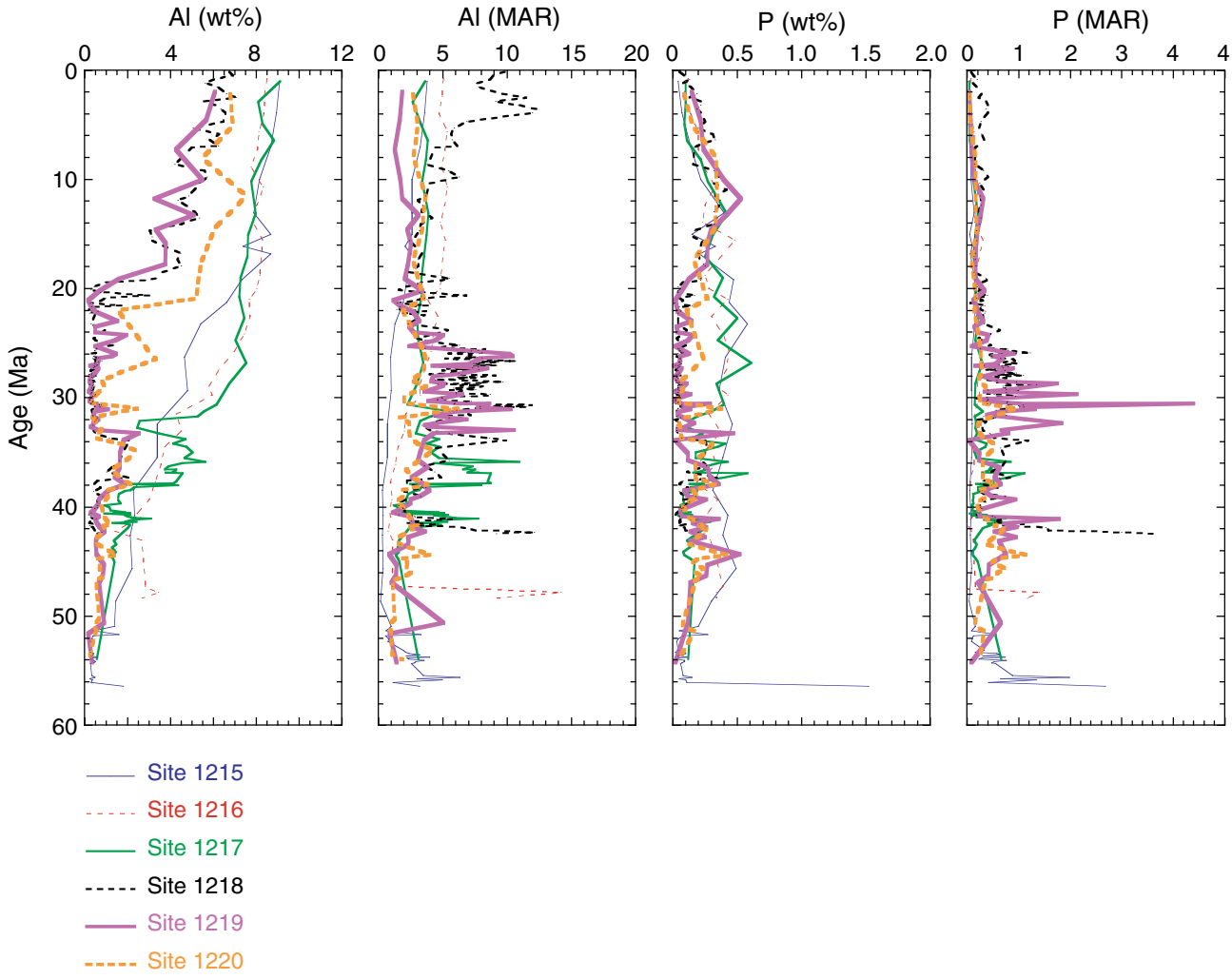

Figure F19. Si/Ti, Ba/Ti, and Al/Ti of Leg 199 sediments. Relatively constant Al/Ti suggests that the detrital sources had similar amounts of these elements. High Si/Ti reflects high biogenic SiO_2 deposition, whereas high Ba/Ti reflects high biogenic Ba burial.

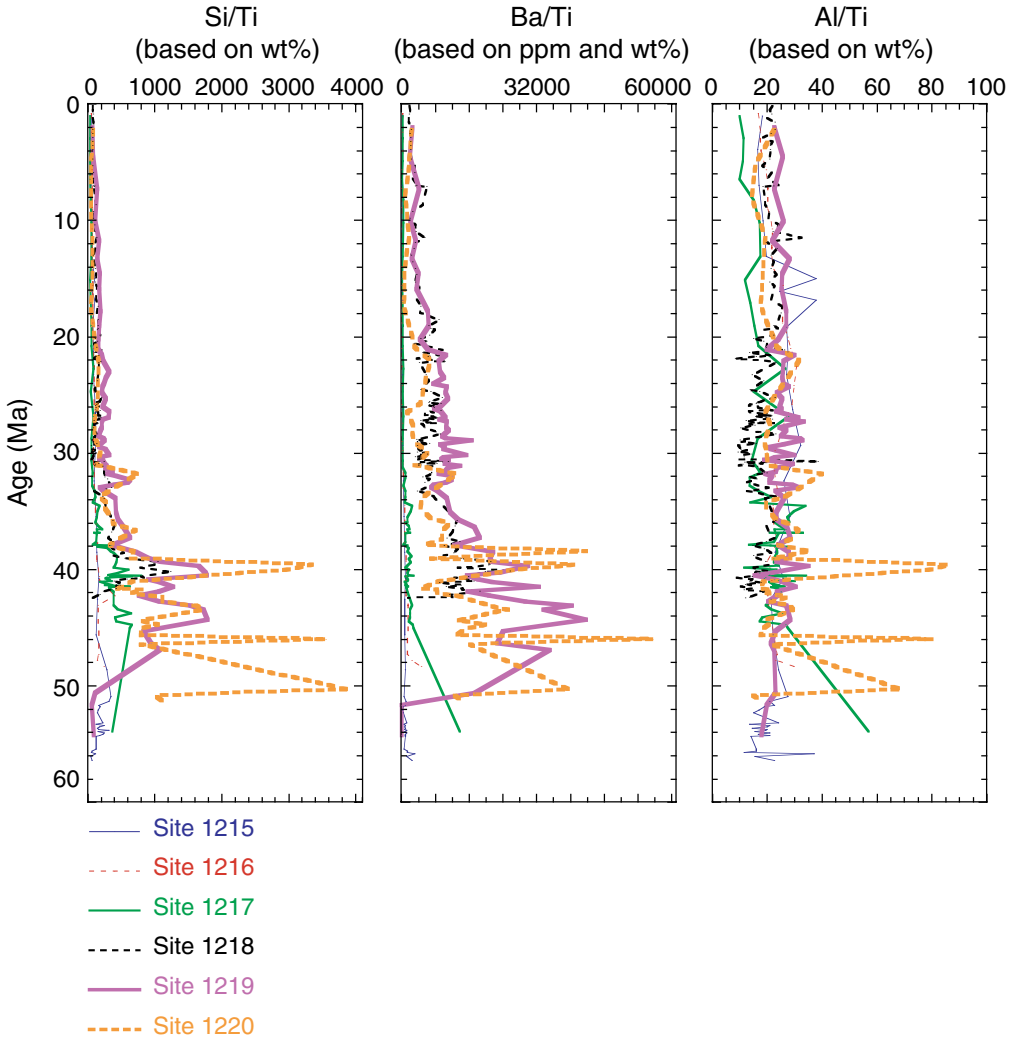

Figure F20. Latitudinal transect of Si mass accumulation rates (MARs) for three time slices: Oligocene (25–34 Ma), middle Eocene (38–45 Ma), and early Eocene (50–55 Ma). Si accumulation in the early Eocene is low and probably has a major contribution from detrital aluminosilicates. Middle Eocene Si accumulation is high, about double modern SiO_2 accumulation at the equivalent longitude. Early Oligocene Si accumulation resembles that of modern sediments (Lyle, 1992).

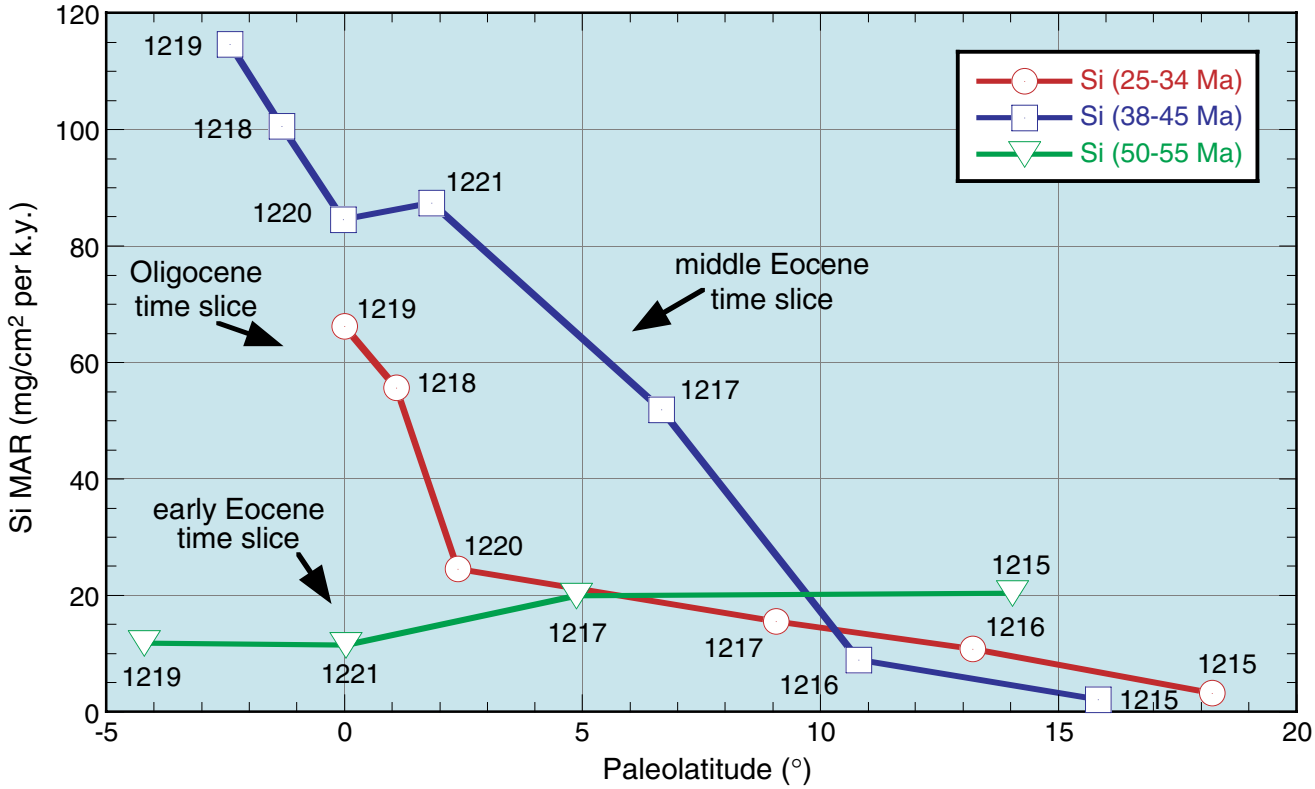

Figure F21. Latitudinal transect of Ca mass accumulation rates (MARs) for three time slices: Oligocene (25–34 Ma), middle Eocene (38–45 Ma), and early Eocene (50–55 Ma). Ca MAR almost exclusively results from the deposition of $CaCO_3$. The Oligocene pattern of Ca MAR is the only one that resembles the Neogene in both shape and magnitude. $CaCO_3$ is essentially absent from middle Eocene sediments along the 56-Ma transect but is present intermittently at the southern end of the transect. The early Eocene Ca MAR is about half of modern flux, and curiously, equatorial Ca MAR is significantly less than the off-axis flux.

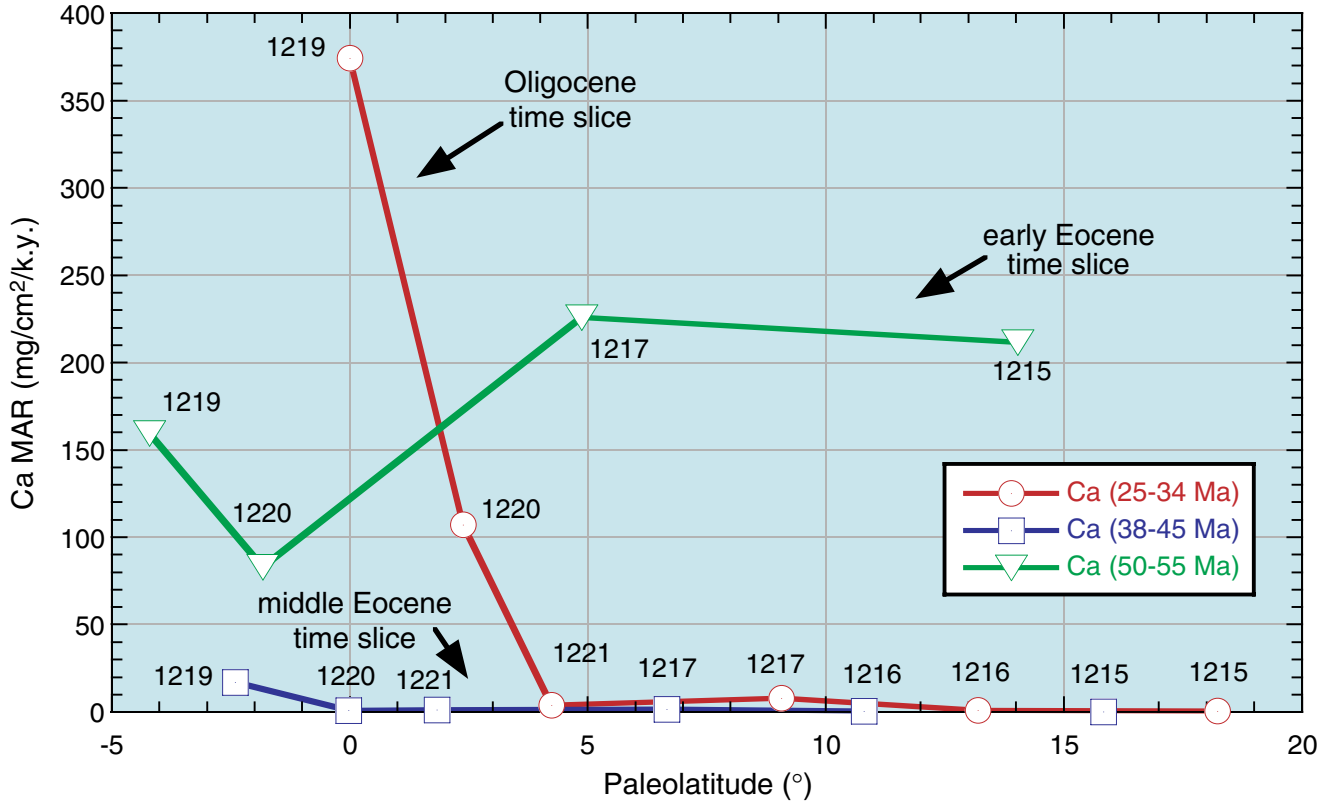

Figure F22. Synthesis of magnetic stratigraphy from four Leg 199 drill sites. Depth scale in mcd is shown on the right of each column, and geographic coordinates are shown at the bottom of each column. Black = normal magnetic polarity, white = reversed magnetic polarity, gray = no polarity assignment possible. Crosses = intervals with no data, dashed lines = correlation between selected chrons to the GPTS (Cande and Kent, 1995).

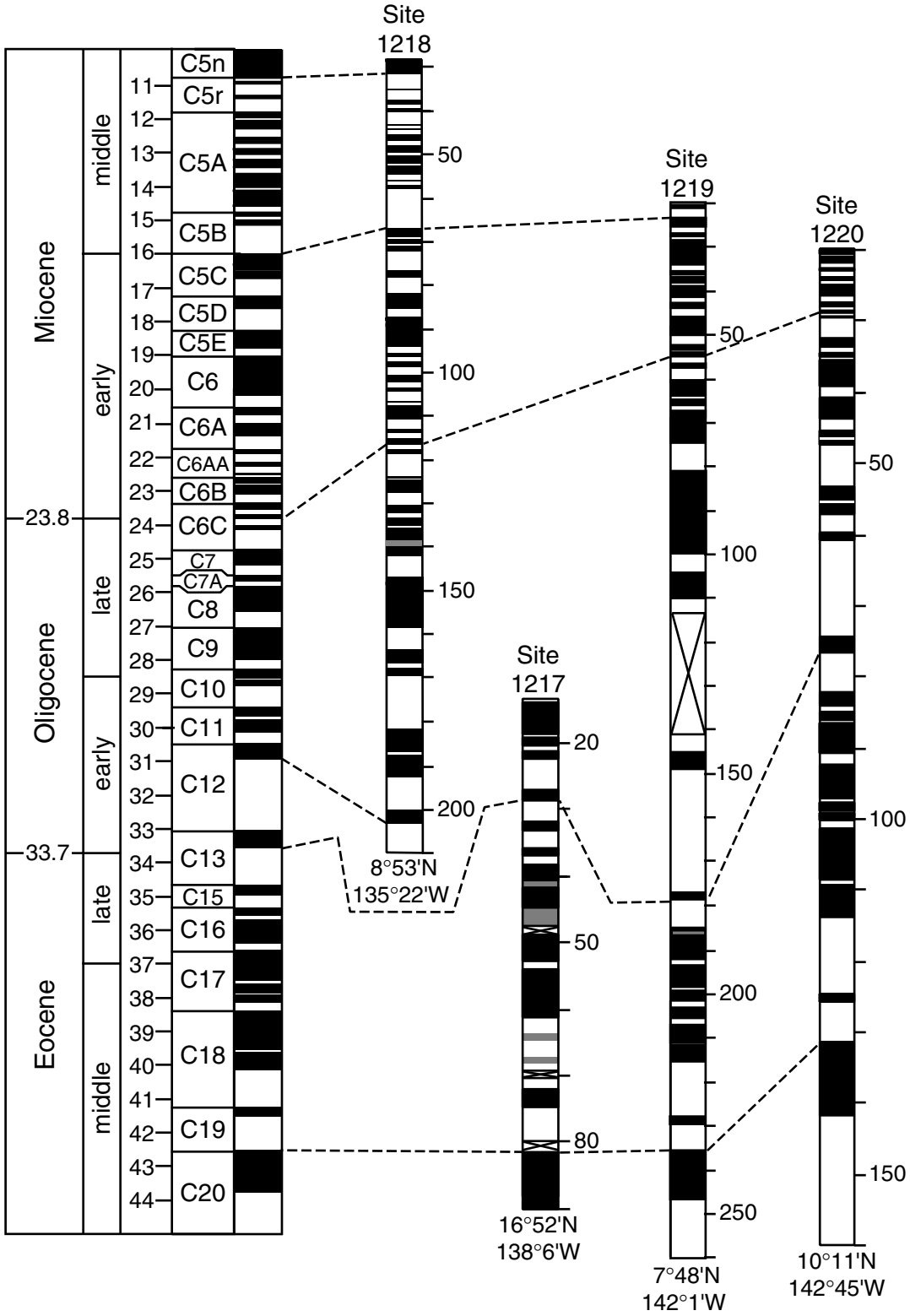

Figure F23. Comparison of estimated ages of radiolarian zones (Sanfilippo and Nigrini, 1998) to age boundaries intercalibrated with magnetic reversal stratigraphy on Leg 199. Significant improvements of zone boundary ages have occurred because of Leg 199 shipboard studies.

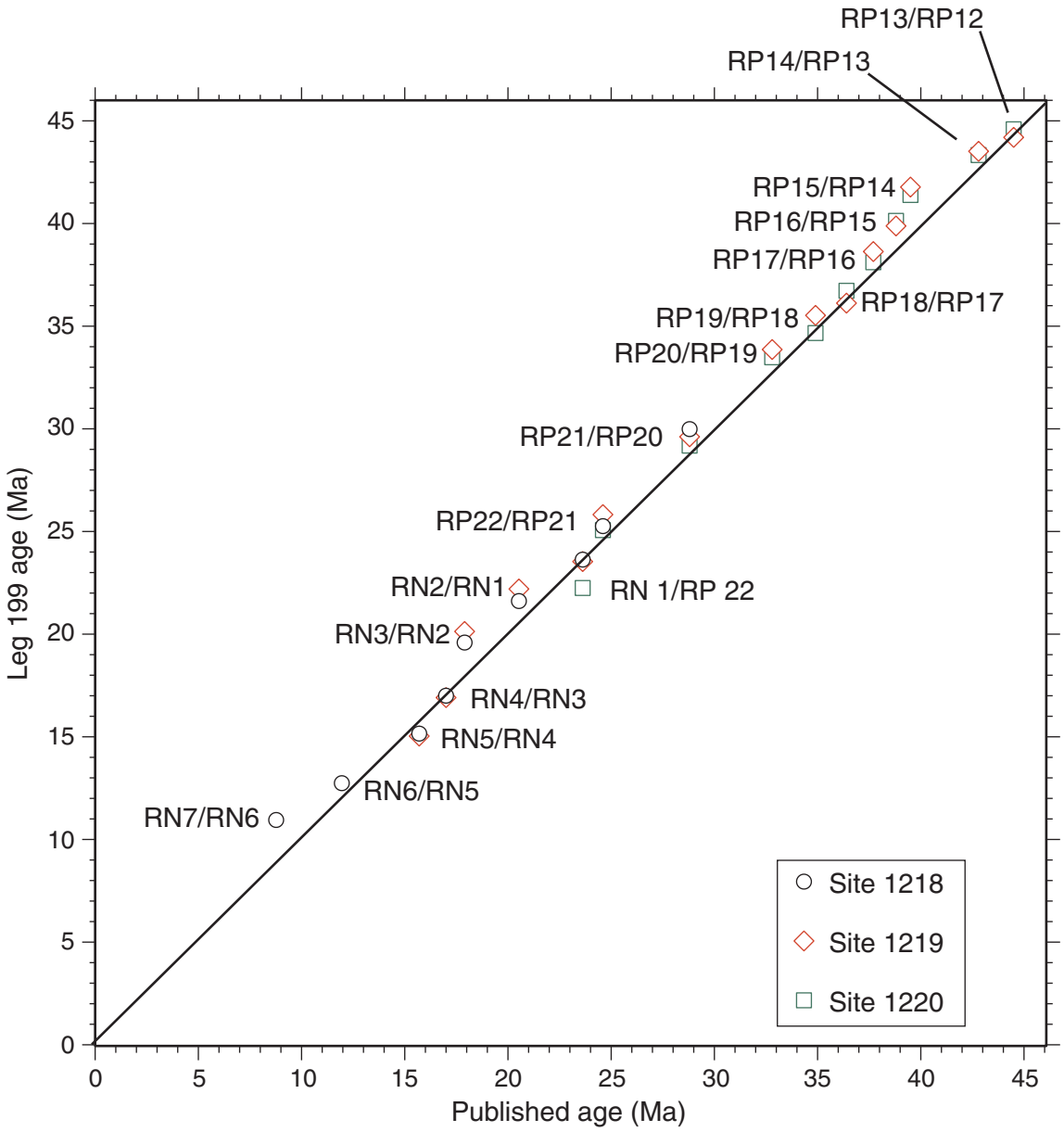

Figure F24. Digital photograph of the record of the Oligocene–Miocene transition and Mi-1 glacial step at Site 1218. Lithology and magnetic susceptibility records show the distinct cyclicity in carbonate content and physical properties observed around the O/M boundary. Together with unambiguous magnetostratigraphy and biostratigraphy, the cycle record contributes to the first high-resolution astronomical-calibrated chronology for the O/M boundary in the Pacific. Bioevents such as the first and last appearance datums of the calcareous nannofossil, *Sphenolithus delphix,* and the appearance datum of the foraminifer *Paragloborotalia kugleri* are identical in current resolution to these same events in the Atlantic Ocean. Hence, we have no doubt that the Site 1218 record will become a standard reference section for the Oligocene–Miocene interval in the Pacific that can be correlated precisely to Atlantic sites that typically lack unambiguous magnetochronologies.

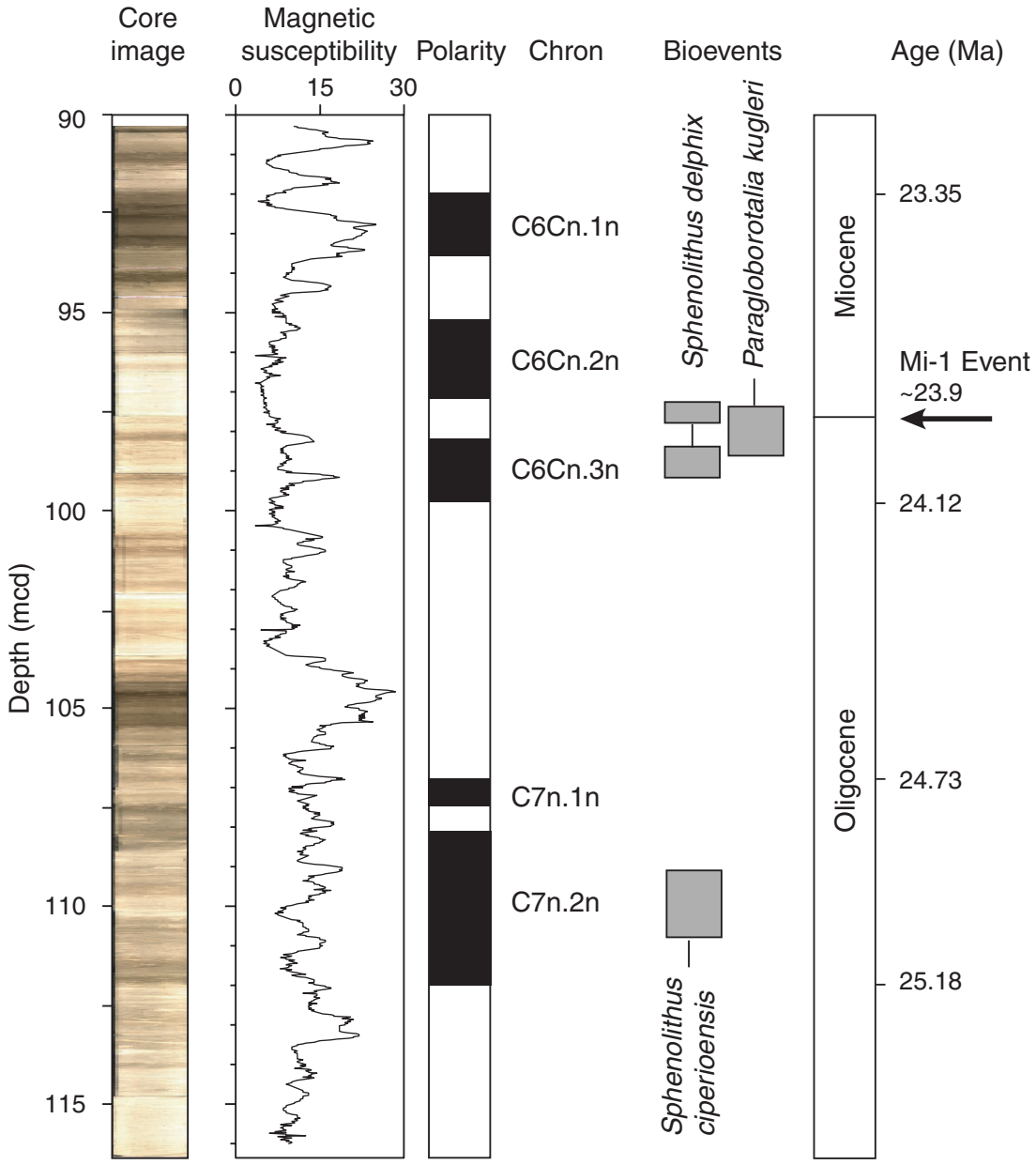

Figure F25. Magnetostratigraphic, biostratigraphic, and MST data from Site 1218 and Site 1219 plotted on a common timescale (developed mainly from magnetic reversal datums that were composited from both sites after matching of lithologic cycles). Note the close correspondence between MST data from the two drill sites and calculated sedimentation rates. Biostratigraphic nannofossil datums and their uncertainty intervals agree well, whereas datums based on certain foraminifers do not agree. Black = normal magnetic polarity, white = reversed magnetic polarity. Ages are based on the GPTS by Cande and Kent (1995). VGP = virtual geomagnetic pole. Biostrat. = biostratigraphy. Sed. rate = sedimentation rate. GRA = gamma ray attenuation. Mag. sus. = magnetic susceptibility. Color refl. L* = color reflectance L*.

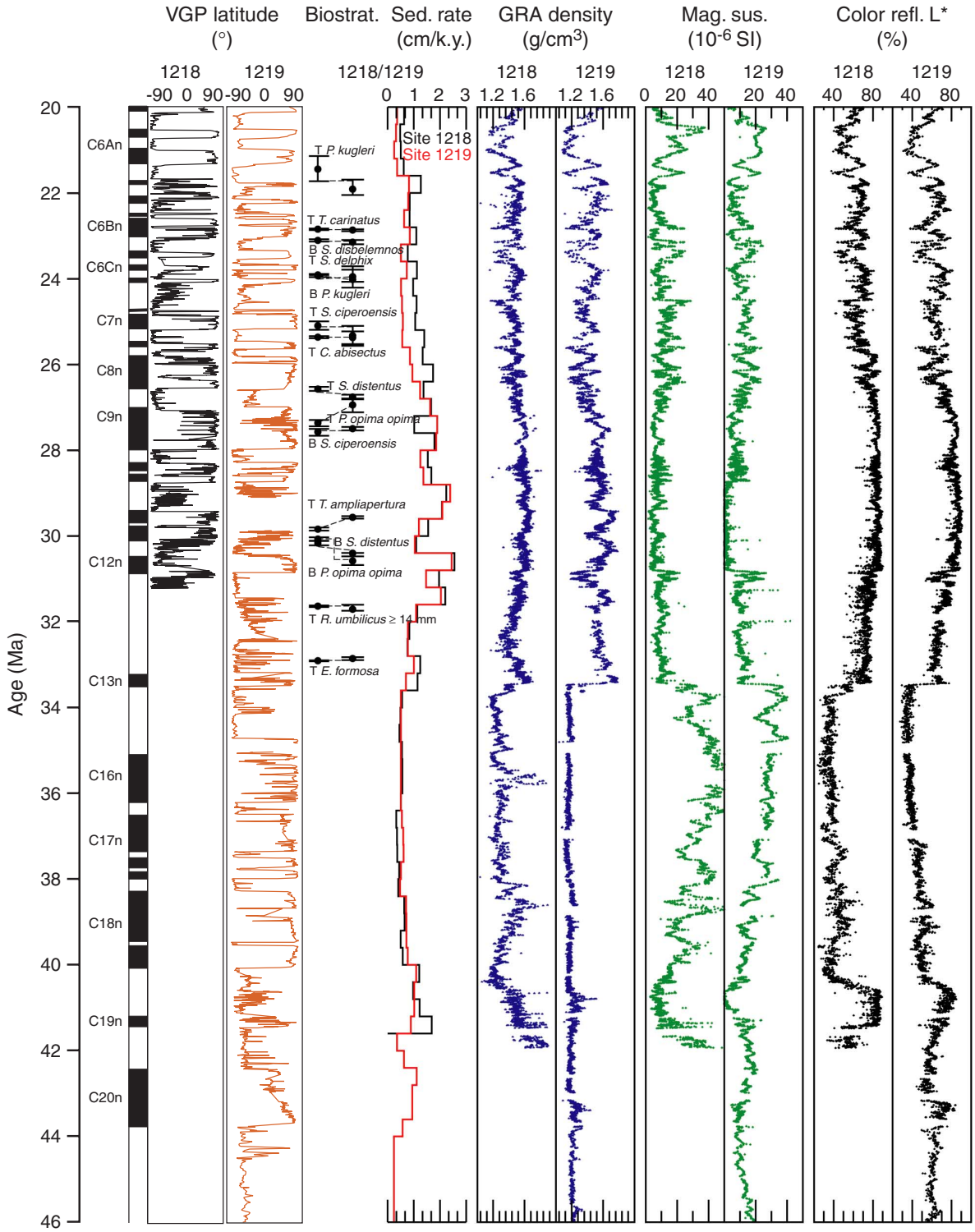

Figure F26. Composite digital photographs showing the Eocene–Oligocene sequence at five sites and composite gamma ray attenuation (GRA) bulk density, magnetic susceptibility, and color reflectance data. The lithologic change from carbonate-rich to carbonate-poor sediments is evident as a two-step decrease in GRA density and an increase in susceptibility at Site 1218.

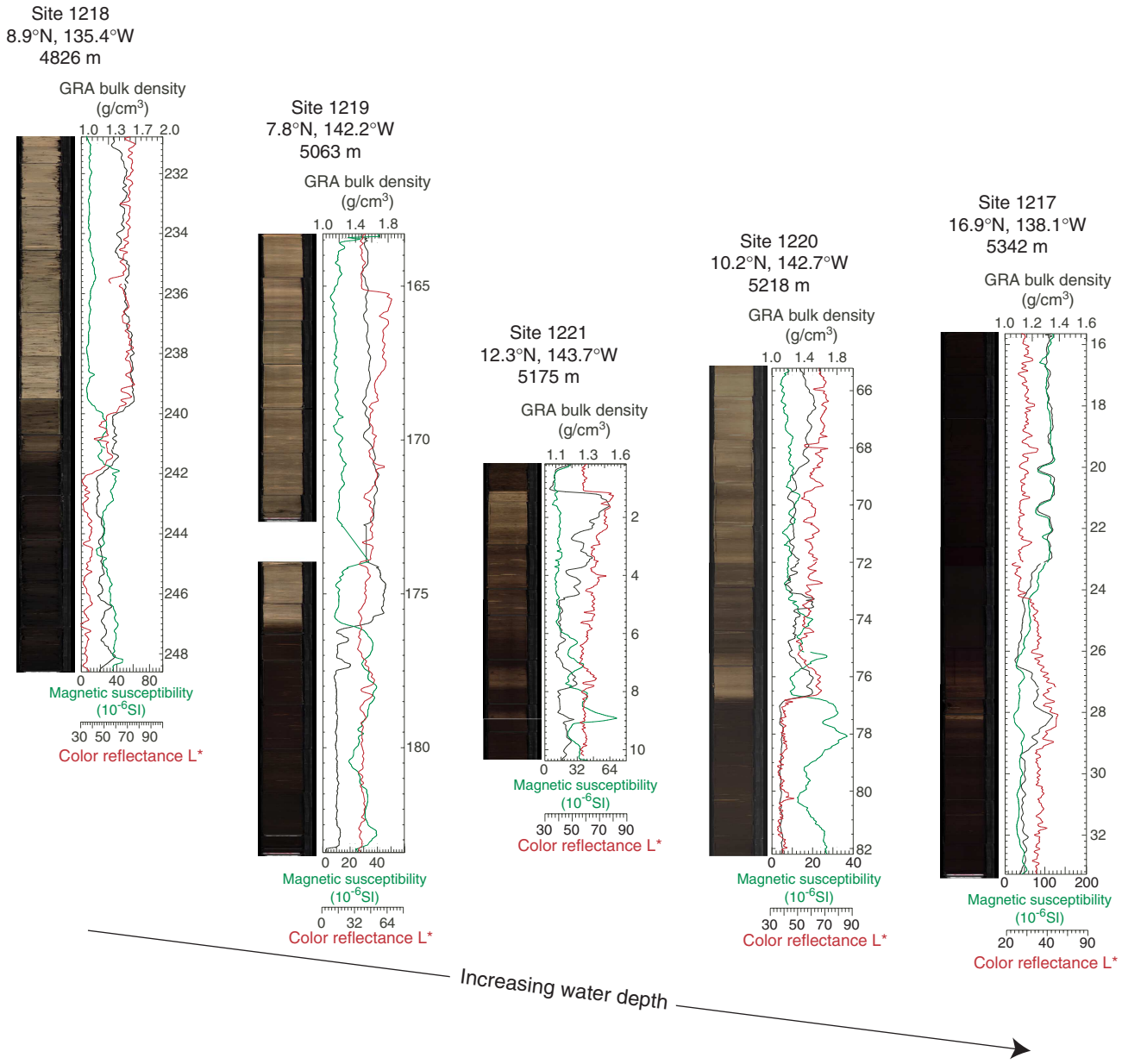

Figure F27. Composite digital photographs of the Eocene/Oligocene (E/O) boundary from Leg 199 using biostratigraphic (nannofossil and radiolarian) and magnetostratigraphic data. Orange dashed line = preliminary position of the boundary (at the 33.7-Ma isochron) as estimated through linear interpolation between paleomagnetic and/or biostratigraphic indications (see Table T2, p. 87). Note that linear interpolations are subject to significant error associated with the change in sedimentation rate that takes place across this transition (see Fig. F25, p. 76). Calc. = calcareous. Paleomag = paleomagnetism.

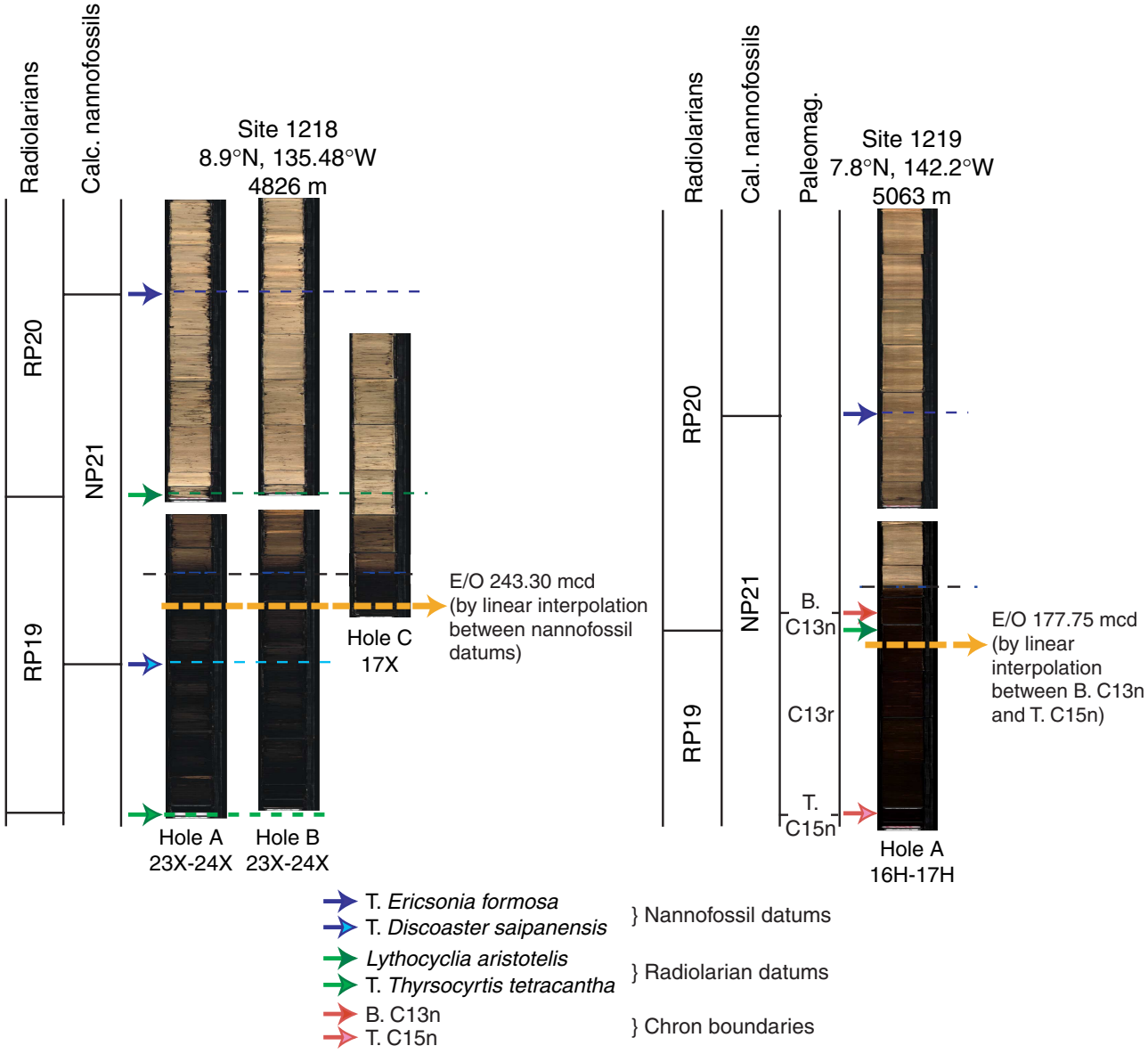

Figure F28. Composite digital photographs of the correlation and comparison of the E/O boundary sections recovered during Leg 199. At four of the five sites from which this interval was recovered, cores from Holes A, B, and C overlap to produce continuous complete sections. At Site 1219 only one hole penetrated the boundary, and a small coring gap is present in the section. Refer to Figure F27, p. 78, and Table T2, p. 87. E/O = Eocene/Oligocene boundary.

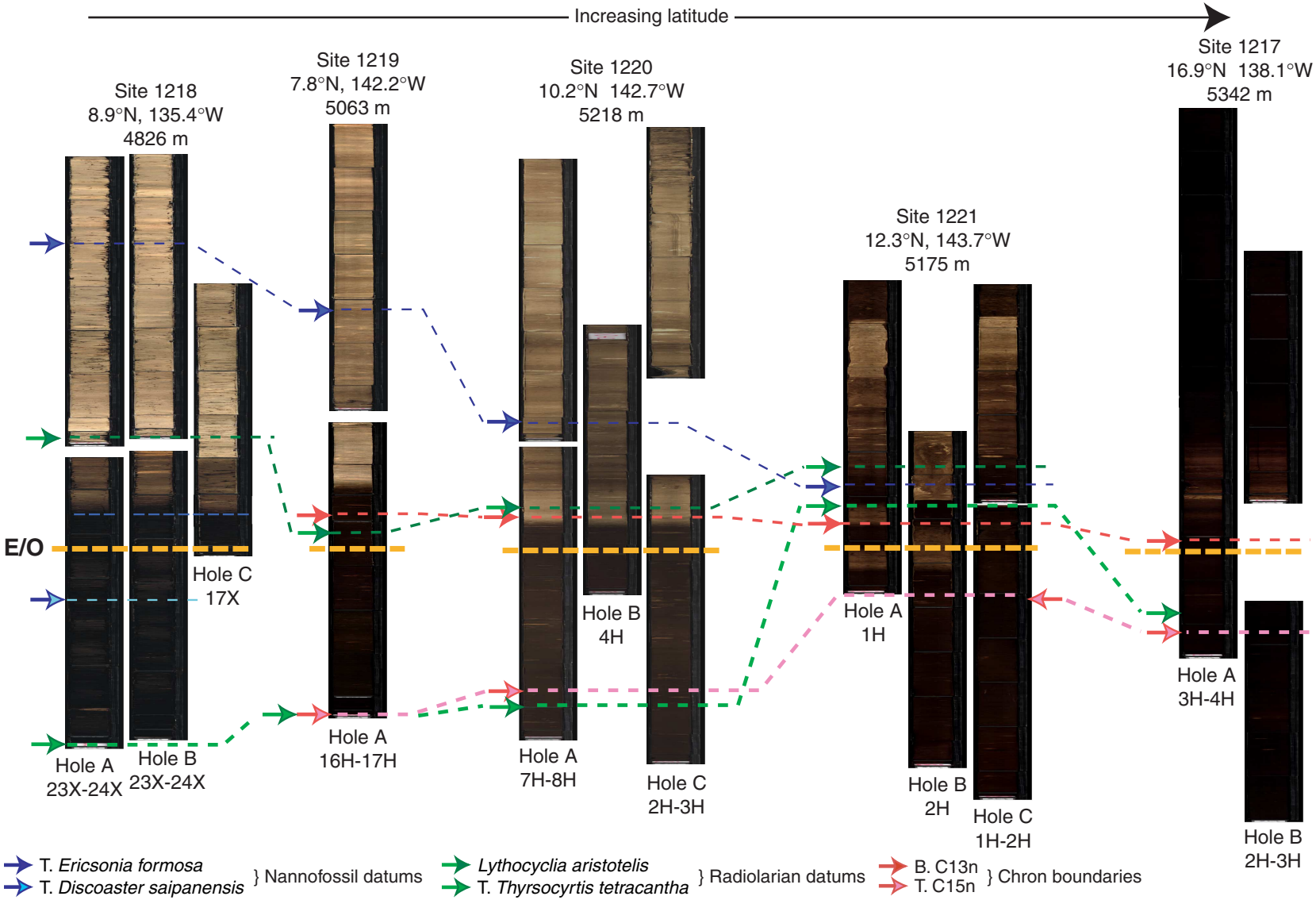

Figure F29. Comparison of diatom events (>5% diatoms in the sediments) to estimated position of equator crossings in lower Eocene–lower Oligocene sediments from the 56-Ma transect. Equator crossings have been estimated by shipboard paleomagnetic results and by using a fixed hotspot model of Pacific plate motion. Diatom events are not clustered at equator crossings. F.Z. = fracture zone.

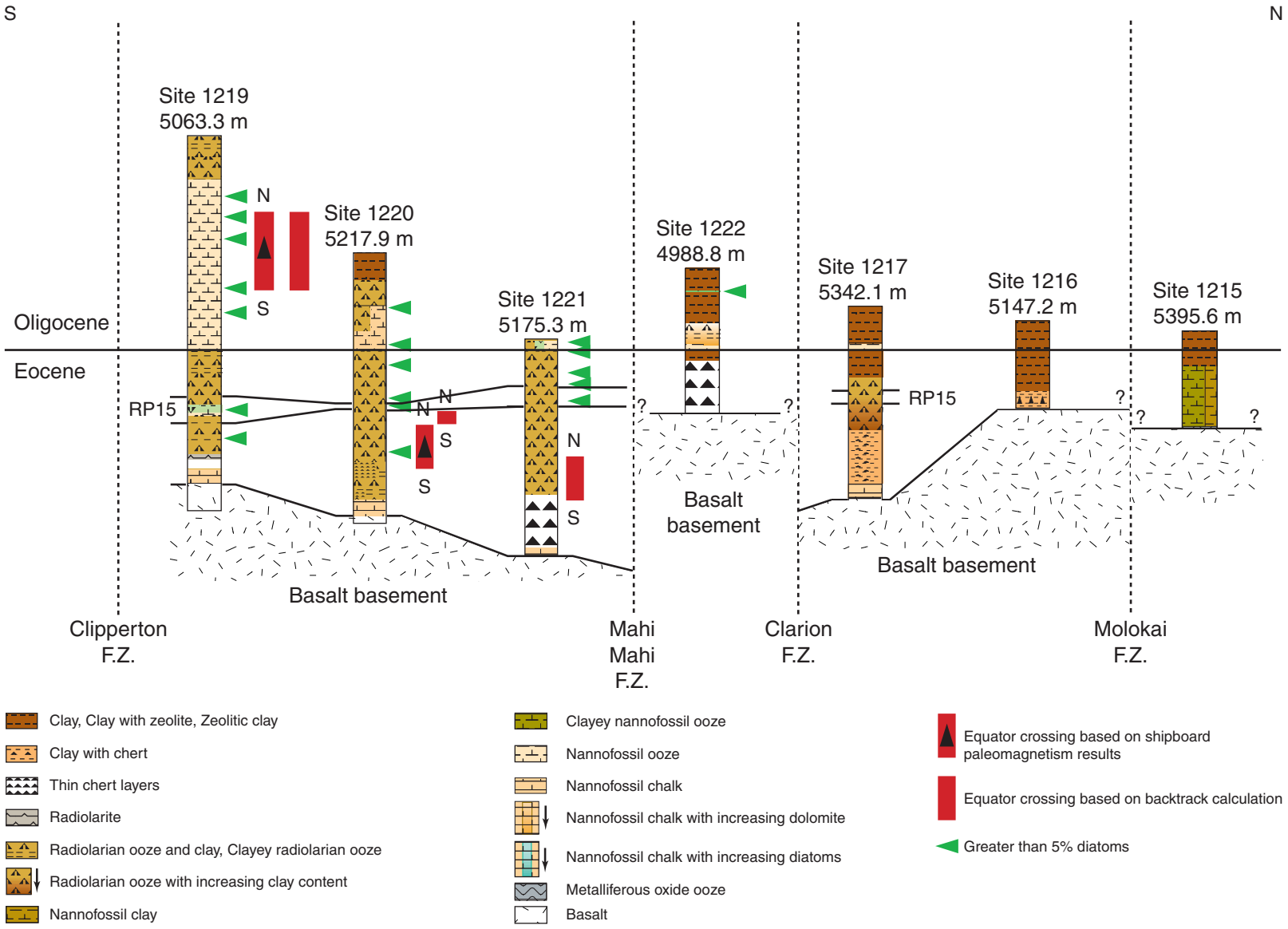

Figure F30. Digital photographs of the P/E boundary sediments recovered at Sites 1220 and 1221. Lower Eocene calcareous chalks grade downcore into multicolored clay-rich lithologies. The last occurrence of Paleocene fauna is recorded at the base of the brown clay, and the first occurrence of Eocene assemblages is at the top of the dark-brown clay. Calcareous fossils are barren to poorly preserved in the multicolored clay layers, and percentage $CaCO_3$ values are very low. FO = first occurrence, LO = last occurrence. Cal = calcareous. P. = pink.

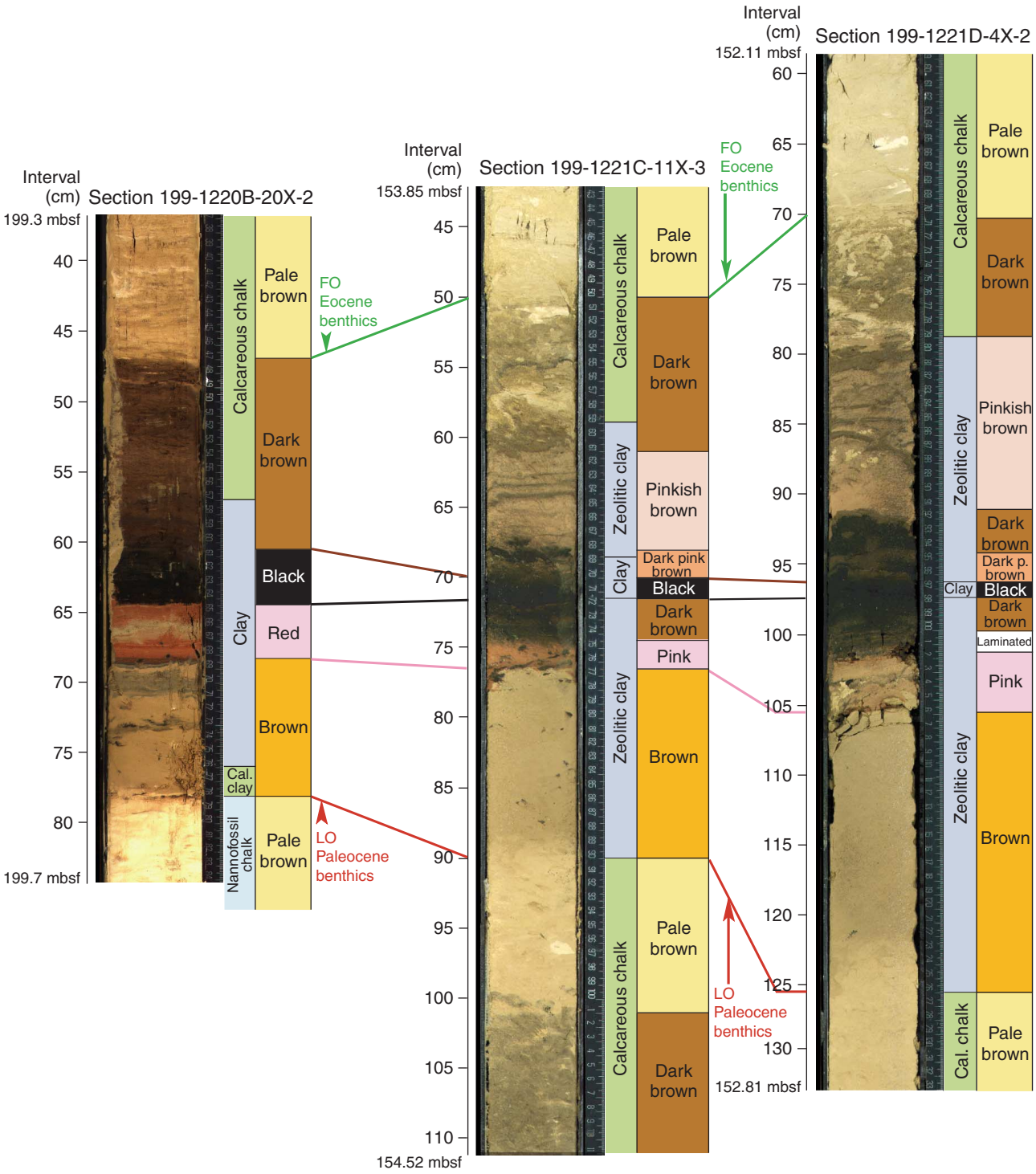

Figure F31. Digital photograph of the >63-µm fraction of surface core scrape washed samples from across the P/E boundary, Section 199-1220B-20X-2. The following major grains are observed at each depth interval: Planktonic foraminifers (intervals 199-1220B-20X-2; 13–20, 28–35, 35–43, and 42–50 cm; 198.90–199.40 mbsf), pink brown grains and dolomite crystals (interval 199-1220B-20X-2; 50–57 cm; 199.40–199.47 mbsf), black grains and sediment lumps (interval 199-1220B-20X-2; 57–64.5 cm; 199.47–199.55 mbsf), large pinkish grains with many dolomite crystals (interval 199-1220B-20X-2; 65–72 cm; 199.55–199.62 mbsf), small pink brown grains with rare planktonic foraminifers and dolomite grains (interval 199-1220B-20X-2; 74–78 cm; 199.64–199.68 mbsf), and dolomite grains and rare benthic foraminifers (interval 199-1220B-20X-2; 77.5–85 and 85–95 cm; 199.68–199.85 mbsf).

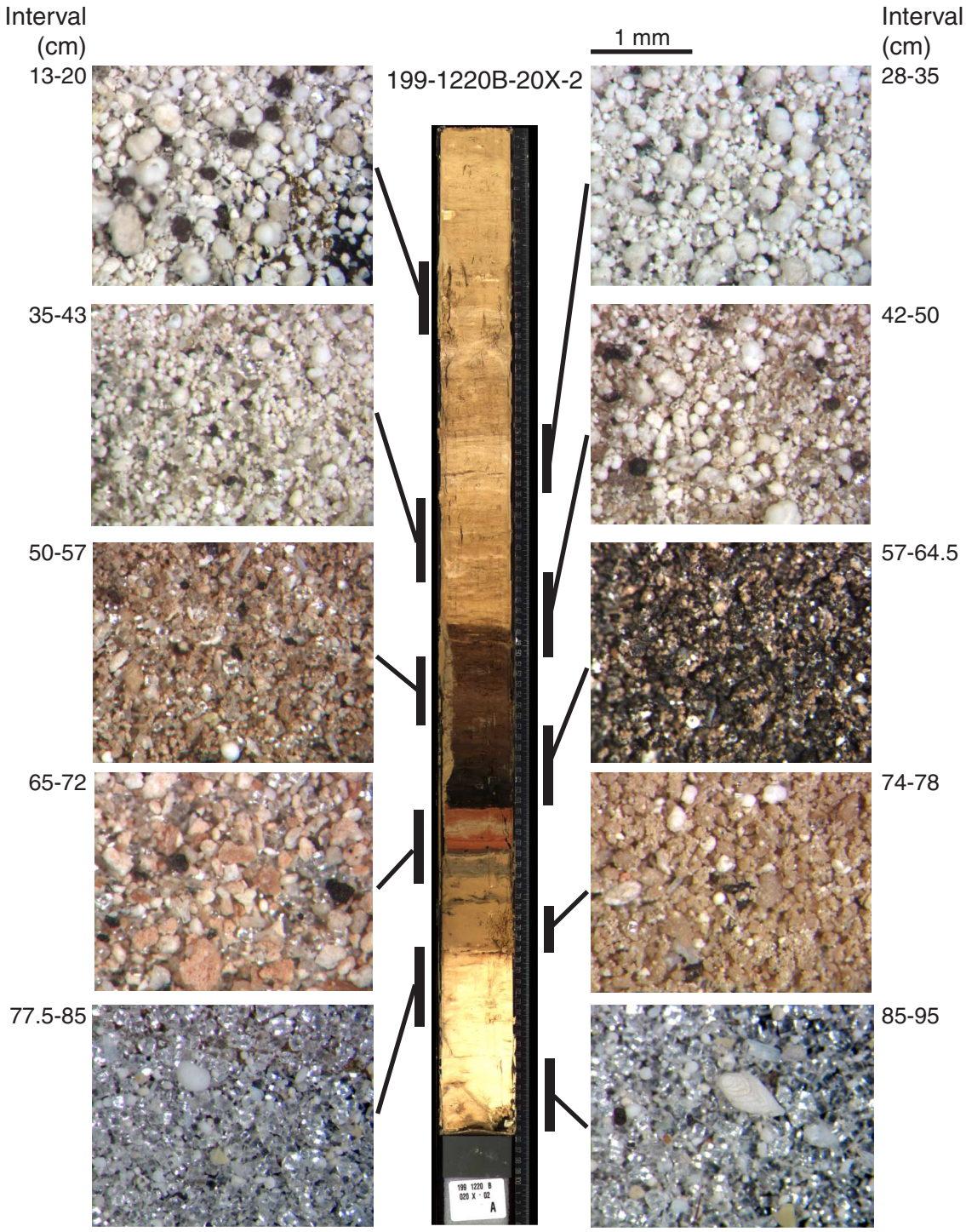

Figure F32. Digital photograph and stratigraphic distribution of benthic foraminifers in Section 199-1220B-20X-2 (198.90–199.85 mbsf). Red triangles at 199.68 mbsf = P/E boundary as represented by the benthic extinction event (BEE).

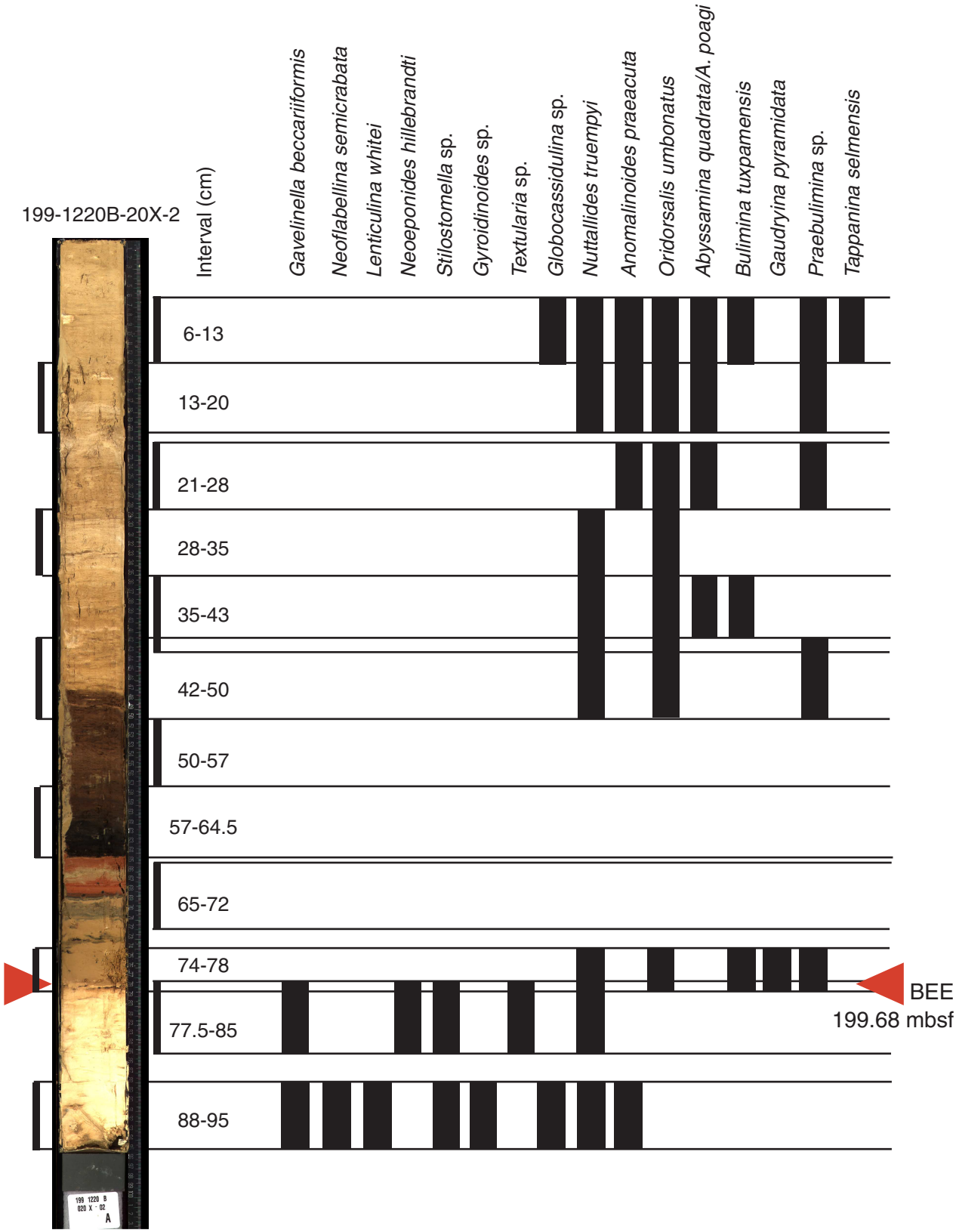

Figure F33. A. Composite digital photograph of shipboard ICP-AES analyses of Si, Al, Ti, Fe, and Mg on 2-cm C_{org} scrapes across the Paleocene–Eocene (P/E) boundary from Sites 1220 and 1221. Elevated concentrations of all these elements in the boundary interval reflect low $CaCO_3$. Different levels of elements through the interval reflect the distinct color bands. (Continued on next page.)

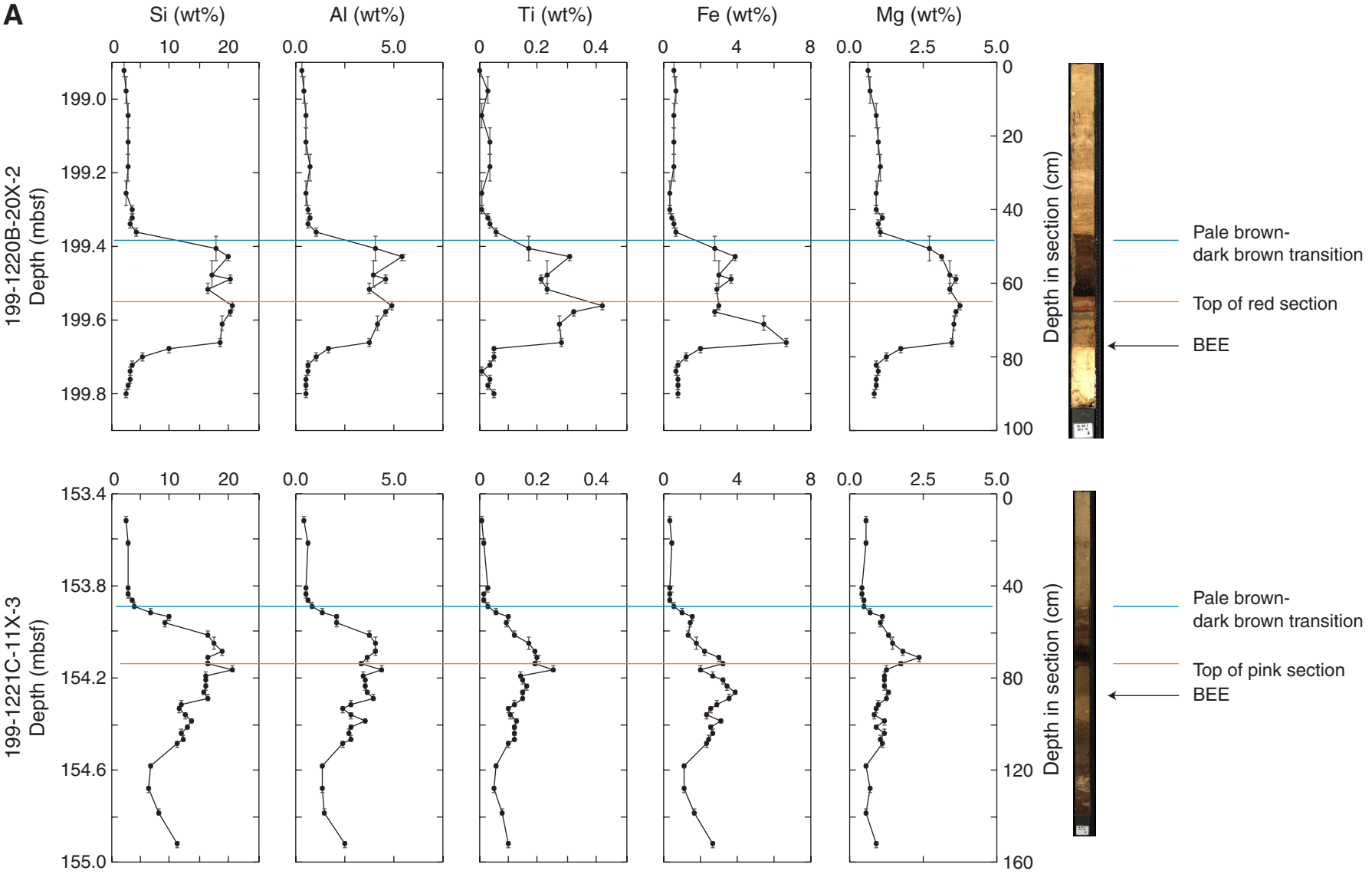

Figure F33 (continued). B. Composite digital photograph of shipboard ICP-AES analyses of Ca, Sr, Ba, P, and Mn on 2-cm C_{org} scrapes across the P/E boundary from Sites 1220 and 1221. The difference in behavior between Ca and Sr reflects recrystallization. A strong Mn peak flanked by P and Ba peaks is characteristic of the boundary interval. BEE = benthic extinction event.

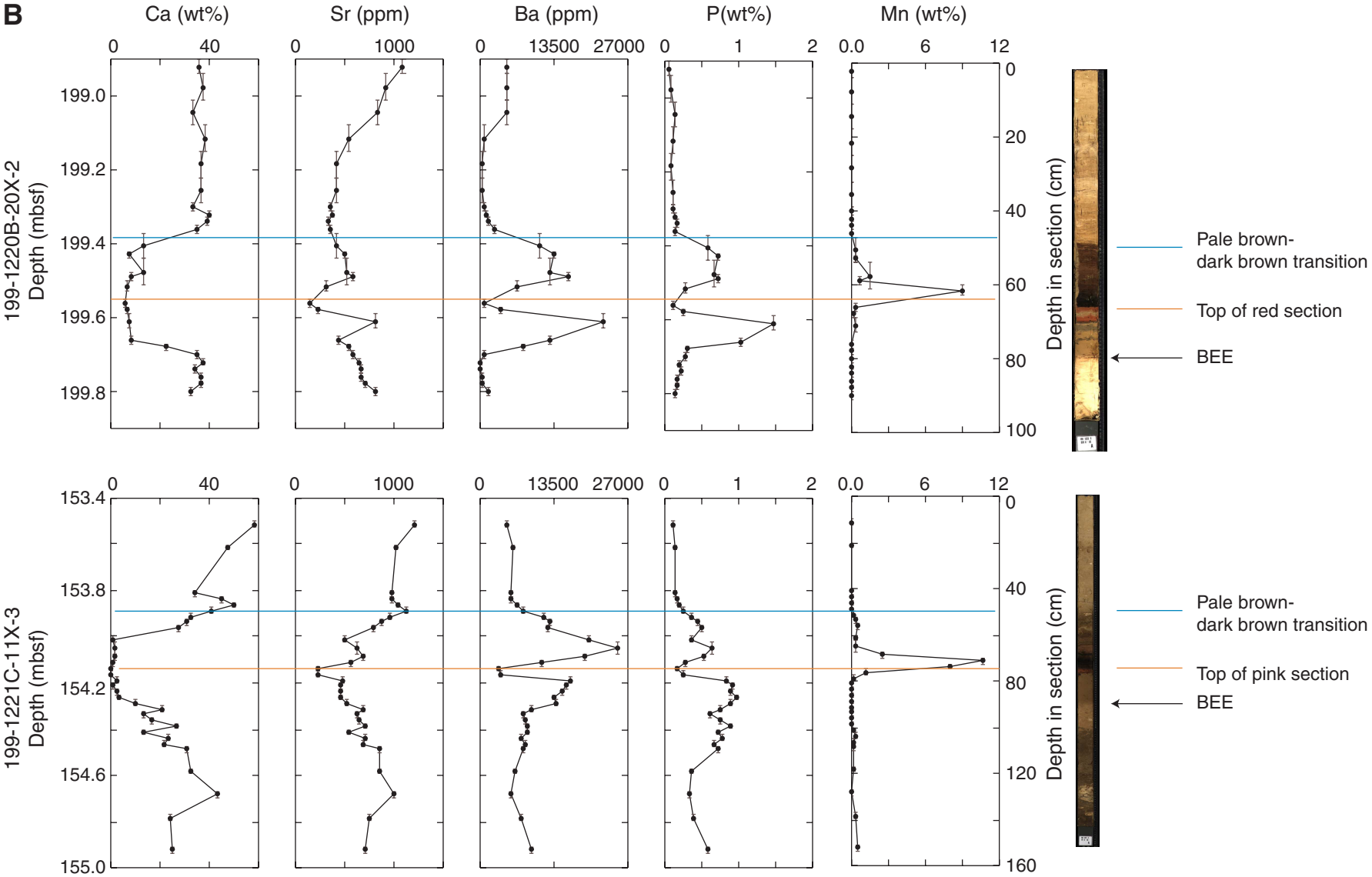

Table T1. Hole summary, Leg 199.

Hole	Latitude	Longitude	Water depth (m)	Number of cores	Interval cored (m)	Core recovered (m)	Recovery (%)	Interval drilled (m)	Time on hole (hr)	Time on hole (days)
1215A	26°01.7734′N	147 55.9906′W	5395.6	10	75.4	68.27	90.50	0	57.50	2.40
1215B	26°01.7626′N	147°55.9906′W	5395.3	11	82.8	58.95	71.20	0	32.00	1.30
		Site 1215 totals:		21	158.2	127.22	80.40	0	89.50	3.70
1216A	21°27.1629′N	139°28.7904′W	5152.5	11	62.2	56.47	90.80	0	31.00	1.30
1216B	21°27.1702′N	139°28.7859′W	5147.2	1	9.5	9.75	102.60	0	11.25	0.50
		Site 1216 totals:		12	71.7	66.22	92.40	0	42.25	1.80
1217A	16°52.0133′N	138°05.9981′W	5342.1	17	145.2	89.94	61.90	0	45.00	1.90
1217B	16°52.0175′N	138°06.0007′W	5342.1	7	66.5	61.49	92.50	20.0	15.00	0.60
1217C	16°52.0234′N	138°06.0012′W	5342.1	5	47.5	46.82	98.60	32.0	19.25	0.80
		Site 1217 totals:		29	259.2	198.25	76.50	52.0	79.25	3.30
1218A	08°53.3667′N	135°22.0002′W	4826.3	30	276.8	266.42	96.30	0	90.00	3.80
1218B	08°53.3777′N	135°21.9995′W	4827.6	29	263.5	259.25	98.40	0	45.65	1.90
1218C	08°53.3885′N	135°21.9997′W	4827.6	21	194.8	198.05	101.70	62.0	44.10	1.80
		Site 1218 totals:		80	735.1	723.72	98.50	62.0	179.75	7.50
1219A	7°48.0097′N	142°0.9390′W	5063.3	27	250.8	240.41	95.90	0	82.42	3.40
1219B	7°48.0186′N	142°0.9397′W	5063.3	15	137.0	138.55	101.20	21.0	40.33	1.70
		Site 1219 totals:		42	387.8	379.01	97.70	21.0	122.75	5.10
1220A	10°10.6008′N	142°45.4917′W	5217.9	12	114.0	118.68	104.10	0	37.75	1.60
1220B	10°10.6001′N	142°45.5028′W	5217.9	20	166.0	144.65	87.10	36.0	54.50	2.30
1220C	10°10.6002′N	142°45.5148′W	5217.9	17	153.6	116.12	75.60	50.5	42.00	1.80
		Site 1220 totals:		49	433.6	379.45	87.50	86.5	134.25	5.60
1221A	12°01.9987′N	143°41.6514′W	5175.3	13	115.6	113.81	98.50	0	47.00	2.00
1221B	12°01.9880′N	143°41.6524′W	5175.1	2	14.2	14.53	102.30	0	12.80	0.50
1221C	12°01.9873′N	143°41.6513′W	5174.4	12	100.2	54.07	54.00	57.1	24.42	1.00
1221D	12°01.9762′N	143°41.6519′W	5174.4	4	17.8	2.28	12.80	138.2	29.50	1.20
		Site 1221 totals:		31	247.8	184.69	74.50	195.3	113.72	4.70
1222A	13°48.9780′N	143°53.3477′W	4988.7	12	107.3	74.64	69.6	0	33.83	1.40
1222B	13°48.9776′N	143°53.3368′W	4990.7	7	64.4	63.77	99.0	0	23.92	1.00
		Site 1222 totals:		19	171.7	138.41	80.6	0	57.75	2.40
		Leg 199 totals:		283	2465.1	2196.92	89.1	416.8	819.30	34.10

Note: This table is also available in **ASCII.**

Table T2. Stratigraphic control around the Eocene/Oligocene (E/O) boundary.

Control points	Age (Ma)	Depth (mcd)	Sedimentation (m/m.y.)	E/O depth (mcd)	E/O depth (mbsf)	E/O position in core
Site 1217:						
Base C13n	33.545	29.88				
Top C15n	34.655	32.83	2.7	30.29	30.03	199-1217A-4H-5, 53 cm
Site 1218:						
Top NP21	32.900	238.68				
Base NP21	34.000	245.03	5.8	243.30	219.84	199-1218C-17X-CC, 1 cm
Site 1219:						
Base C13n	33.545	176.92				
Top C15n	34.655	182.84	5.3	177.75	152.42	199-1219A-17H-4, 58 cm
Base C16n.2n	36.341	190.99	4.8	177.67	152.34	199-1219A-17H-4, 50 cm
Site 1220:						
Base C13n	33.545	76.97				
Top C15n	34.655	82.67	5.1	77.77	70.13	199-1220A-8H-3, 63 cm
Site 1221:						
Base C13n	33.545	8.11				
Top C15n	34.655	10.65	2.3	8.46	9.02	199-1221A-1H-7, 2 cm

Note: The mcd and mbsf depths of the E/O boundary (set at 33.7 Ma) are extrapolated from the rates and datum points given in the age, depth, and accumulation columns.